FINITE ELEMENT ANALYSIS OF HOT-MIX ASPHALT LAYER INTERFACE BONDING

by

MATTHEW J. WILLIAMSON

BS, Kansas State University, 2003
MS, Kansas State University, 2007

AN ABSTRACT OF A DISSERTATION

submitted in partial fulfillment of the requirements for the degree

DOCTOR OF PHILOSOPHY

Department of Civil Engineering
College of Engineering

KANSAS STATE UNIVERSITY
Manhattan, Kansas

2015

Abstract

Tack coat is a thin layer of asphaltic material used to bind a newly-placed lift of hot-mix asphalt (HMA) pavement to a previously-placed lift or a new HMA overlay/inlay and existing pavement. The purpose of a tack coat is to ensure that a proper bond occurs so that traffic loads are carried by the entire HMA structure. Proper bonding exists when HMA layers act as a monolithic structure, transferring loads from one layer to the next. This depends on appropriate selection of tack coat material type and application rate, and is essential to prevent slippage failure and premature cracking in the wearing surface. This study focuses on development of a three-dimensional finite element (FE) model of HMA pavement structure in order to assess HMA interface bonding. The FE model was constructed using commercially available ABAQUS software to simulate an Accelerated Pavement Testing (APT) experiment conducted at the Civil Infrastructure Systems Laboratory (CISL) at Kansas State University. Mechanistic responses measured in the CISL experiment, such as localized longitudinal strain at the interface, were used to calibrate the FE model. Once calibrated, the model was used to predict mechanistic responses of the pavement structure by varying the tack coat property to reflect material characteristics of each application. The FE models successfully predicted longitudinal strains that corresponded to APT results.

FINITE ELEMENT ANALYSIS OF HOT-MIX ASPHALT LAYER INTERFACE BONDING

by

MATTHEW J. WILLIAMSON

BS, Kansas State University, 2003
MS Kansas State University, 2007

A DISSERTATION

submitted in partial fulfillment of the requirements for the degree

DOCTOR OF PHILOSOPHY

Department of Civil Engineering
College of Engineering

KANSAS STATE UNIVERSITY
Manhattan, Kansas

2015

Approved by:

Major Professor
Dr. Mustaque Hossain

Abstract

Tack coat is a thin layer of asphaltic material used to bind a newly-placed lift of hot-mix asphalt (HMA) pavement to a previously-placed lift or a new HMA overlay/inlay and existing pavement. The purpose of a tack coat is to ensure that a proper bond occurs so that traffic loads are carried by the entire HMA structure. Proper bonding exists when HMA layers act as a monolithic structure, transferring loads from one layer to the next. This depends on appropriate selection of tack coat material type and application rate, and is essential to prevent slippage failure and premature cracking in the wearing surface. This study focuses on development of a three-dimensional finite element (FE) model of HMA pavement structure in order to assess HMA interface bonding. The FE model was constructed using commercially available ABAQUS software to simulate an Accelerated Pavement Testing (APT) experiment conducted at the Civil Infrastructure Systems Laboratory (CISL) at Kansas State University. Mechanistic responses measured in the CISL experiment, such as localized longitudinal strain at the interface, were used to calibrate the FE model. Once calibrated, the model was used to predict mechanistic responses of the pavement structure by varying the tack coat property to reflect material characteristics of each application. The FE models successfully predicted longitudinal strains that corresponded to APT results.

Table of Contents

List of Figures

List of Tables

Acknowledgements

I wish to express my sincere appreciation to Dr. Mustaque Hossain for guiding me through this research endeavor. As a professor and advisor he has provided direction, support, and encouragement. My thanks also go to Dr. Robert W. Stokes, Dr. Sunanda Dissanayake, and Dr. Xiaojiang “Jack" Xin for serving on my doctoral committee. Thank you also to Dr. Kristan Corwin for serving as the outside chair of this committee.

I would like to thank my fellow graduate students, Daniel Mealiff and Milad Saghebfar, for their efforts. Their willingness to share their experiences in accelerated pavement testing and finite element modeling made my work possible.

My deepest thanks to my loving wife, Rebecca, without whom I could not have completed this journey. Thank you for the countless hours you gave to allow for the completion of this work. Your love and support are truly a gift to me. Thank you to my family who supported me throughout.

Dedication

To my wife, Rebecca, and my children Rachel, Leah, and Benjamin.

Chapter 1 - Introduction

1.1 Introduction

According to ASTM D8, *Standard Terminology Relating to Materials for Roads and Pavements*, "Tack coat (bond coat) is an application of bituminous material to an existing, relatively non absorptive surface to provide a thorough bond between old and new surfacing" (ASTM 2004). Figure 1.1 illustrates tack coat application using a distributor truck. Tack coat is used to bind a newly-placed layer, or lift, of hot-mix asphalt (HMA) pavement to a previously-placed lift or new HMA overlay/inlay and existing pavement. Inlay refers to the HMA overlay when the existing pavement is milled and replaced by an overlay with thickness equal to the milling depth. The purpose is to ensure a proper bond so that traffic loads are transmitted and carried throughout, the entire HMA structure. Proper bonding exists when HMA layers act as a monolithic structure, transferring loads from one layer to the next. This depends on appropriate selection of tack coat material type and application rate, is essential to prevent slippage failure and premature cracking in the wearing surface. Khweir and Fordyce (2003) reported that improper bonding, where pavement layers displace independently, could lead to 40% to 83% loss in predicted life of the pavement. Such a reduction in pavement service life leads to increased maintenance and construction costs, user delays and lost productivity, and unnecessary use of valuable resources, such as aggregate, binder, and fuel, utilized in the production of HMA pavement.

Figure 1.1 Tack Coat Application (Mealiff 2015)

Hot paving asphalt cement, cutback asphalt, and emulsified asphalt have all been employed by owners and contractors as tack coat materials (West et al. 2005). Emulsified asphalt (or asphalt emulsion), the most common type for tack coat material use, is produced by mixing solid asphalt and water in the presence of an emulsifying agent in a colloid mill. During the mixing process, extremely small (less than 5 -10μm) globules or asphalt cement droplets are produced and become suspended in water. Electric charge imparted by the emulsifying agent ensures that the globules do not coalesce. These bituminous materials are liquid at ambient temperature. The water evaporates when applied to the existing clean pavement surface, leaving a thin layer of asphalt cement on the surface to which it was applied. This evaporative process is known as "breaking" or "setting." This thin layer of asphalt cement promotes bonding between the layers or lifts of

HMA, resulting in maximum structural capacity of the pavement cross section and prevention of delamination and premature failure.

The most commonly used tack materials include slow-setting (SS) emulsions, such as SS-1, SS-1h, CSS-1, and CSS-1h, and rapid-setting (RS) grades of emulsion, such as RS-1, RS-2, CRS-1, CRS-2, CRS-2P ("P" stands for polymer-modified), and CRS-2L ("L" stands for latex-modified). In these designations, "C" designates the emulsion as being cationic. The "h" indicates that a "hard" grade asphalt has been used in the emulsion production. Emulsions with "2" designation typically have higher viscosities than emulsions with "1" designation.

1.2 Problem Statement

As mentioned, lack of bond between HMA pavement layers can lead to premature failure in the form of debonding and potential fatigue cracking, resulting in reduced pavement life. Slippage cracking, an additional type of HMA pavement failure associated with inadequate bonding between layers, occurs most often in locations of vehicle acceleration, especially braking and turning. Application of asphalt emulsion or other tack coat materials most often facilitate the bond between HMA layers. Although some form of tack coat material is used in nearly all forms of HMA pavement, exact materials and application rates vary greatly by location and agency. Based on a survey of state transportation agencies, Paul and Scherocman (1998) found that a majority of agencies use SS emulsions for tack coat, including SS-1, SS-1h, CSS-1, and CSS-1h. Results showed that the Kansas Department of Transportation (KDOT) commonly uses SS-1hP and Emulsion Bonding Liquid (EBL). SS-1hP is a slow-setting, polymer-modified suspension of asphalt in water, and EBL is a polymerized asphalt emulsion (Mealiff 2015).

Mechanistic pavement design is often based on an assumption of fully-bonded interface layers. However, recent studies have shown significant variations in mechanistic responses when

layer interfaces are treated as other than fully-bonded (Hu and Walubita 2011; Willis and Tim 2007; King and May 2003; Roffe and Chaignon 2002). Many studies have been undertaken to thoroughly understand the mechanistic response of HMA structures relative to their bonded and unbonded interfaces. Studies that have included Accelerated Pavement Testing (APT) are of particular importance because these studies simulate loading similar to in-service pavement loading but within a controlled environment (Hossain et al. 2012; Leng et al. 2008; Romanoschi 1999; Metcalf 1996). Other relevant studies have focused on modeling relevant pavement structure-vehicle loading interactions (Saevarsdottir and Erlingsson 2014; Maina and Matsui 2004; Huang et al. 2001; DeBondt and Scarpas 1994). Use of finite element modeling (FEM) software is instrumental in this area. Various studies have also emphasized HMA interface bonding (Hu and Walubita 2011; Yan-qing et al. 2009; Wu 2001; Yoo and Al-Qadi 2008; Duncan et al 1968). Continued utilization of FEM and APT are necessary in order to increase understanding of mechanistic responses of HMA pavement structures given variable application rates and types of tack coat.

1.3 Objective

The objective of this study was to develop a three-dimensional (3D) FEM model that would assess interface bonding condition using mechanistic analysis of HMA pavement structures. This study utilized FEM software and APT experimental data to appropriately characterize the interface with a property such as the reaction modulus in order to vary types and application rates of tack coat material. The model was built to characterize the materials, geometry, and loading of a previously conducted APT experiment at the Civil Infrastructure Systems Laboratory (CISL) at Kansas State University, Manhattan, Kansas. Later, the model was calibrated with APT results derived from that experiment.

1.4 Research Approach

An extensive literature review was conducted to assess the knowledge base of tack coat bonding performance, mechanistic responses of HMA pavement structures relative to interface bonding, accelerated testing of HMA pavement structures, and relevant FEM.

A full-scale APT experiment was constructed and monitored at the CISL facility to study HMA interface layer bonding. This test was conducted on existing pavement structures that were milled and overlaid with a new layer of HMA. During overlay construction, various material types and application rates were used to apply tack coat on the test sections. Tack coat material types and application rates were intended to be the only variables among the sections, but some variation in overlay thicknesses and existing HMA layers occurred. The overlay was placed in a test pit over two previously-paved lanes with existing HMA layers. Variations in response and performance among test sections were the focus of the APT experiment and FE modeling.

Using commercially available ABAQUS software, a numerical model was built to simulate the APT experiment performed at the CISL facility. Essential elements of this model included the geometry and material properties of the APT sections, appropriate simulation of applied wheel loads, and an interaction that appropriately simulated various bonding conditions. The model was calibrated so that mechanistic responses in the FEM, specifically the strain at the interface layer, adequately matched mechanistic responses measured in the APT portion of the study.

1.5 Dissertation Outline

This dissertation is divided into six chapters. Chapter 1 contains the introduction, Chapter 2 presents a literature review, and Chapter 3 describes APT of the test sections at CISL. Chapter 4 and 5 discuss FEM and analysis results, respectively. Chapter 6 presents conclusions and recommendations from this study.

Chapter 2 – Literature Review

2.1 Introduction

Owners, agencies, and contractors involved in the design, construction, maintenance and operation of HMA pavements have recognized the importance of interface bonding in HMA pavement structures. Although proper bonding to ensure long-term pavement performance has been well established, improper bonding and subsequent failures continue to occur. Therefore, valuable, ongoing research to describe the mechanics of HMA interface layer bonding must continue.

2.2 Hot-Mix Asphalt Pavements

HMA is comprised of a mixture of coarse aggregate, fine aggregate (sand), and bituminous binder. Depending on availability, natural and/or manufactured aggregates may be used to achieve desired gradation and angularity properties. These HMA mixtures are used in construction of pavements for facilities such as parking facilities, streets, and major highways. HMA pavements are aptly named flexible pavements because all layers deform under traffic loads, in contrast to rigid pavements commonly made from Portland Cement Concrete (PCC)

HMA pavements are constructed by placing multiple lifts, often approximately 2 in. thickness, on top of one another. HMA also is frequently used as an overlay of existing flexible and rigid pavements and as overlay/inlay for flexible pavements. However, the lifts must be well-bonded in order to monolithically mobilize the structural capacity of separately-placed lifts. Therefore, tack coats are typically applied between HMA layers to ensure bonding.

2.3 Tack Coat

As mentioned, tack coat refers to material used to bind HMA layers to previously-placed HMA layers or existing flexible or rigid pavements. However, asphalt binder must be in a liquid

state for tack coat application at ambient or slightly elevated temperature. Heating asphalt is one option for achieving a liquid state, but this alternative is less effective and more dangerous than use of emulsions. Emulsions are formed by using an emulsifying agent to suspend asphalt binder globules in water (Brown et al. 2009). Asphalt particles are naturally neutral, thereby requiring ionization to prevent them from adhering to each other in suspension. Asphalt emulsions are liquid at ambient temperature; this liquid is light brown when applied to an existing layer of asphalt or concrete pavement. As water evaporates from the emulsion, a residual layer of sticky asphalt binder remains on the asphalt or pavement. This evaporative process is known as "breaking" (Brown et al. 2009).

In addition to emulsions, other available tack materials include EBL and Trackless Tack. According to KDOT, "EBL is a polymerized emulsion used primarily undiluted at rates that depend on the existing pavement macro-texture" (KDOT 2007). EBL is a proprietary material used in specially-designed spray pavers that place EBL directly ahead of the HMA mat because, unlike emulsions, EBL does not need to break. This placement protects EBL tack coat from pickup on truck tires. Trackless tack, although applied similarly to traditional tack coat, quickly becomes non-adhesive after placement, thereby also avoiding pickup by truck tires (Clark et al. 2010). Figure 2.1 shows tracking of tack coat on the tires of trucks carrying HMA mix that may be eliminated using EBL or Trackless tack. Tracking removes tack material from the existing pavement surface, potentially producing improper bonding in the pavement structure.

Figure 2.1 Tack Pickup by Truck Tire (Mealiff 2015)

2.4 Laboratory Evaluation of Tack Coat

A majority of previous studies characterizing HMA interface bonding have focused on laboratory results, and many laboratory tests have been proposed to quantify bonding characteristics of tack coat. Failure modes in these tests included tension, shear, and torque.

Romanoschi's (1999) direct shear test method improved previous direct shear methods such as Iowa Test Method No. 406 (Grove et al. 1993). Unlike previous methods, Romanoschi introduced a constant normal stress to the specimen that remained constant while a shear load was applied with a constant rate of displacement. When the test was repeated with multiple applied normal stresses, a relationship was found that yielded the reaction modulus, or the slope of the resulting stress versus displacement plot.

Romanoschi and Metcalf (2001) used direct shear tests to formulate a constitutive, two-state model for the asphalt layer interface. Before failure, the model indicated that the interface would undergo increasing shear stress with increasing shear displacement until reaching a

maximum shear stress value. The slope of this linear region was defined by a reaction modulus, k in lb/in^3 (MPa/mm). This modulus, or layer stiffness, was also the basis other works such as Ozer et al. (2008). In addition to critical shear displacement, the coefficient of friction, μ, characterized the interface (Romanoschi and Metcalf 2001), as shown in Figure 2.2. Direct shear laboratory testing has generally determined the maximum shear stress value for this model. The linear portion of this interface model was used to characterize the asphalt interface layer in the 3D-FEM portion of the study presented here. Maximum shear stress values were unknown because direct shear tests were not performed. However, the linear portion of the model was adequate for this study because test sections did not show distresses related to shear failure.

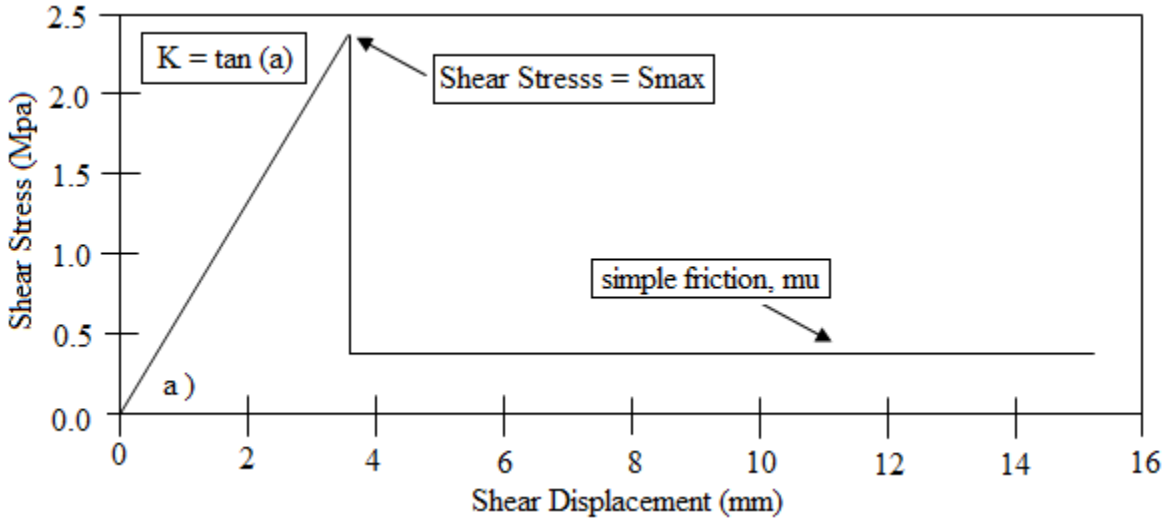

Figure 2.2 Interface Shear Behavior (Romanoschi and Metcalf 2001)

Additional notable shear tests have been developed since Romanoschi and Metcalf (2001), including Canestrari's Layer-Parallel Direct Shear (LPDS) tester (Canestrari et al. 2005). LPDS shears 6-in. diameter core samples at a rate of 2 in./min. The Strategic Highway Research Program (SHRP) developed the Superpave shear tester (SST) to evaluate interface bond strength. SST applies a shear load at a specified rate in a temperature-controlled chamber until the specimen fails.

The Louisiana Interlayer Shear Strength Test (LISST) is one of two test methods developed by Mohammad et al. (Mohammad et al. 2012) as part of the project NCHRP 9-40: "Optimization of Tack Coat for HMA Placement." The LISST evaluates the effects of several bonding parameters, such as existing pavement type and surface condition, tack coat material type, and tack coat application rate, using test hardware designed to fit in a universal testing machine (UTM).

Researchers at Kansas State University (Mealiff 2015) conducted an APT experiment to determine optimum application rates of SS-1hP, EBL, and Trackless tack materials. In addition to a full-scale APT experiment, Mealiff (2015) also utilized a direct tension pull-off test similar to KDOT's KT-78 test method described in Section 2.5. In the laboratory portion of that study, cores of existing HMA pavements were bonded to new HMA overlay with various rates of SS-1hP, EBL, and Tackless tack (Mealiff 2015). Figure 2.3 shows a sample of core loaded in the UTM that was formed by applying tack coat on a core of existing HMA pavement in order to bond the overlay material compacted on top of the tack coat in a gyratory compactor. The cored sample remained in mold at room temperature, but the loose mixture for the overlay was hot and compacted by a fixed number of revolutions in the gyratory compactor. The compacted overlay contained approximately 7% air voids to represent the as-constructed overlay in practice in which 93% compaction of the theoretical maximum specific gravity is desired. Trial and error was used to determine the number of gyrations necessary to achieve 93% compaction (Mealiff 2015).

Figure 2.3 Bond Testing Specimen in UTM (Mealiff 2015)

2.5 In-Service Evaluation of Tack Coat

When they are able to be used, in-service studies provide valuable data because pavements are under actual load and environment during the studies. Researchers have previously performed in-situ tests to compare interface bonding variables within in-service pavement structure. Deysarkar (2004) used a Pull-Off test to measure tensile strength of tack coat in the field before an HMA overlay was placed. A torque wrench was used to apply a contact plate to the tack coat material that had been allowed to set. A normal load was applied to the plate until the plate adhered to the tack coat. When the normal load was removed, the torque wrench was used to twist off the plate from the tack coat. Previous knowledge regarding the developed relationship of tensile strength and torque required to detach the plate allowed tensile strength to be recorded from the measured torque (Deysarkar 2004).

The Tack Coat Evaluation Device (TCED) by Instro Tek, in which an aluminum plate is attached to the tack coat with normal force and then detached by tension, torque, or shear force,

has the ability to assess tensile and torque or shear strength of the tack coat. Woods (2004) used the TCED to evaluate tack coat application rates.

An interface bond study in Illinois placed test pavements on high-volume highways with variables such as material type, application rate, application procedure, surface cleaning method, and existing surface (Salinas et al. 2013). However, conclusions regarding optimum application rates were made based on laboratory shear tests performed on specimens from the test sections.

KDOT recently developed KT-78, "Method for Determining the Tensile Adhesive Strength of Asphalt Pavement Tack Coat" (KDOT 2007), a modification of the ASTM standard test method, ASTM D4541 "Standard Test Method for Pull-Off Strength of Coating Using Portable Adhesion Tester". The standard gives guidance for use of a mobile pull-off apparatus to separate two bonded layers in direct tension (ASTM D4541). Mealiff modified KT-78 protocol to perform direct tension tests in a UTM environment in order to characterize tack coat applications of test sections in an APT experiment at Kansas State University's CISL facility (Mealiff 2015).

2.6 Finite Element Modeling of HMA Pavements with Interface

Asphalt pavements exhibit viscoelastic and viscoplastic responses under traffic and thermal loads. This complexity has increased popularity of FEM for studying mechanistic responses of HMA pavement structures. Since 1965, FEM has been utilized for HMA pavements (Huang 2003). Because FEM has become the tool of choice for modern pavement engineers, Huang's 2003 study was undertaken to study interface bonding of two HMA layers using FEM. Other tools, such as the layered elastic analysis, are unable to provide detailed information about the interface because they can only model slip. In addition, because of ever-increasing computational capabilities of personal computers, most researchers currently use commercially available FEM software for pavement modeling: ABAQUS and ANSYS are the two most commonly used software packages.

Wu (2001) proved that 3D-FEM is a viable tool for analyzing HMA pavement structures under APT. In his study, creep models for HMA layers and Drucker-Prager (DP) models for granular layers helped capture nonlinear behavior of materials used in the HMA structure. Wu's work focused on permanent deformation, or rutting, of the HMA wearing surface. However, modeling approaches such as simulation of APT loading are largely applicable to the study presented here in regards to interfacial bond behavior.

Huang et al. (2001) developed a 3D-FEM to simulate an APT experiment at the Louisiana Accelerated Loading Facility. Similar to this study, material modeling was done with creep parameters and a moving wheel load. Study results concluded that FEM with visco-plastic materials could accurately predict pavement responses with respect to rutting.

A French and Swiss team performed EM analysis with APT laboratory experimentation, similar to Huang et al. (2001), that emphasized HMA rutting (Ali et al. 2006). The study used constitutive materials modeling approaches and loading similar to other studies. Previous studies emphasized model development and analysis with respect to rutting behavior. Recent work has developed models to analyze layer interface behavior. The study for this paper varied from other studies because a two-dimensional (2D) plane strain model was used instead of 3D models possibly due to an increase in available computing resources.

Yoo used the FEM approach to investigate fatigue cracking in HMA (2008). That study investigated variables such as tire configuration, HMA depth, wheel load, and wheel speed. Responses predicted by FEM were compared to measurements taken on the Virginia Smart Road. This study meticulously described differences in loading types used in FEM approaches, supporting use of 3D dynamic loading compared to conventional static, normal loading. Although the loading method differed substantially from modeling done here, other methods used here and

commonly throughout the literature provided a basis for the work presented here. Yoo and Al-Qadi (2008) utilized commonly-used C3D8R elements also chosen for this analysis. HMA materials were defined as viscoelastic, utilizing the same parameters (resilient modulus, Poisson's ratio, and creep parameters) as models created in this study.

Another study used the Coulomb friction model to represent interface layers in an HMA pavement structure (Yan-qing et al. 2009). That study investigated the effect of semi-rigid bases for reducing fatigue cracking. The study by Yan-qing et al. focused specifically on horizontal tensile stresses at the interface layer with the conclusion that increase in the model's Coulomb friction coefficient led to reduced tensile stresses at the bottom of the HMA layer above the interface (Yan-qing et al. 2009).

Hu and Walubita (2011) created a 3D-FEM to simulate fully-bonded and fully- unbonded interfacial conditions. Strains for both conditions were considered for flexible, semi-rigid, and rigid base materials. The study concluded that bonding condition does not significantly influence responses at the top of the wearing course, but it does significantly impact tensile strains at the bottom of the wearing course. This work was performed using arbitrary pavement structure sections without calibration to any type of actual testing. Although the experiment considered fully bonded and unbonded conditions, it did not consider the partially-bonded condition that may exist between those extremes.

Liu and Hao (2012) considered mechanistic responses of the HMA interface layer, similar to the study for this work. Liu and Hao measured maximum transverse tensile and maximum transverse shear stresses, primary indicators of cracking at the bottom of the HMA layer and rutting and transverse slippage, respectively. Several bonding types were considered for asphalt-to-asphalt and asphalt-to-base interfaces. When considering the effect of asphalt-to-asphalt interfaces, only

fully-bonded or "tied" interface properties were used in the asphalt-to-base layer interface. Results showed that stresses and strains are significantly re-distributed when layer interfaces are not treated as completely bonded, as is common in mechanistic analysis and design approaches. Their study demonstrated the significance of proper layer interface modeling in order to achieve more accurate design outputs.

A case study in Arkansas used FEM analysis and ABAQUS software to analyze potential causes of distresses seen in relatively new pavement structures on I-40 (Zou et al. 2012). The study showed that depth of maximum shear stresses was consistently 1.6 to 2.3 in. below the surface regardless of the thickness of the wearing course. The study also revealed that horizontal loads had little to no impact on shear stresses at depths below 1.6 in. Horizontal loads impacted shear stresses at the surface but were significant only when horizontal load coefficients were above 0.3.

A study similar to work described in this dissertation was recently conducted in Illinois (Ozer et al. 2012). That study used 3D FEM, with an APT experiment to analyze the effect of interface bonding for HMA overlays on PCC pavement. The work established a framework for developing an FE model that compared predicted responses to responses measured in the APT environment. The friction model utilized by Ozer et al. (2012) was previously developed by the same researcher (Ozer et al. 2008). The research of Ozer et al. significantly contributes to knowledge in applied to the study presented here, because it focused on HMA overlays on existing asphalt pavement.

2.7 Accelerated Pavement Testing

APT has been a viable means of characterizing the mechanistic response of pavement structures under loading since the 1930's, with significantly increased popularity and versatility in recent years. An APT is "the controlled application of a prototype wheel loading, at or above the

appropriate legal load limit to a prototype or actual, layered, structural pavement system to determine pavement response and performance under a controlled, accelerated accumulation of damage in a compressed time period" (Metcalf 1996). Hugo and Martin (2004) proposed a broader definition, such that APT is "…the controlled application of wheel loading to pavement structures for the purpose of simulating the effects of long-term in-service loading conditions in a compressed time period." A primary benefit of APT experiments is the ability to reduce time required to acquire meaningful data compared to in-service experiments. A variety of test tracks, in-situ test roads, and indoor facilities such as CISL are available to study various pavement features. Details of these facilities are presented in the Transportation Research Board (TRB) website administered by Dr. Stefan Romanoschi (https://sites.google.com/site/afd40web/home).

Results from several recent APT experiments were published at the 4th International Conference on Accelerated Pavement Testing in September 2012. Those experiments included a study in which a flexible pavement test road was built and tested in an APT to investigate their performance in order to validate a mechanistic-empirical pavement design. Various wheel loadings and tire pressures were applied with single- and dual-tire configurations. Measurements for permanent deformation were taken at the beginning and after 100,000 load repetitions. Deformation obtained from modeling was in good agreement with the observed permanent deformation (Saevarsdottir and Erlingsson 2012).

Ritter et al. (2012) described a German study in which researchers sought to understand long-term structural performance of flexible road pavements under heavy vehicle traffic. Impulse loading simulated heavy vehicle traffic on two test sections of varying lengths. Embedded sensors indicated mechanistic responses under loading. Transverse profile measurements indicated

accumulated permanent deformation. Increased elastic strain at the bottom of the asphalt base course and decreased bearing capacity were observed as loads accumulated (Ritter et al. 2012).

2.8 Summary

Asphalt pavements have been and continue to be critical elements of the U.S. transportation infrastructure. Pavement longevity has become a priority of owner-agencies and other stakeholders from economic and sustainability perspectives. Therefore, understanding mechanics of the asphalt interface layer and its importance to the life of the asphalt pavement structure is essential. Ongoing research of these mechanics continues with utilization of tools such as APT and FEM. FEM has proven to be a valuable tool for modeling, understanding, and predicting mechanistic responses and distresses in pavement structures. This study builds on previous works by connecting an FEM study to an APT experiment of HMA overlay on an existing HMA pavement structure.

Chapter 3. Accelerated Pavement Testing

3.1 Introduction

The APT portion of this study was conducted at CISL, the location at which APT studies have been conducted since 1998 (Hossain et al. 2012). Many tests in this facility have been used to conduct side-by-side comparisons of pavement processes and materials. This study adds to the work of an experiment designated CISL 17. CISL 17 is the 17th APT experiment conducted at CISL. The previous 16 experiments have been described by Hossain et al. (2012).

3.2 Civil Infrastructure Systems Laboratory

The CISL at Kansas State University has an APT facility capable of testing large-scale asphalt and concrete pavement sections under full-scale truck traffic loading (Figure 3.1). CISL has three pits for test section construction. Two of the pits are 20 ft. long, 16 ft. wide, and 6 ft. deep. The third pit is 20 ft. long, 14 ft. wide, and 6 ft. deep. The wheel assembly is belt-driven by a 20-HP electric motor, and hydraulic pressure controls the load (Lewis et al. 2008). Travel distance of the APT machine is approximately 20 feet, and the machine applies single or dual axle load with air-bag suspension.

The loading mechanism at CISL can be controlled with respect to hydraulic pressure, tire pressure, and test speed. In this test, a 20-kip single axle load with airbag suspension was applied on dual tires. Tire pressure was 90 psi and the longitudinal speed of the loading mechanism was 7 mph. The APT machine can wander laterally during passes, thereby simulating realistic trafficking on highways. A ±6 in. wander was applied in a truncated normal distribution with 676 repetitions for one wander cycle, as shown in Figure 3.2.

Figure 3.1 APT machine (Saghebfar 2014)

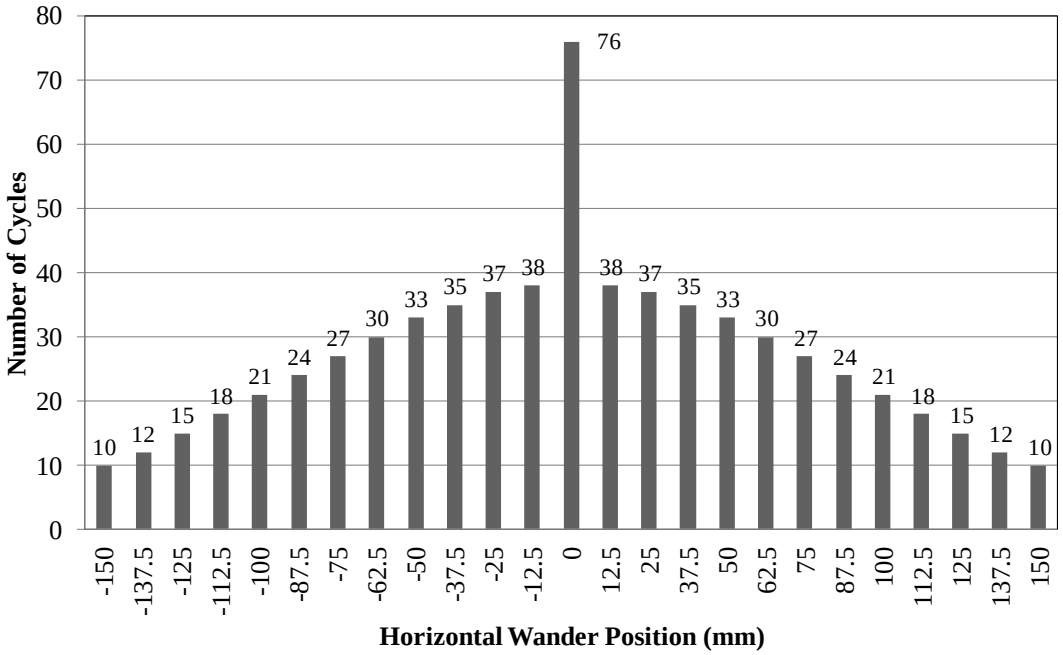

Figure 3.2 Truncated Wander of APT Machine at Kansas State University (Saghebafar 2014)

Test pavements are typically built in pits as layered structures that include soil subgrade, aggregate base, and HMA/PCC layers. Previous studies have analyzed permanent vertical deformation (rutting) of various HMA mixes. The APT related to this study was built as a mill-and-overlay of previous test sections. Material properties for previously-placed materials were assumed to be identical to properties reported in a previous study (Romanoschi et al. 2014).

3.3 Construction of CISL 17

Pavement test sections of CISL 17, were constructed as a mill-and-overlay of test sections of a previous CISL 14 experiment. Test sections for this study were laid out in a 20-ft long by 14-ft wide pit, divided into test sections of 6.66-ft by 7-ft., as shown in Figure 3.3. In the original experiment, the north lane (wheel path) was designated as MO-1, and the south lane (wheel path) was designated as MO-2 (Onyango 2009). The original CISL 14 experimental pavement section consisted of 4 in. of 0.5-in. (12.5 mm) Nominal Maximum Aggregate Size Superpave mix. This pavement was placed over 6 in. of AB-3 granular base over a subgrade of soil classified as A-7-6 clay to a total depth of 6 ft. Romanoschi et al. reported details and results of CISL 14 (Romanoschi et al. 2014). From the existing HMA layer, 2.0 in. were milled off the top and the surface was cleaned by compressed air. EBL was applied to half of the pit as tack coat over three sections at rates of 0.07, 0.22, and 0.16 gal/yd^2, as shown in Figure 3.3. SS-1HP was applied to the other half of the pit at rates of 0.013, 0.05, and 0.025 gal/yd^2. After milling, cleaning, and applying the tack coat, the SR-12.5A HMA overlay was placed (Mealiff 2015).

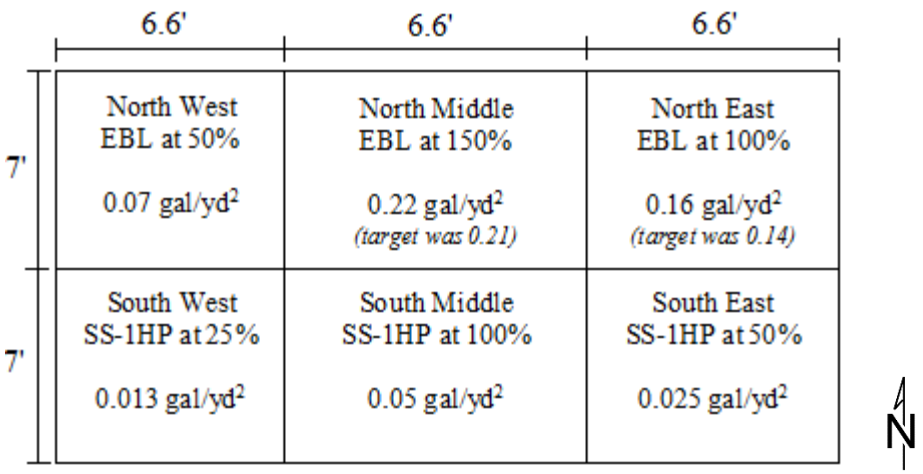

Figure 3.3 Layout of Test Sections for CISL 17

Mix properties for the new SR-12.5A overlay mixture are shown in Table 3.1. The mix satisfied all criteria specified by KDOT for SR-12.5A HMA mixture. The original HMA layer moduli backcalculated by Romanoschi et al. (2014) and shown in Table 3.2 have been used in this study. Other HMA mixture properties tested and used by Onyango (Onyango 2009) were used for MO-1 and MO-2 lanes. Saghebfar (2014) derived CISL 17 material properties used in this study and shown in Table 3.3.

Table 3.1 CISL 17 Overlay Mix Properties (Mealiff 2015)

Mix Properties	
% AC by Mass of Mix	5.63
% Aggregate by Mass of Mix	94.37
Sp. Gr. of AC	1.0315
Bulk Sp. Gr. of Aggregate	2.555
Theoretical Max. Sp. Gravity	2.430
Bulk Sp. Gr. of Mix	2.340
Effective Sp. Gr. of Aggregate	2.644
Absorbed Asphalt Content (%)	1.36
Effective Asphalt Content (%)	4.35
% VMA	13.6
% Air Voids	3.70
% VFA	73
Eff. Film Thickness (μm)	8.44
Dust/Binder Ratio	1.1

Table 3.2 Existing Layer Material Properties from CISL 14 (Onyango 2009; Romanoschi et al. 2014)

Parameter	MO-1	MO-2
HMA Elastic Modulus (ksi)	382.98	319.80
HMA Poisson's Ratio	0.35	0.35
HMA Creep Parameter A	4.50E-09	5.00E-09
n	0.5	0.6
m	-0.5	-0.5
Base Modulus (ksi)	125.63	116.23
Base Poisson's Ratio	0.4	0.4
Subgrade Modulus (ksi)	8.33	7.98
Subgrade Poisson's Ratio	0.45	0.45

Table 3.3 Material Properties for CISL 17 Overlay Mix (Saghebfar 2014)

Parameter	Unit	Value
HMA Elastic Modulus	ksi	300
HMA Poisson's ratio		0.35
HMA Creep A		3.50E-08
n		1.01
m		-0.8

3.4 Instrumentation

Before application of tack coat materials at their specified rates, strain gages were placed. For each test section, two H-bar strain gages from Tokyo Sokki Kenkyujo Co. Ltd. were placed in the longitudinal direction on top of the milled, existing HMA layer, as shown in Figure 3.4 (Mealiff 2015).

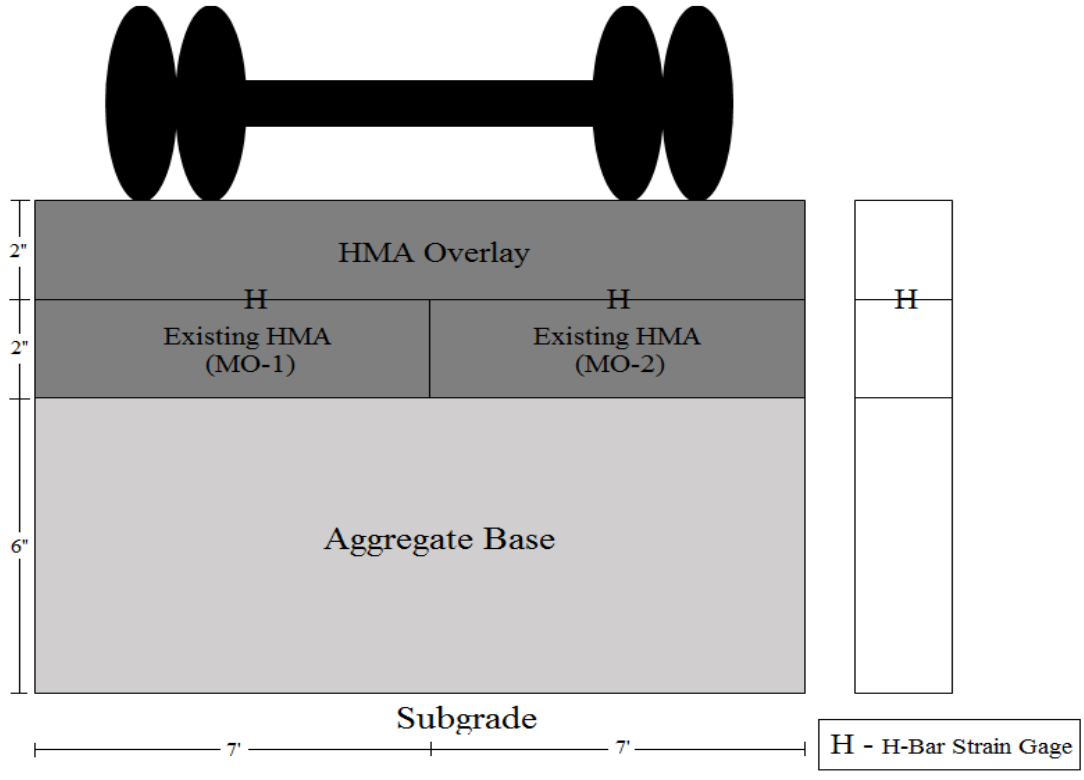

Figure 3.4 Schematic of Instrumentation Layout in Test Sections for CISL 17

The gages were attached with epoxy to aluminum bars and then stapled to the milled surface. Special care was taken to shield the wires to the gages from the hot paving mixture placement and compaction. Small quantities of loose HMA mixtures were placed over the gages and hand-compacted before the paver and roller ran. Initial gage length was 2.36 in. with resistance of 120 ± 0.5 Ω. The gage factor was 2.09 ± 1%, defined as follows (Saghebfar 2014):

$$GF = \frac{\frac{\Delta R}{R}}{\varepsilon} = \frac{\frac{\Delta \rho}{\rho}}{\varepsilon} + 1 + 2\nu \quad (1)$$

where
ε = strain,
ν = Poisson's ratio,
ρ = Resistivity,
ΔR = change in strain gage resistance, and
R = unstrained resistance of strain gage.

Data collected from these strain gages were used to calibrate the FE model of the APT experiment. After construction, only six of the 12 installed gages were operational. Gages in the Southwest and Southeast segments of the experiment failed during loading.

3.5 Loading

As mentioned, the APT assembly was equipped to apply rolling wheel loads from a single axle with a dual-tire configuration. Dual tires applied the 20-kip load on a single axle at a constant velocity of 7 mph across the entire wheel path of 20 ft. The single axle assembly was guided longitudinally along two beams, while the load was applied through a hydraulic pump, as shown in Figure 3.1. Because no acceleration was present over the length of the section, horizontal loads were neglected in the study. Location of the wheel path included a "wander" of up to 6 lateral inches in each direction. The number of passes in each location was distributed in a truncated normal pattern, as shown in Figure 3.2. This wander was programmed into the loading to provide

a loading cycle that more accurately represented in-service traffic loading in the wheel path of highway pavement. The 3D-FEM exceeded reasonable computing time for completion of this study in order to include the small lateral changes. Therefore, wander was ignored during the modeling process.

3.6 Strain Measurements

Longitudinal strain measurements in the longitudinal direction were taken with in-place strain gauges connected to the CISL data acquisition system via the LabView interface software. H-Bar strain gages from Tokyo Sokki Kenkyujo Co. were placed at the overlay/existing HMA interface, two in each test section. Similar instrumentation had been previously used (Webster 1992). Figure 3.5 shows the strain gages. Heat shrinking sheaths were used in which 22 American Wire Gauge (AWG) leads were connected to the gages (Saghebafar 2014). The sheathing and heavier gage lead were both measures taken to protect the instrumentation. In addition to strain measurements, rut depth measurements were taken periodically.

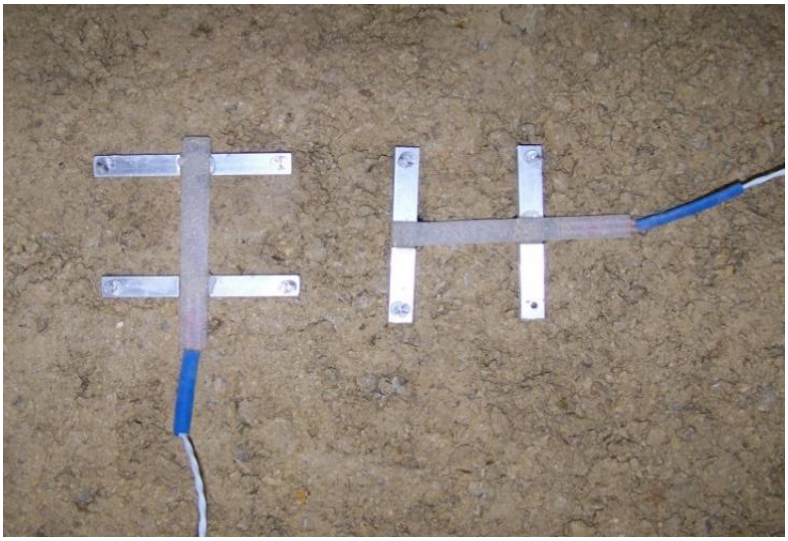

Figure 3.5 H-bar Strain Gages (Saghebafar 2014)

3.7 Rut Depth Measurement

In this study, transverse profiles were taken on all test sections at 0.5-in. intervals using a Chicago Dial Indicator digital gage shown in Figure 3.6. The gage, a Linear Variable Differential Transformer, produced a digital output that could be stored in a computer in spreadsheet format. Three fixed reference points at every 4.55 ft. of lane length were placed on the HMA outside the lanes, and measurements were taken with reference to these monuments (Lewis 2008). Average rut depth was taken over the middle 5 in. of wheel path with readings every 0.5 in.

Figure 3.6 Transverse Profiler at CISL (Saghebfar 2014)

3.8 Quality Control

Factors that impact interface bonding for in-service pavement structures include temperature, surface texture, moisture, debris, existing HMA material, and tack coat material and application rate (Mealiff 2015). The APT experiment in CISL 17 limited these variables to tack coat material and application rate. The APT loading apparatus was contained in a temperature-controlled unit and great care was taken during preparation and construction to prevent moisture or debris from affecting the tack coat interface (Mealiff 2015).

3.9 Laboratory Testing

Prior to APT test section construction, a laboratory experimental program was performed to characterize bonding of tack coat materials under the APT test (Mealiff 2015). Specimens were prepared by applying various tack coat materials and application rates on 6-in. diameter cored samples overlaid with an HMA layer, and compacted in a gyratory compactor. Then 2-in. diameter specimens were cored out of this composite core for testing in direct tension mode. A longitudinal displacement at a rate of 0.7-in./minute was used in the UTM. These tests provided a basis for tack material performance in the laboratory, and were compared to results of the APT experiment. Figure 3.7 presents output obtained in the laboratory test. As shown in the figure, peak stress and fracture energy were found for various combinations of tack coat material type and application rate. Fracture energy is the area under the load-displacement curve.

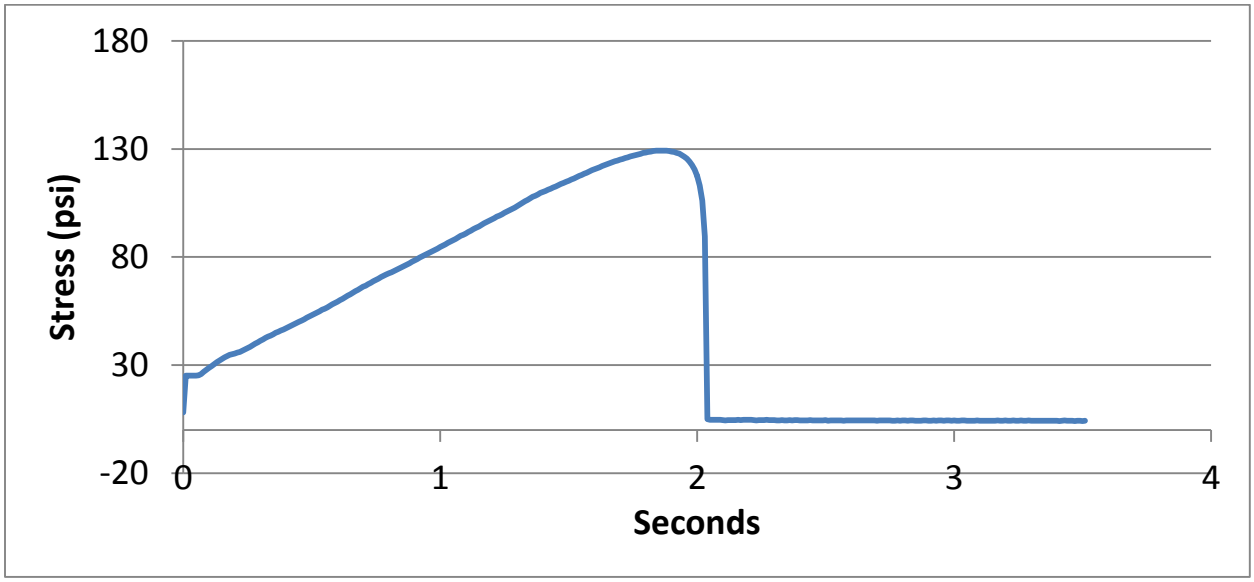

Figure 3.7 Stress versus Time for Typical Bond Test Sample Break (Mealiff 2015)

3.10 APT Results

Daniel Mealiff reported Results from the APT portion of the study (Mealiff 2015). Figures 3.8 and 3.9 summarize rut depth (south lane) and strain (both lanes) developments with load repetitions, respectively. These results were compared to FEM analysis predictions. Rut depth is included in this study because it was used as output from analyses described in Chapter 5. Results indicated a steady increase in rut depth with loading for test sections in the south lane. However, strain measurements for sections fluctuated with load, indicating change in stress condition of this interface layer with increased load repetitions.

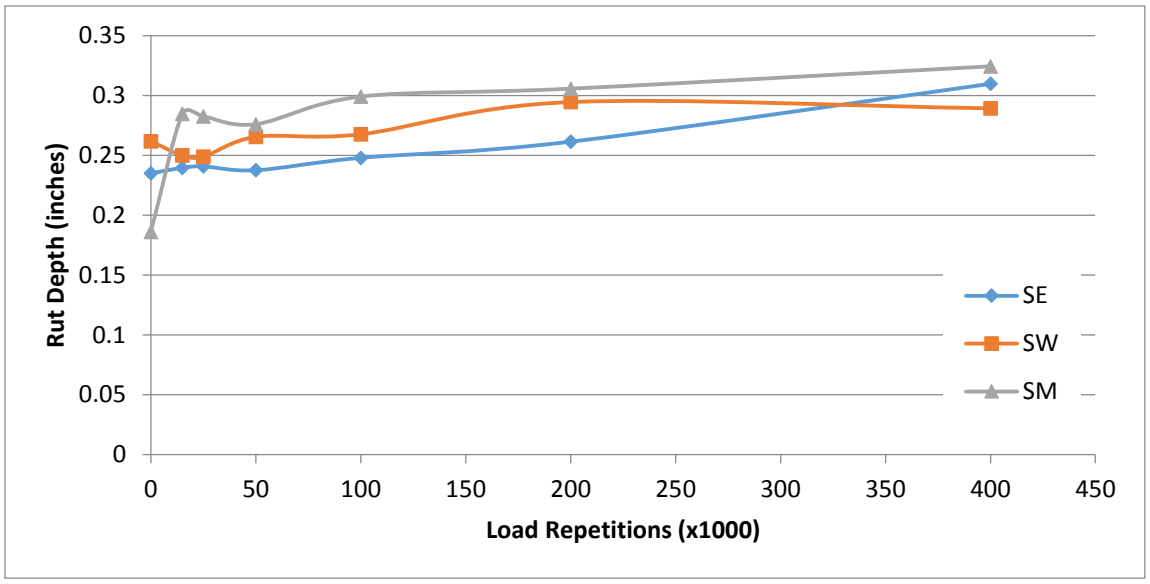

Figure 3.8 Typical Rut Depth versus Load Repetitions for CISL 17 Experiment (Mealiff 2015)

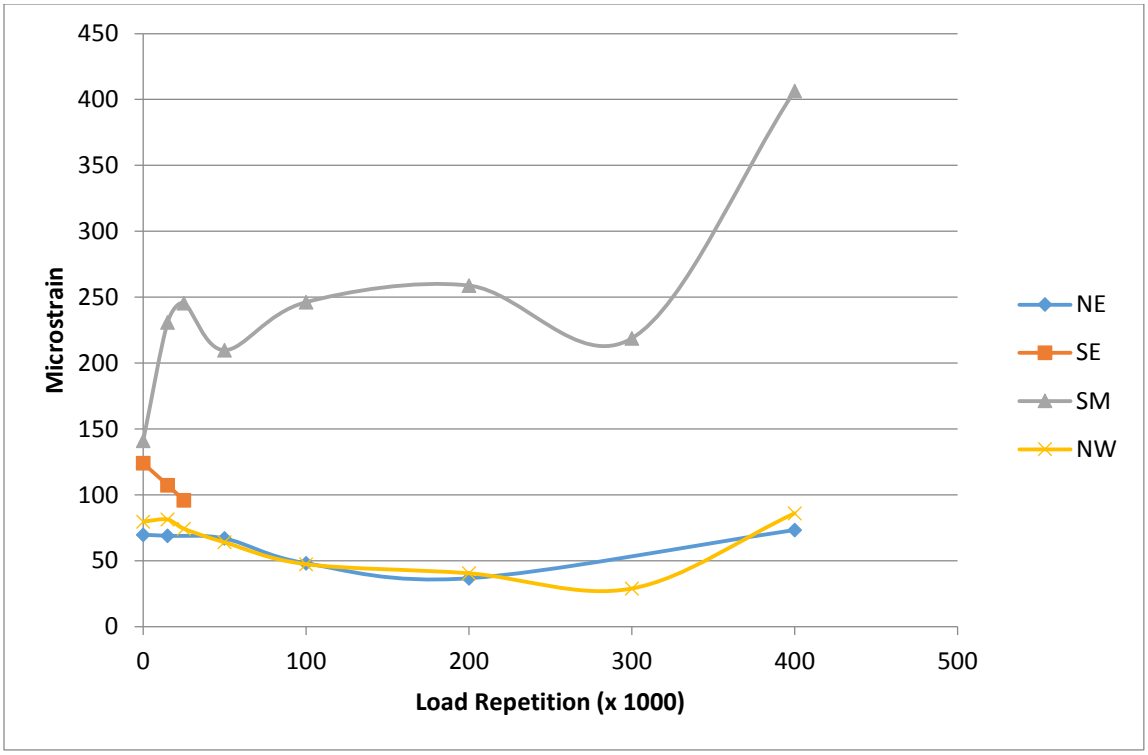

Figure 3.9 Typical Longitudinal Strain versus Load Repetitions for CISL 17 Experiment (Mealiff 2015)

Chapter 4 – Finite Element Modeling

4.1 Introduction

In order to fulfill study objectives, a 3D-FEM capable of predicting mechanistic pavement responses was created. The study focused on longitudinal strains at the interface layer when various tack coat material types and application rates were applied to bond the newly-placed HMA pavement to the underlying existing HMA pavement. The model was then calibrated using data from APT test sections at the CISL facility at Kansas State University. Therefore, geometry, boundary conditions, and material properties of the model were selected to match properties at the APT facility.

4.2 ABAQUS

ABAQUS software uses several modules to simulate physical interactions of loads and materials as defined by the user. Key user inputs include part and assembly geometry, material properties, loading, boundary conditions, and part interactions.

4.2.1 Part Module

The ABAQUS Part Module allows the user to create and edit 2D or 3D geometry of parts to be used in the analysis. Parts created in other modeling software may be imported to the Part Module. However, parts created by ABAQUS can be exported to other software. Figure 4.1 demonstrates the part module interface.

4.2.2 Property Module

In ABAQUS, users define material properties such as bulk and mechanical and thermal properties in the Property Module. Materials used in the sections may be defined as solid, shell, or beam elements. Material properties are assigned to the sections, and the sections are subsequently

assigned to model geometry, typically parts. Solid and shell elements may be further defined as homogeneous, composite, surface, or Eulerian.

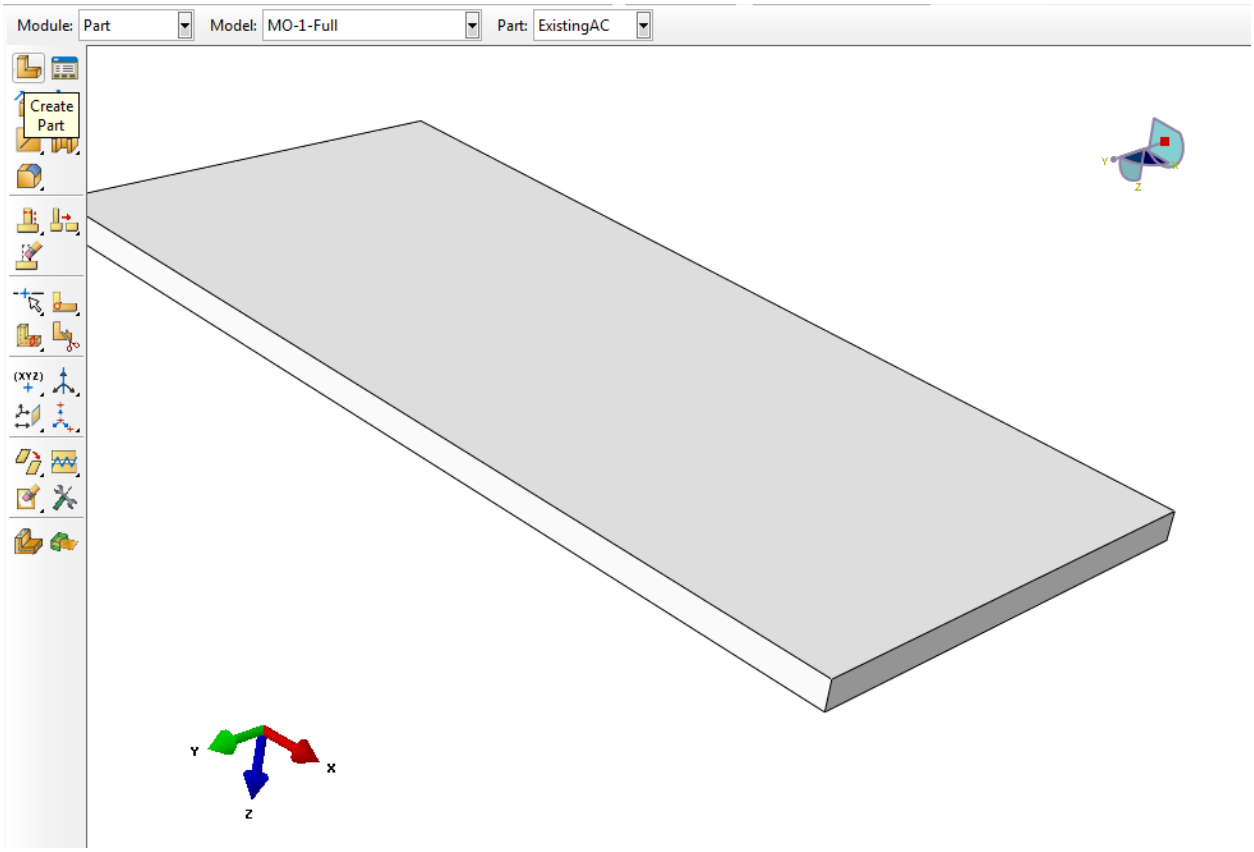

Figure 4.1. Part Creation in ABAQUS Part Module

4.2.3 Step and Load Modules

ABAQUS requires that users define a specific time step in order to define time-dependent changes in other modules. For this study, steps had to be created to load each pair of tire footprints on the pavement surface in the step module. A new time step was created for each movement of the simulated load to a new area on the surface. The number of steps used in each analysis was included as a portion of the study's sensitivity analysis. An increased number of steps more accurately modeled mechanics of APT and in-service pavement sections. The APT experiment was conducted with 400,000 load cycles. Modeling as many as ten load cycles required days of

computing. Use of a realistic number of loading cycles is not feasible because of the requirement of extensive, necessary computing resources.

The Load Module in ABAQUS allows the user to define several types of loads, their magnitude, direction, and location. This study used pressure loads applied to defined areas on the pavement surface to simulate physical tire pressure (resulting from the load) onto the pavement structure. Each load was created in a defined step. Consequently, every load was propagated in subsequent steps, which was undesirable for this study. Therefore, each load had to be deactivated in the step after the load was created. For each analysis, an additional step was defined in which all previous loads were deactivated, thereby allowing the user to analyze the pavement structure as it would appear after all loads were removed.

4.2.4 Interaction Module

The Interaction Module in ABAQUS gives the user the ability to govern how parts or surfaces interact. This module is often used to define how non-contacting surfaces will behave if they come into contact during analysis. In this study, the interaction module was critical component because it was initially used to "tie" together parts that existed below the existing HMA layer in the pavement structure. The "tied" interaction prevented displacement of nodes on one surface relative to adjacent nodes on the tied surface. Subsequent testing showed that removing the "tie" interaction and replacing it with a friction interaction did not change strain outputs obtained in this study.

The primary function of the interaction module for this study was the ability to define interaction behavior between surfaces in contact, such as normal, tangential, and cohesive behavior. The cohesive behavior model was readily applicable for modeling the tack coat interface. Cohesive interaction requires the definition of two surfaces but eliminates the need to create

cohesive elements in analysis between the overlay and existing HMA layers. This interaction is recommended in order to model delamination at interfaces in terms of traction versus separation (ABAQUS 2011).

Various stiffness or reaction modulus values to characterize an interface were used in this study. These values fell in the range of values found experimentally by Romanoschi and Metcalf (2001). As mentioned, the reaction modulus indicates the relationship between shear strain and shear displacement. Reaction moduli were applied in an isotropic manner for this study. Figure 4.2 shows the interaction property dialog in the ABAQUS software in which interaction inputs were made.

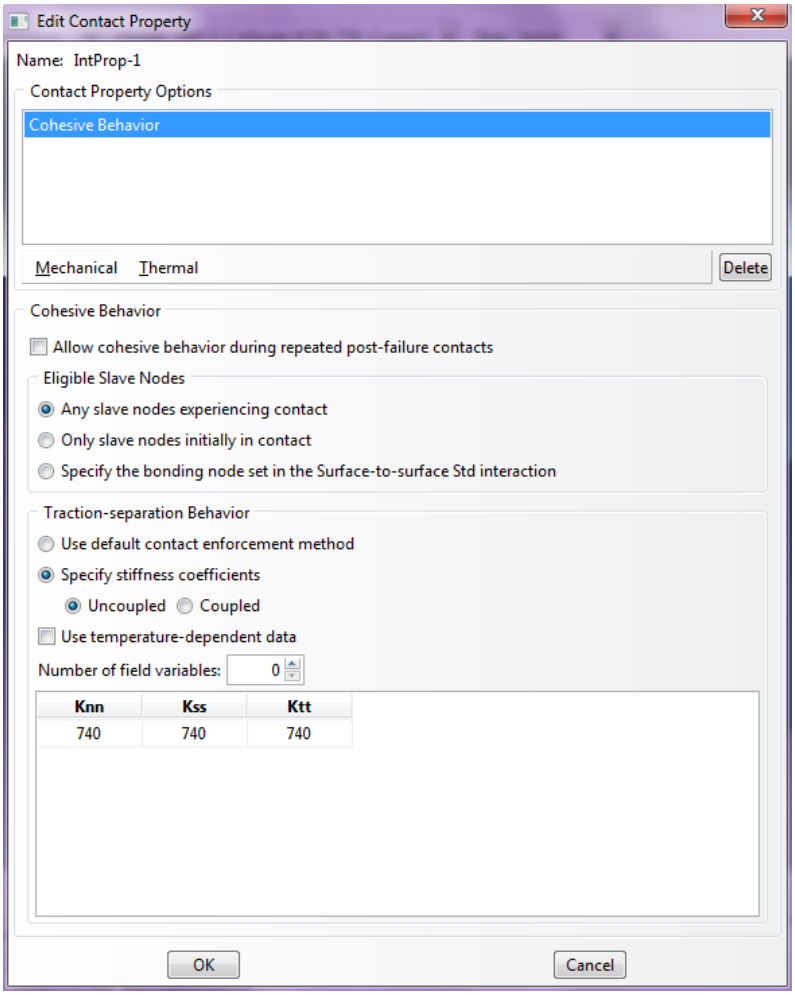

Figure 4.2 Interaction Property Dialog Box

4.2.5 Job Module

Analysis began after creation of an appropriate model geometry that included parts, materials, steps, loads, boundary conditions, and interactions to mimic those of the CISL 17 experiment. In ABAQUS software, FEM analysis occurs in the Job Module. Jobs specifically perform the analysis described in a particular model. Each job must be assigned a model to analyze. The job performed the analysis based on previously described inputs and returns with outputs as designated by the user in the Field Output Request and History Output Request fields of the model. In this study, only total strain and total displacements were requested as Field Output Requests.

4.2.6 Visualization Module

Post-processing in ABAQUS occurs in the visualization module in which the user can analyze outputs as requested in the job module. Deformed and non-deformed shapes are available for viewing at any step and for any output previously requested. In addition to using color-coded legends for output values, the user may use several probing tools. The query tool is useful for determining values at specific nodes on the model geometry. Results of these queries are easily saved as text files for future analysis. Figures 4.3 through 4.6 illustrate examples of strain and deformation visualizations under loading and after all loads have been removed.

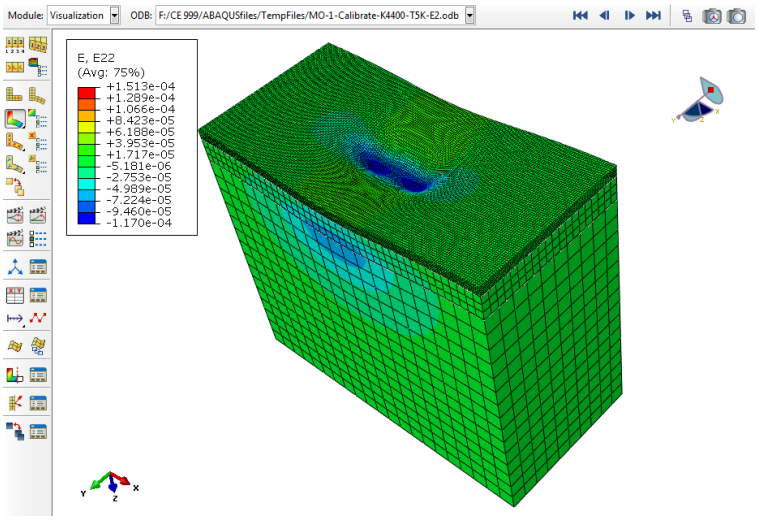

Figure 4.3 Visualization of Longitudinal Strain under Loading

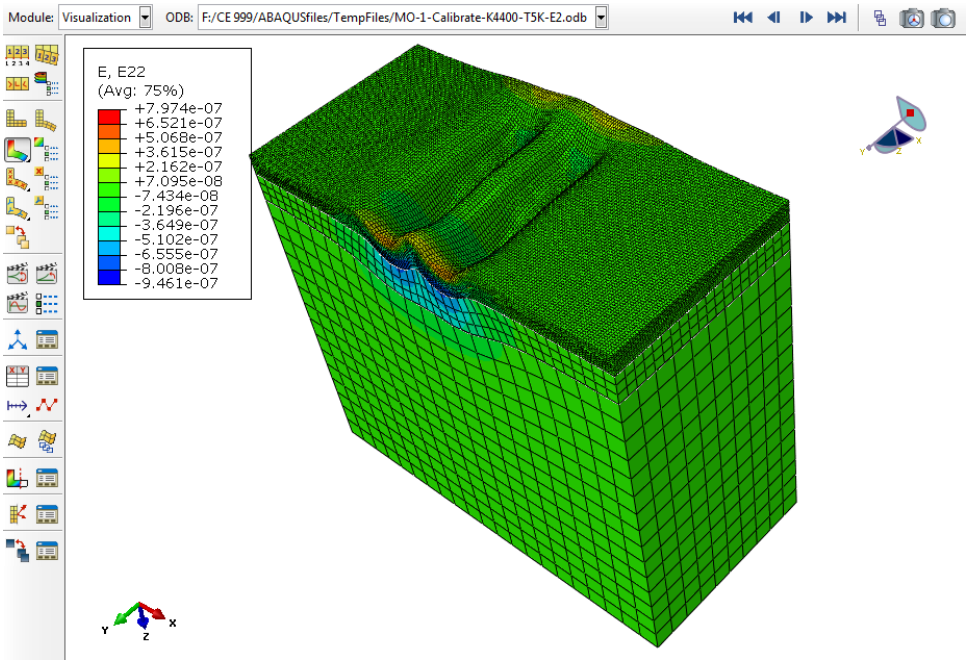

Figure 4.4 Visualization of Longitudinal Strain After Loading

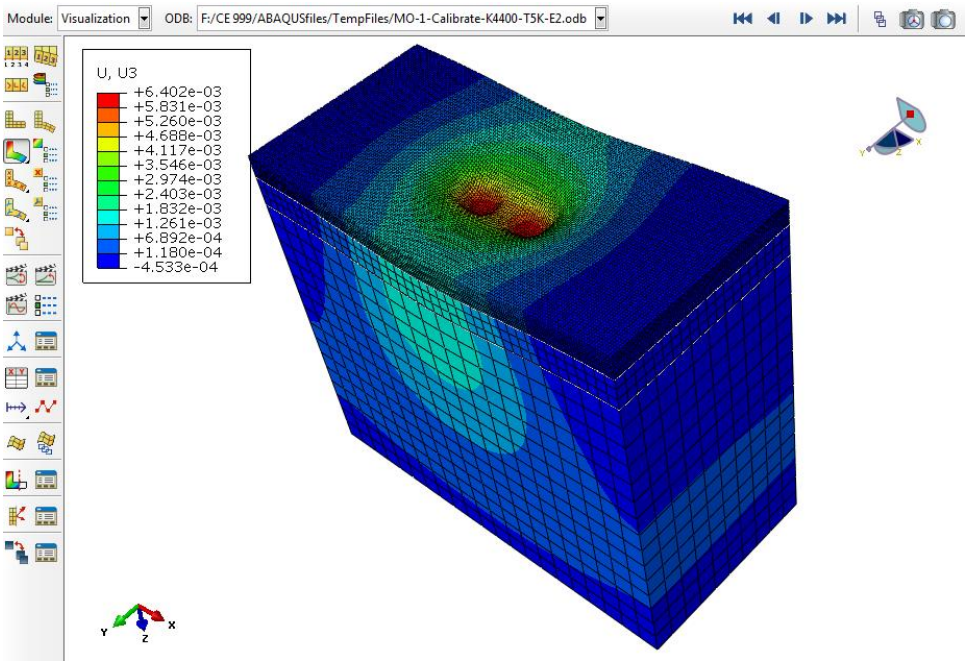

Figure 4.5 Visualization of Vertical Displacement under Loading

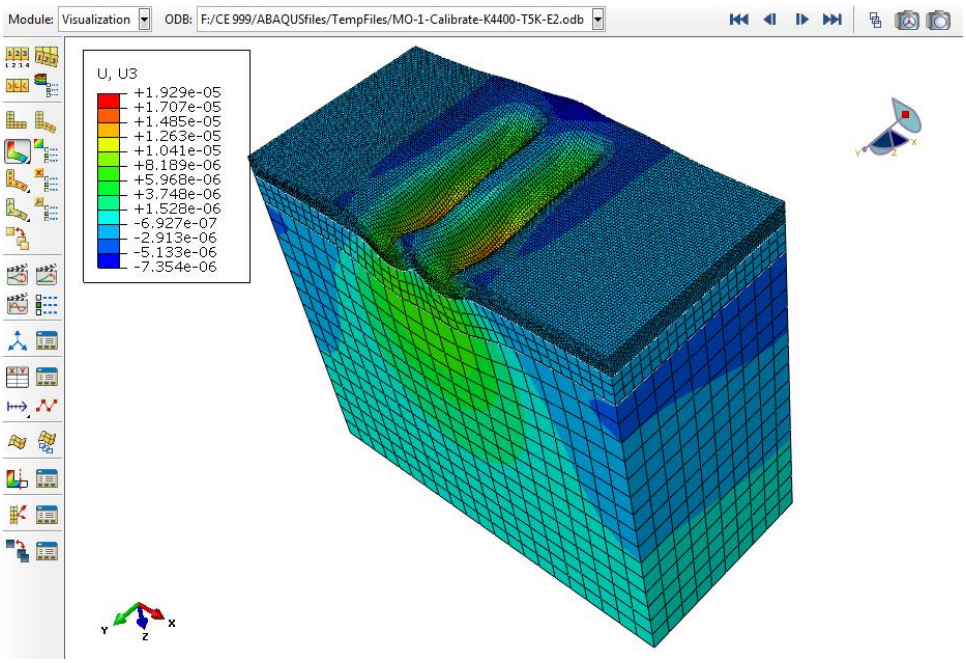

Figure 4.6 Visualization of Vertical Displacement after Loading

4.3 Model Geometry

The modeled 3D pavement test section had a width equal to the width of the lane on the test section of the APT facility: 84 inches (one-half of 14-ft total pit width). The test section's length in the longitudinal direction, or the direction of travel, was 40 inches. This dimension is 40 in., and represented a portion of the section that was half that of the 80-in. long APT test section. Symmetrical boundary conditions in the longitudinal direction were used to reduce the length of the model, and errors or concentrations due to proximity to test pit walls at the ends of each section were ignored. This 40 in. length was chosen in order to reduce model complexity and computing time. Sensitivity analysis was completed by varying these model dimensions, and depth of each layer corresponding to layer thickness in the test section was recorded. New HMA overlays were approximately 2 in. over 4 in. of existing HMA pavement. In each test section, HMA layers were placed over 6 in. of granular base and soil subgrade. The total depth of each complete section was 72 in. (6 ft.), the depth of pits constructed at the CISL facility.

The model created for this study was comprised of C3D8R elements. This commonly used element is an 8-node, linear block with reduced integration. The element name identifies its key characteristics. For example, the letter 'C' names the element as a continuum element. Other element types include shells, beams, and membranes. Continuum type elements work well for solids with shapes that do not lend itself to other named types. The second portion of the element name, '3D', identifies the element as a three-dimensional element. The number '8' indicates the number of nodes in the element. The chosen 8-node element takes the shape of a rectangular solid which lends itself well to the pavement structure geometry analyzed in this study. Finally, 'R' indicates reduced integration. Almost all elements in an explicit code use reduced integration in order to reduce computational load. ABAQUS literature recommends use of quadrilateral and hexahedral elements because they provide equivalent accuracy at less computational cost than the more geometrically versatile tetrahedral elements (ABAQUS 2011).

4.4 Boundary Conditions

Boundary conditions define known quantities in any solution variable (ABAQUS 2011). For this analysis, zero-valued boundary conditions for displacements and rotations of the pavement structure had to be defined. The bottom face of the soil subgrade was set as a fixed boundary because this boundary is far from the loaded surface and relatively rigid, resting on a reinforced concrete base. The left edge of the test section, where the pavement structure was contained by a reinforced concrete wall, was fixed with respect to translation in the transverse direction (x-axis). Nodes on the left edge of the model had 5 degrees of freedom and only x-direction translation was zero (U1 = 0). On the right edge of the model, faces were given x-symmetry boundary condition to represent the presence of nearly identical, adjacent pavement structures in the same pit. The application of this symmetry boundary condition is shown in Figure 4.7. Analysis software treats

these faces as though identical analysis tools, including parts, loads, and boundary conditions, were mirrored about the symmetry boundary. In the direction of travel, the front and back faces were bound by symmetry in the longitudinal direction (y-axis). This symmetry caused the model to be viewed as a thinner "cut" of an infinitely long pavement structure. One benefit of this boundary condition was to allow modeling of a smaller section, thereby reducing computing time. However, this boundary condition was only applicable when measurements were taken at locations far from the east and west walls of the test pit.

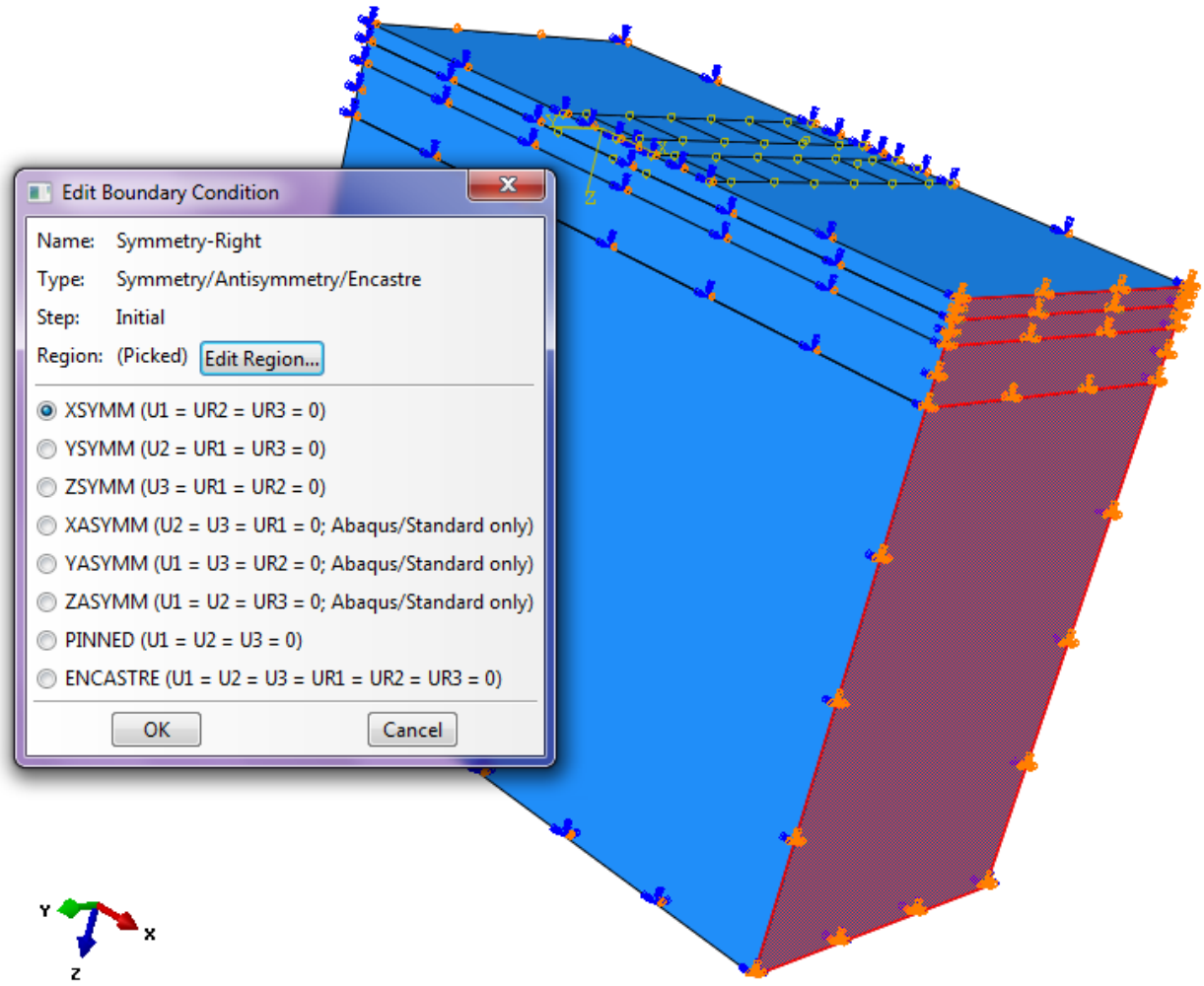

Figure 4.7 Application of Symmetry Boundary Condition

4.5 Loading

Repeated loading of the single axle, dual-tire assembly was difficult to simulate on the test section. Several approaches, such as applied pressure on circular, semi-circular, and rectangular areas, have been discussed throughout the literature. Other approaches deconstruct these shapes into smaller areas to more closely resemble the pattern of tire tread in contact with the pavement surface. However, modeling the tire tread in such detail is computationally costly, and the rolling movement complicates simulation of tire pressure loads. This study used uniform pressure applied to rectangular areas with dimensions approximating dimensions of the dual-tire contact area. This loading concept, in addition to uniform pressure over the entire length of the wheel path, has been successfully used in previous studies. The entire-path loading approach was evaluated in the sensitivity analysis portion of this study and found to be adequate for evaluating vertical displacements, but unsuitable for estimating strains at the layer interface.

The load was applied to the rectangular area for 0.05 sec. time, equal to the time required for the tire to move a distance equal to the length of the rectangle. This time was derived from the speed of the axle (7 mph) during the APT experiment. The load was then moved to an equal, adjacent rectangular area in the longitudinal direction for an equal length of time. This process was repeated until the load moved across the test section. To simulate repeated passes of the wheel load, the applied time was multiplied by the number of passes. For example, in order to simulate 100,000 load cycles, each rectangular area was loaded for 5,000 seconds. This method was significantly more efficient than creating new steps for each pass of the applied load. Two wheel paths were loaded simultaneously. Although the APT performed at the CISL facility included wheel-path "wander," the simulated wheel paths remained constant in this study. Modeling small horizontal changes in wheel paths that comprise real-world phenomenon, or "wander," would be

a taxing exercise unessential for this analysis. Because the APT load moved across the test section at constant velocity, no horizontal loads were modeled in the study. Figure 4.8 shows the model and its basic geometry. Wheel paths and uniform pressure loading on rectangular areas are also illustrated.

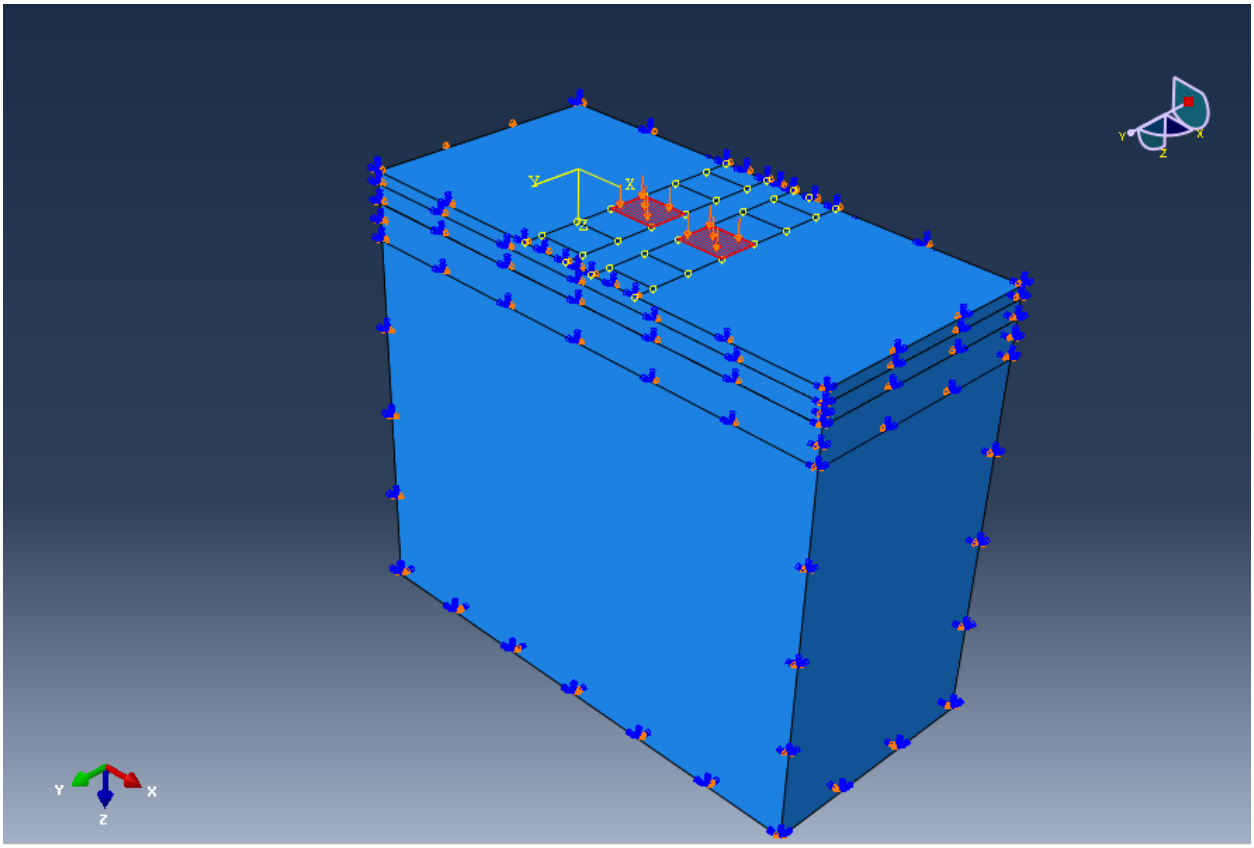

Figure 4.8 3D-FEM Geometry and Loading

4.6 Material Properties and Constitutive Models

Each material represented in the 3D-FEM was solid, homogeneous, and isotropic. Granular base and soil subgrade materials were modeled as elastic materials. However, this selection ignored the plastic behavior of each material and was made based on their distance from the investigated interface. Onyango (2009) found this method to be reliable for rutting prediction, but plastic responses in these layers may affect strains observed in the interface layer.

Asphalt materials, existing and overlay, must be modeled to capture their viscoplastic behavior by including their time-hardening creep parameters. These parameters were obtained from laboratory tests performed for previous studies (Saghebfar 2014). Creep is the time-dependent behavior of a solid material to continue to deform under a constant stress less than the yield stress of the material. Creep occurs in three stages: primary, secondary, and tertiary. Creep strain occurs rapidly in the first stage, is slowed by strain hardening in the second phase, and increases speed again in the third stage, often accompanied by necking, until failure. These stages are demonstrated in Figure 4.9.

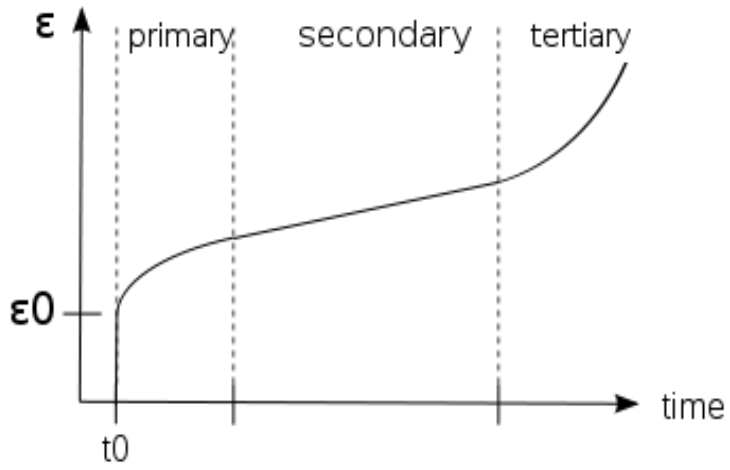

Figure 4.9 Creep Stages (ABAQUS 2011)

Viscoplastic strain in HMA is given by the following equation (Hua and White 2002):

$$\epsilon^{vp} = A'\sigma^{n}t^{m+1} \quad (2)$$

where *A*, *m*, and *n* are creep parameters determined by laboratory testing.

In the ABAQUS software, creep strain is given by Equation 3:

$$\dot{\bar{\varepsilon}}^{cr} = A\bar{\sigma}^{n}t^{m} \quad (3)$$

This equation is a time-hardening version of the power-law creep model. Creep strain is a function of deviator stress (σ) and time (t). The constants *A* and *n* must be positive, and the value of *m* must be greater than -1 and less than or equal to zero.

Laboratory tests were performed to obtain *A*, *m*, and *n* constants for the HMA overlay material used in CISL 17. Loose HMA material was collected from the paving site and compacted into 6-in. diameter, 6-in. tall cylinders in a Superpave gyratory compactor. From these cylinders, 4-in. diameter cores were taken for creep testing. The cores were cyclically loaded at room temperature with a deviator stress equal to 30 psi (Saghebfar 2014). The creep test setup and typical output chart are shown in Figures 4.10 and 4.11. Creep parameters were derived through statistical analysis using this output chart.

Figure 4.10 Creep Test on HMA Samples (Saghebfar 2014)

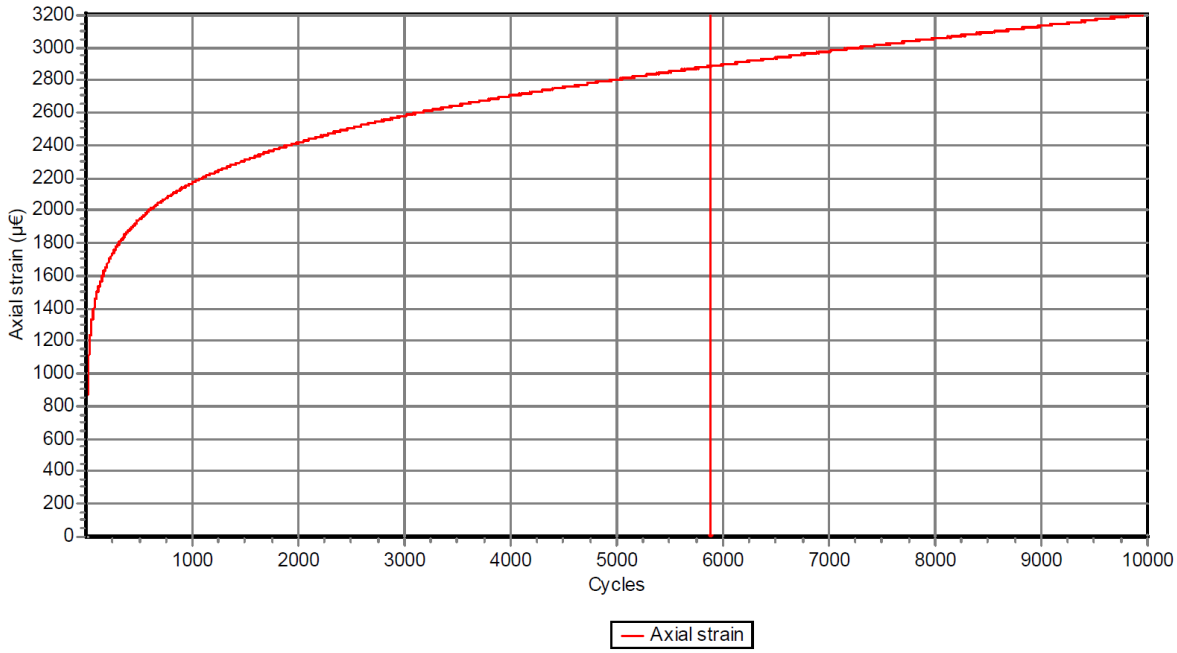

Figure 4.11 Typical Creep Test Results (Saghebfar 2014)

Back-calculation software was used to find the elastic modulus of each layer from falling weight deflectometer (FWD) data. Properties for the overlay material, granular base, and soil subgrade were obtained from previous and concurrent studies that used the same material. Similar data were used for the existing HMA layer, and laboratory tests were conducted to determine its relevant properties, including density, elastic modulus, and creep parameters. Material properties in Table 4.1 were used to model sections in the north and south lanes of this experiment.

Elastic deformations in this study are subject to the generalized Hooke's Law,

$$\varepsilon_i = \frac{\sigma_i}{E} - \nu\frac{\sigma_j}{E} - \nu\frac{\sigma_k}{E} \quad (4)$$

where

ε_i = strain in the i-direction,
σ_i = normal stress in the i-direction,
σ_j = normal stress in the j-direction,
σ_k = normal stress in the k-direction,
υ = Poisson's ratio, and
E = Young's modulus

Table 4.1 Material Properties Modeled by Lane 14 (Onyango 2009; Romanoschi et al. 2014; Saghebfar 2014)

Parameter	North Lane	South Lane
Existing HMA Elastic Modulus (ksi)	382.98	319.80
Existing HMA Poisson's Ration	0.35	0.35
Existing HMA Creep Parameters: A	4.50E-09	5.00E-09
n	0.5	0.6
m	-0.5	-0.5
Base Modulus (ksi)	125.63	116.23
Base Poisson's	0.4	0.4
Subgrade Modulus (ksi)	8.33	7.98
Subgrade Poisson's	0.45	0.45
Overlay Elastic Modulus (ksi)	300	300
Overlay Poisson's Ratio	0.35	0.35
Overlay Creep Parameters: A	3.50E-08	3.50E-08
n	1.01	1.01
m	-0.8	-0.8

4.7 Layer Interaction Properties

Several types of surface interactions are available in the ABAQUS software, including interactions labeled “tied” or “rough” that allow no relative movement between nodes on the surfaces of adjacent bodies. These interactions are used for layer interfaces away from the existing overlay HMA interface. Rough interaction is also used as a lower-bound comparison at the overlay interface. This study created interaction properties that closely follow the understood mechanics of tack coat interfaces. The characteristic reaction modulus, or “k-value,” proposed by Romanoschi and Metcalf (2001) and used in another study (Ozer et al. 2012) was similar to the reaction modulus in this study. This parameter was the key element in modeling the interaction at the interface of existing and overly HMA layers.

Model interactions modify the relative behavior of adjacent elements. Interactions are not comprised of additional elements and do not have volume or mass. Utilizing interactions to model

tack coat bonds has been successfully demonstrated (Ozer et al. 2012). ABAQUS also provides means to model cohesive elements with individual volume and mass, thereby differing from interaction properties. Those elements may provide an alternative method of modeling asphalt tack coat and should be evaluated as such in the future.

Ozer et al. (2008) presented a complex, user-defined interaction property to capture the multifaceted mechanics of tack coat interaction. Although the tack coat remained properly bonded throughout the CISL 17 experiment, the following equation relates interface stresses to displacements:

$$\begin{Bmatrix} \sigma_{nn} \\ \tau_{ns} \\ \tau_{nt} \end{Bmatrix} = \begin{bmatrix} k_{nn} & 0 & 0 \\ 0 & k_{ns} & 0 \\ 0 & 0 & k_{nt} \end{bmatrix} \times \begin{Bmatrix} \delta u_n \\ \delta u_s \\ \delta u_n \end{Bmatrix} \quad (5)$$

where

n, s, and t = normal (n), and tangential (s and t) coordinates,
σ_{nn} = normal traction,
τ_{ns} and τ_{nt} = tangential tractions,
k_{nn}, k_{ns} and k_{nt} = normal and tangential stiffnesses, and
δu_n, δu_s and δu_t = displacement jumps at the interface.

Within the ABAQUS model, an interaction property was created as cohesive behavior between the overlay and existing AC layer. Stiffness of cohesive interaction was the key variable in this study. Romanoschi experimentally found values ranging from 740 to 4,400 lb/in^3 using direct shear testing (Romanoschi 2001).

Chapter 5 – Results and Analysis

5.1 Predictive Model Results

The objective of this study was to develop a 3D-FEM that would accurately predict the mechanistic response of an HMA pavement structure for various interface bonding conditions. Specifically, the goal of this study was to use the FEM software, coupled with APT experimental data, to appropriately characterize the interface in terms of reaction modulus for various types and application rates of tack coat material. Previously discussed analysis in this study has focused solely on one test section. Varying model inputs on one model led to a more accurate model that can be used on other sections. Ultimately, these sections allowed a reaction modulus, or "k-value," to be assigned to each tack coat application. Once a k-value was assigned, models could be used to predict responses for loading beyond that were used in the CISL 17 APT experiment.

Each section was modeled based on cores taken from outside the wheel path of the CISL 17 experiment. The HMA overlay and existing layer thicknesses, determined from the cores, are given in Table 5.1 and duplicated in the modeled sections of this study.

Table 5.1 Section Pavement Thickness Revealed by Coring outside the Wheelpaths (Mealiff 2015)

NW (EBL 0.07 gal/yd^2)	NM (EBL 0.22 gal/yd^2)	NE (EBL 0.16 gal/yd^2)
2" top 3" base 5" total	2" top 2.25" base 4.25-4.5 total	1.75" top 3.5" base 5.25-5.75 total
SW (SS-1HP 0.013 gal/yd^2)	SM (SS-1HP 0.05 gal/yd^2)	SE (SS-1HP 0.025 gal/yd^2)
2" top 3.25" base 5.25" total	2" top 3" base 5-5.5" total	1.75" top 3.25" base 5" total

With each section uniquely defined for layer thickness and material properties, a series of analyses were done to observe the variation of longitudinal strain at the interface layer as the k-

value was varied. The strain of interest was the longitudinal strain, noted as E22 in the ABAQUS software for model orientation. Modeled values recorded and analyzed were at the top of the existing HMA layer directly below the applied loads. Results of those analyses are shown in Figures 5.1 and 5.2.

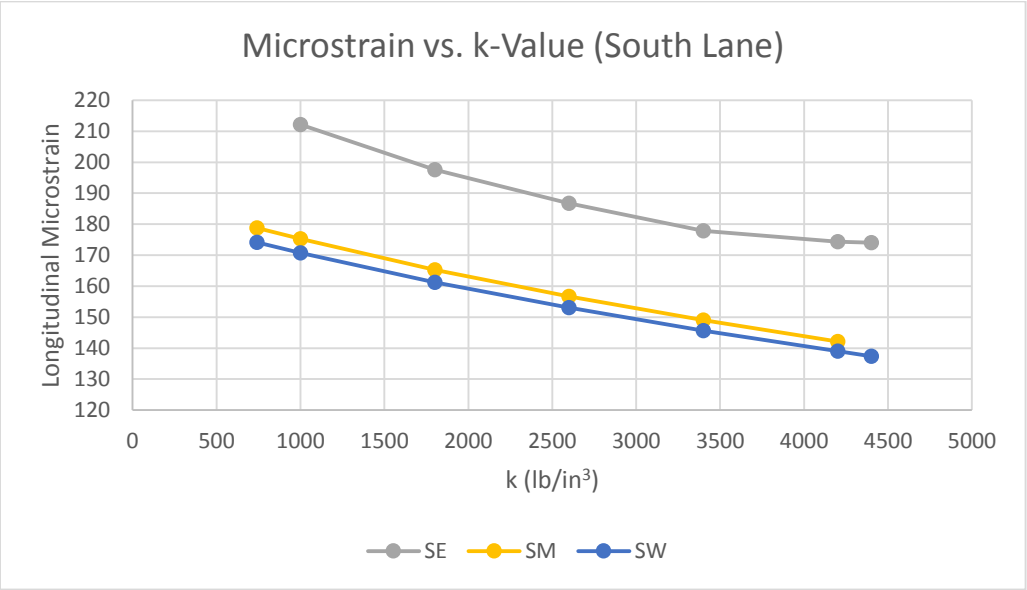

Figure 5.1 Microstrain versus k-value (south lane)

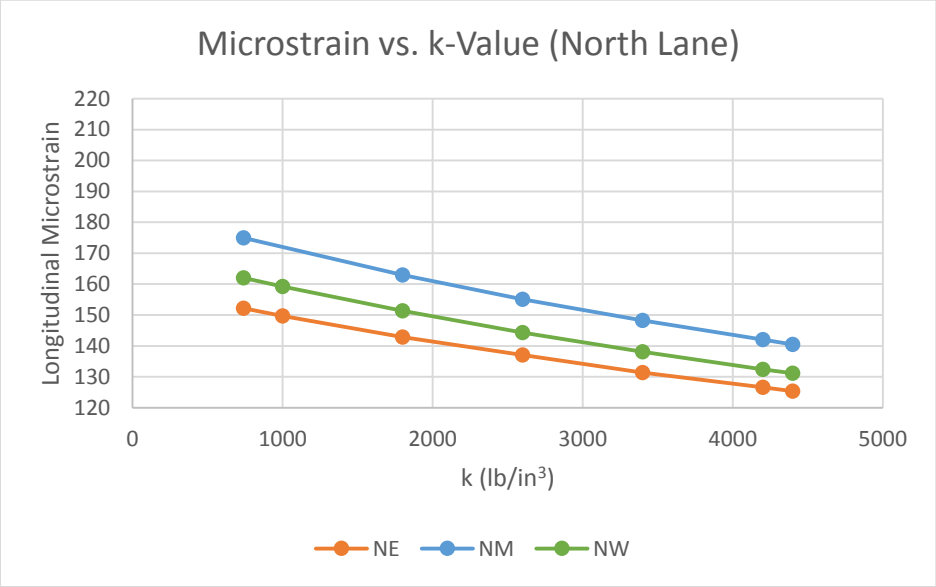

Figure 5.2 Microstrain versus k-value (north lane)

These figures show that, with available input data such as material properties, loading, and geometry, each section had a range of potential longitudinal strains depending on the reaction modulus, k, of the interface layer. These values are reasonable compared to strains measured under loading in the CISL 17 experiment (Figure 3.8). Predicted strain values for the northeast (NE) and northwest (NW) sections were slightly higher than strain values measured during the CISL 17 experiment. Additional FEM results are presented in Section 5.2.2, in which the reaction modulus was raised to values above 4,400 lb/in^3.

Predicted values for the south middle (SM) section closely matched values measured by the CISL 17 experiment. Model-predicted strain values for the southeast (SE) section were slightly higher than APT results throughout the range of k-values.

Table 5.2 Material Properties for Existing AC Layers (Onyango 2009 and Romanoschi et al. 2014)

Parameter	MO-1	MO-2
HMA Elastic (ksi)	382.98	319.80
HMA Poisson's Ratio	0.35	0.35
Creep Parameters: A	4.50E-09	5.00E-09
N	0.5	0.6
M	-0.5	-0.5
Base Modulus (ksi)	125.63	116.23
Base Poisson's Ratio	0.4	0.4
Subgrade Modulus (ksi)	8.33	7.98
Subgrade Poisson's Ratio	0.45	0.45

5.2 Calibration of 3D-FEM with APT Data

In this portion of analysis, results from the 3D-FEM were compared to those measured by the APT instrumentation, especially the relationship between measured and predicted strains at the overlay interface. This step allowed for modeling inputs such as material and interface properties to be manipulated in order to create a model that closely reflected measured results from the APT. Strain measurements were taken as part of the previously described CISL 17 experiment. Table 5.3 shows measured longitudinal strains (microstrain) derived from 30 peak values during the experiment for one wander cycle of APT (676 passes). Peak strain values occurred whenever the loading wheel passed closest to train gages in the wheel path (lane).

Table 5.3 Longitudinal Strain (Microstrain) during Loading (Mealiff 2015)

Passes (x1,000)	NE EBL 100%	SE SS-1HP 50%	SM SS-1HP 100%	NW EBL 50%
0	70	124	141	80
15	69	107	231	81
25		96	245	74
50	67		210	64
100	48		246	47
200	37		256	40
300			219	29
400	73		406	86

Notes: CISL 17 did not return strain values in the EBL 100% section at 25,000 and 300,000 load repetitions; Strain gages failed before 50,000 load repetitions in the SS-1HP 50% section.

Vertical deformation at the surface was used in the first portion of this study to analyze model sensitivity to several factors. Those values were useful for identifying trends in mechanistic responses of the model. Predicted values for vertical deformation were not, however, calibrated to APT results of CISL 17. Although Drucker-Prager material properties of the granular base and subgrade layers were not necessary in the modeling to capture the strain response at the interface

of the overlay and existing HMA layers, omission of those properties resulted in predicted vertical deformation many times smaller than measured values.

5.2.1 Longitudinal Strain Under Loading

During sensitivity analysis of this study, strains were calculated during a time step after all loads were applied and subsequently removed. Strain values measured in the CISL 17 experiment were substantially larger than values obtained during sensitivity analysis. Predicted longitudinal, strain values were on the order of 10^{-7}, while values in Table 5.3 were on the order of 10^{-4}. An accurate comparison could only be made when strain values obtained in the CISL 17 APT experiment were compared to model-predicted strains during loading time steps, specifically strain values while the load was near the center of the model section and away from the boundaries.

These strains could be viewed in the ABAQUS Visualization Module after the "Job" was completed. The "Overlay" part instance was removed from view to enable the user to directly view the top surface of the existing AC layer, as shown in Figure 5.3.

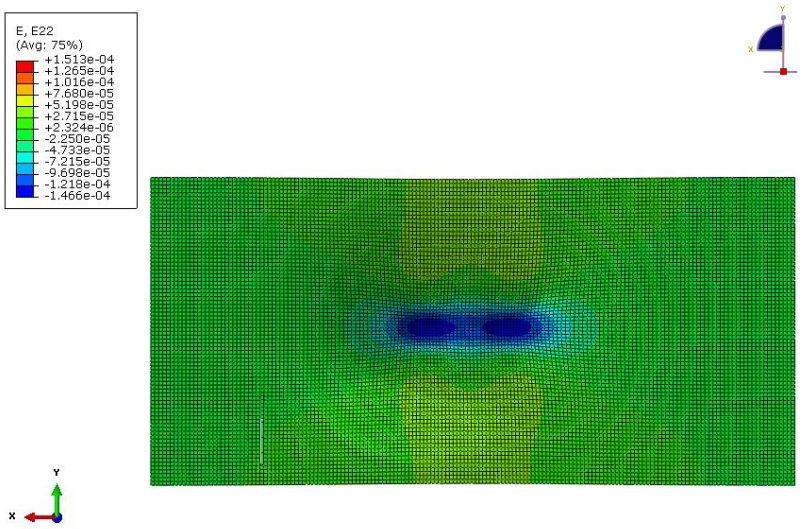

Figure 5.3. Visualization of Longitudinal Strain on Existing HMA Layer

Longitudinal strain predicted by the model when a load was applied at the pavement surface was not affected by loading time. For models that included repetitive load cycles, predicted

strain was constant for each load cycle and remained constant regardless of the number of cycles, as shown in Figure 5.4. These strains varied with mesh size and stiffness of the existing overlay HMA layer interface (Figure 5.5)

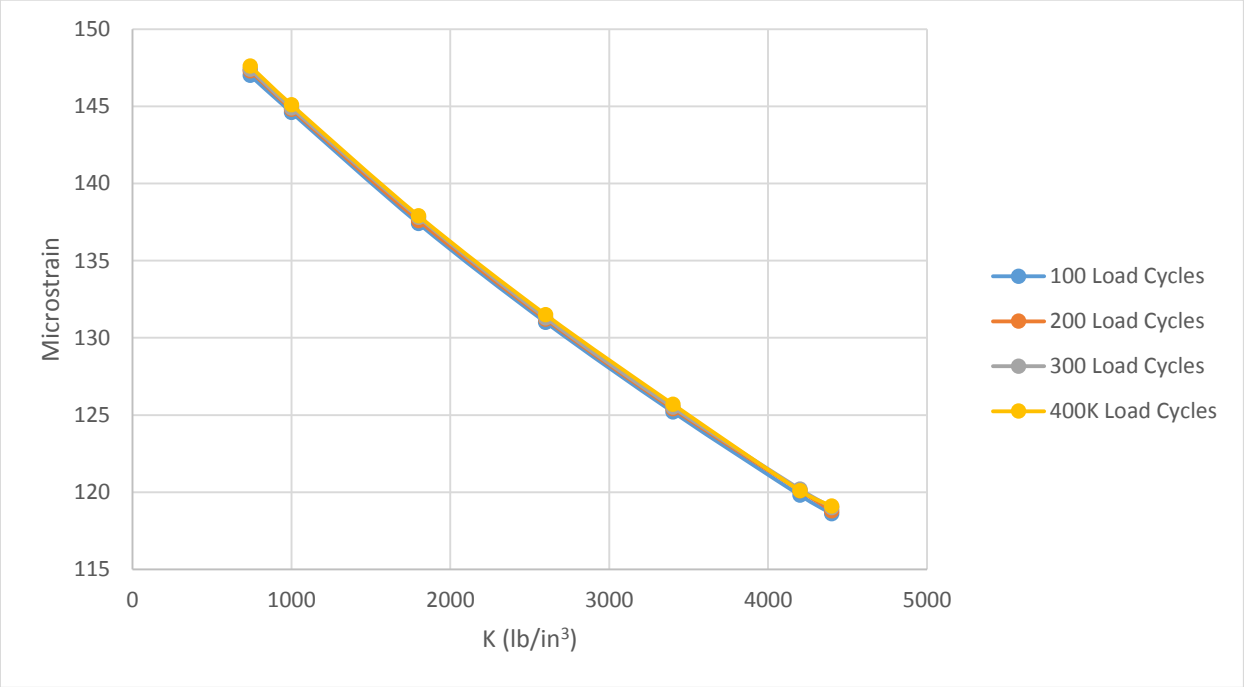

Figure 5.4 Variation of Microstrain versus Interface k-value for Increasing Load Cycles

Figures 5.4 and 5.5 show that predicted longitudinal strain at the interface of the overlay and existing HMA layer varied significantly with interface stiffness, or k-value, assigned to define the cohesive property of the interface. However, predicted longitudinal strain only varied slightly with the number of load cycles applied. These load cycles were modeled simply with a varied time quantity attached to one cycle of loading across the pavement structure model.

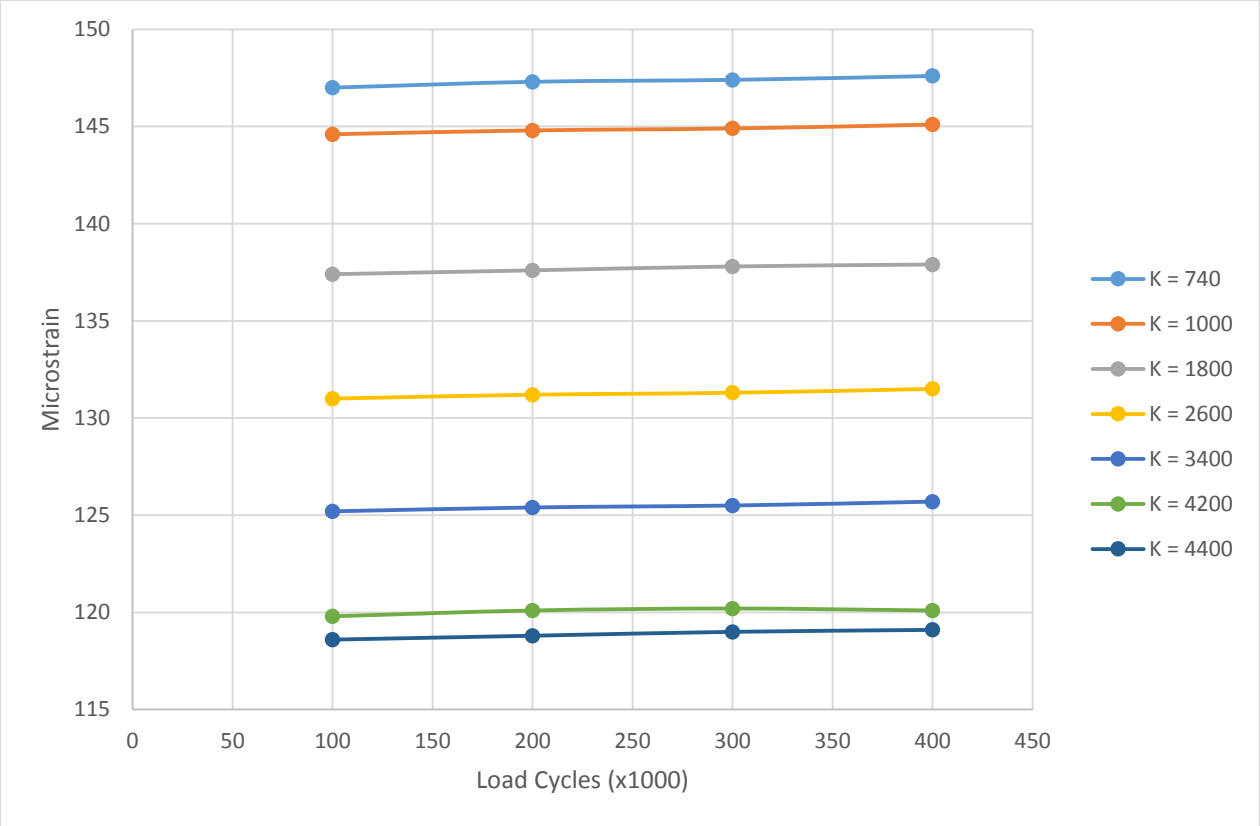

Figure 5.5 Variation of Microstrain versus Number of Applied Load Cycles for Varying Interface Stiffness

In the north lane, Mealiff (2015) collected multiple data points in the NE and NW end sections. Microstrains measured under loading in those two sections were nearly linear with load repetitions, and the range of measured microstrains in those two sections was very small. For the NE section, a majority of measured microstrain values were found to be between 67 and 73. Similarly, on the NW section, measured strains were primarily between 74 and 86 microstrain. These values were similar to values predicted in the ABAQUS model when the interaction property defining the friction between the overlay and the existing HMA layer was set to a k-value near 4,400 lb/in^3 which represents the largest stiffness found by Romanoschi and Metcalf (2001). However, that value is not necessarily the physical limit of bonding value in the direct shear test.

The SM section also had several strain data points in the CISL 17 experiment. These measurements showed a wide variation from the beginning to the end of loading. However, the first and last data points in this set appeared to be outliers. The portion of this data set between these terminal points was within a much smaller range, from approximately 220 to 260 microstrain. Linearity of these strain values appeared to support FEM models developed in this study.

5.2.2 Calibration by Overlay Elastic Modulus

Further attempt was made to make model results more closely reflect APT results by modifying the elastic modulus of the overlay material. The original value derived by Saghebfar (2014), used throughout the models of this study, was 300,000 psi. If that elastic modulus varied from 250,000 to 400,000 psi, longitudinal strain at the interface varied a few microstrains, as shown in Figure 5.6. Although this material property provides some contribution to the interface response, the contribution is not substantial.

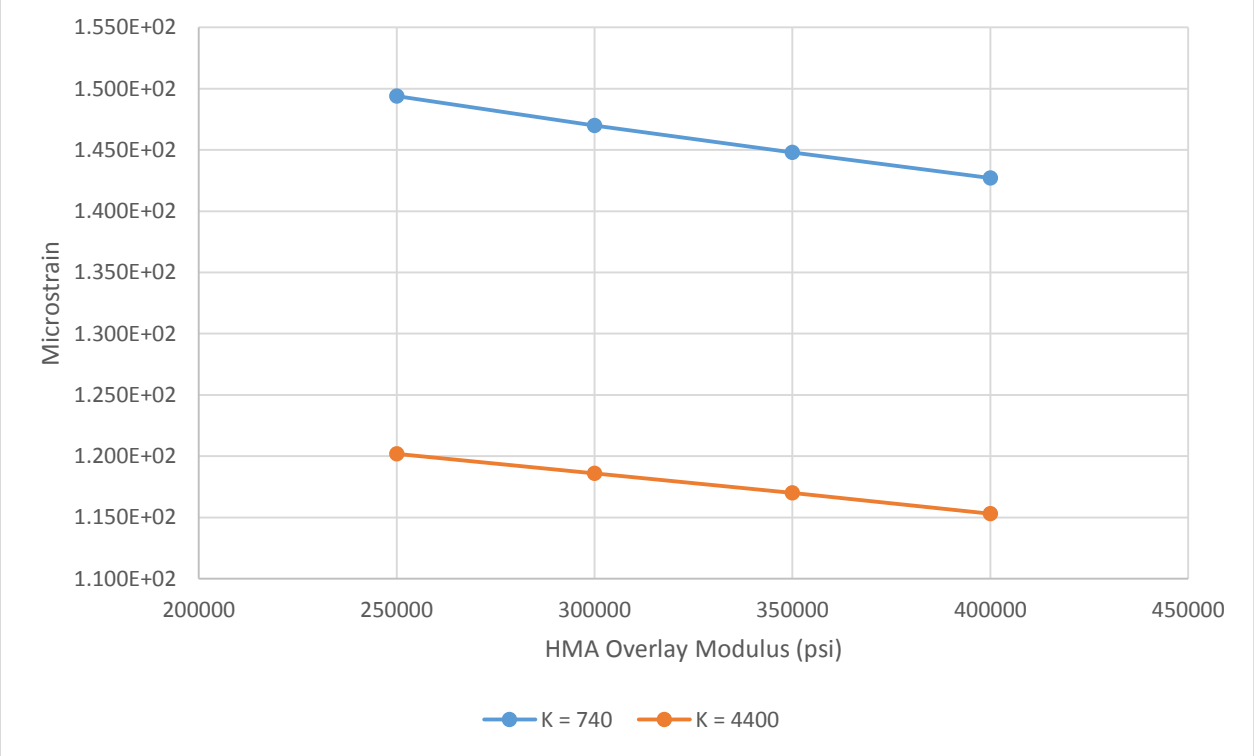

Figure 5.6 Interface Longitudinal Strain (Microstrain) versus Overlay Elastic Modulus

Figure 5.7 shows the change in longitudinal strains predicted by the FEM, as reaction moduli is increased well above 4,400 lb/in^3. This value was previously used as an upper bound of this analysis because it corresponds to the upper limit of the values obtained by Romanoschi (2001) from direct shear testing. While these calculated longitudinal strain values continually move toward smaller values, they are still not approaching the much smaller strain values measured in the CISL 17 APT experiment (Mealiff 2015). Beyond 4,400 lb/in^3, strain values continue in a very linear regression. Linear regression analysis was, therefore, applied to the results in Figure 5.1 and 5.2. The relevant resulting equations are as follows:

NE (EBL 100%): $\varepsilon = -0.0073(k) + 156.73$ ($R^2 = 0.9957$) (6)

NW (EBL 50%): $\varepsilon = -0.0084(k) + 167.26$ ($R^2 = 0.9955$) (7)

SE (SS-1HP 50%): $\varepsilon = -0.011(k) + 218.99$ ($R^2 = 0.9471$) (8)

SM (SS-1HP 100%): $\varepsilon = -0.0107(k) + 185.6$ ($R^2 = 0.9946$) (9)

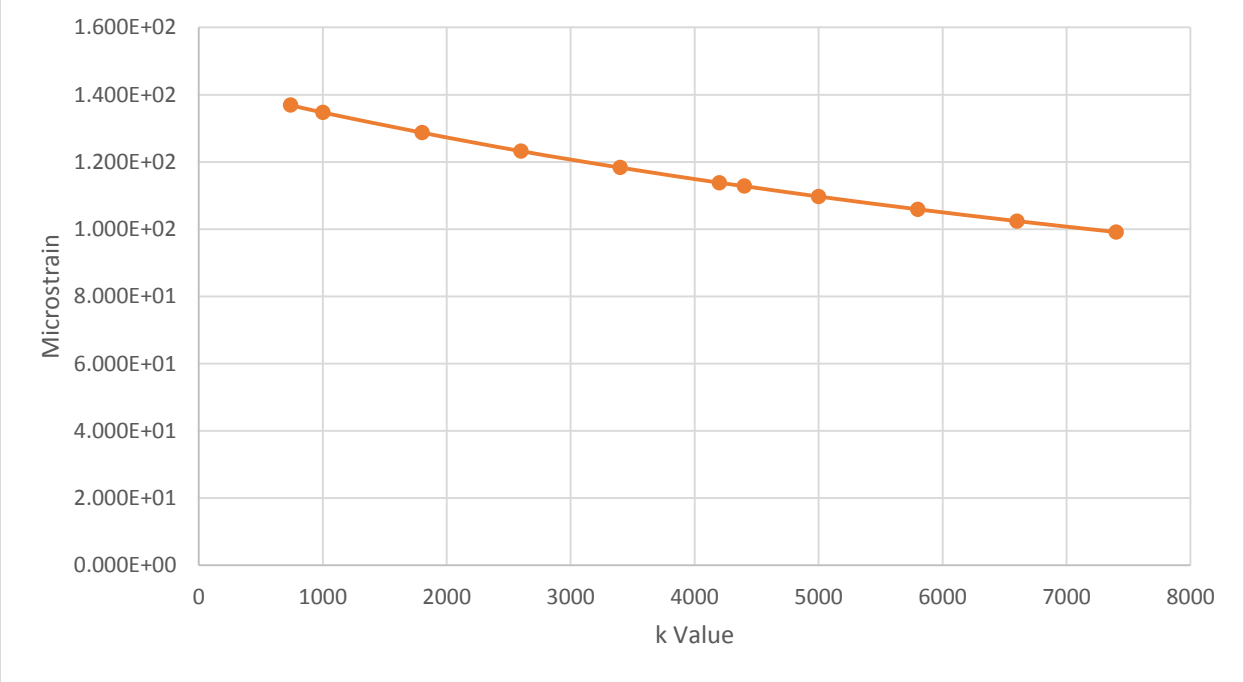

Figure 5.7 Microstrain versus k-value beyond 4,400 lb/in^3 in NE Section

The CISL 17 APT experiment was performed by overlaying the north and south lanes of the previously performed CISL 14 experiment. The two lanes were distinct in their existing HMA material. The following calibration was conducted to measure significance of underlying material on interface layer performance. The elastic modulus of the existing HMA was hypothetically varied. Figure 5.8 shows strain results of models with various existing HMA layer moduli. Little variation was evident in the resulting strain.

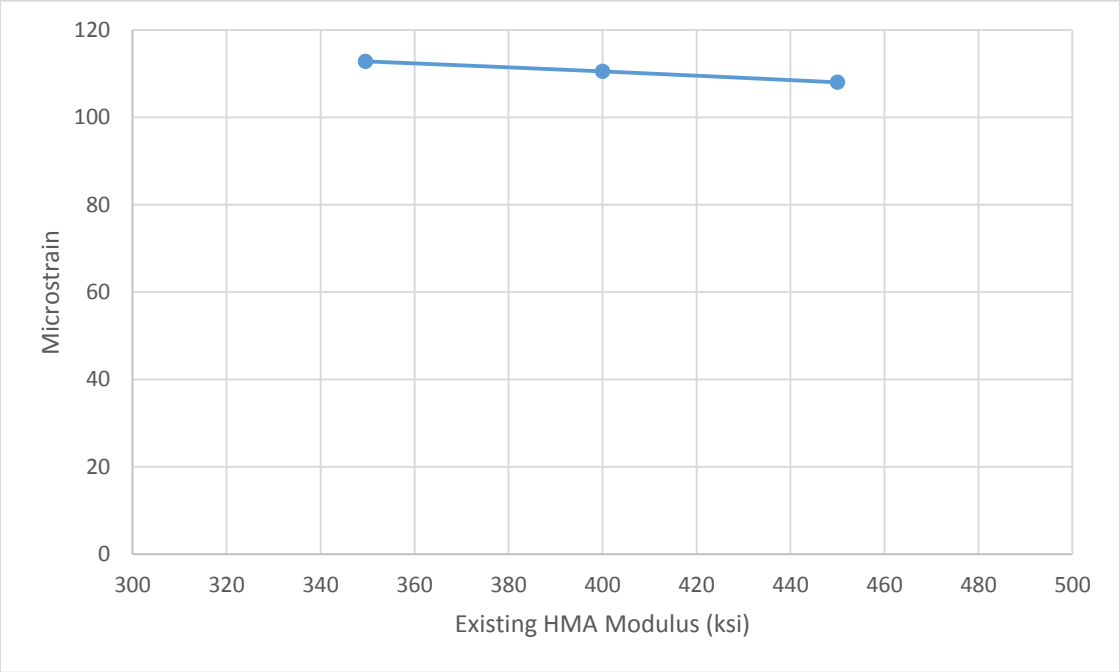

Figure 5.8 Microstrain versus Modified Existing HMA Elastic Modulus

5.2.3 Comparison to APT Distress Survey Results

As a part of the CISL 17 experiment, periodic distress surveys were performed to assess cracking in the wheelpath. Those surveys revealed cracking beginning in the southeast and south middle sections at 200,000 load repetitions were applied. Cracking was evident in all sections at 300,000 and 400,000 load repetitions, though the later cracks were described as “hairline” and “not visible except when closely searched for” (Mealiff 2015). Figures 5.9 through 5.11 show the results of the CISL 17 distress surveys.

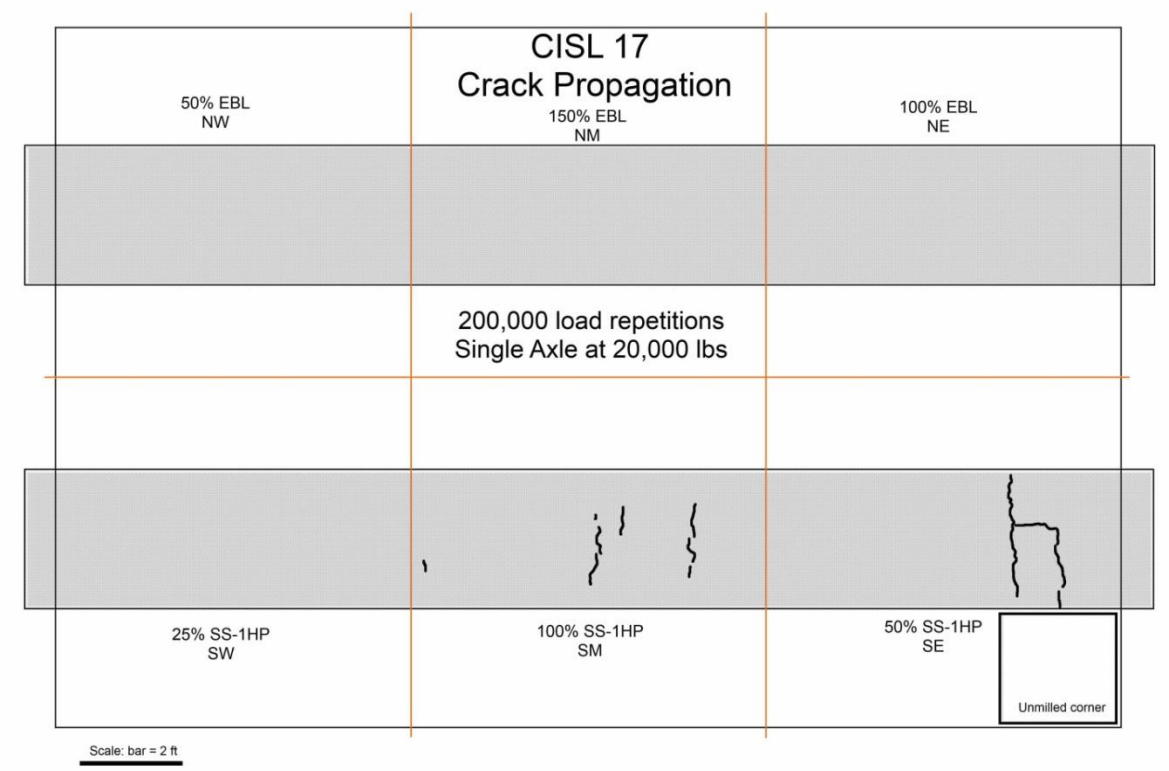

Figure 5.9 Cracks at 200,000 load repetitions

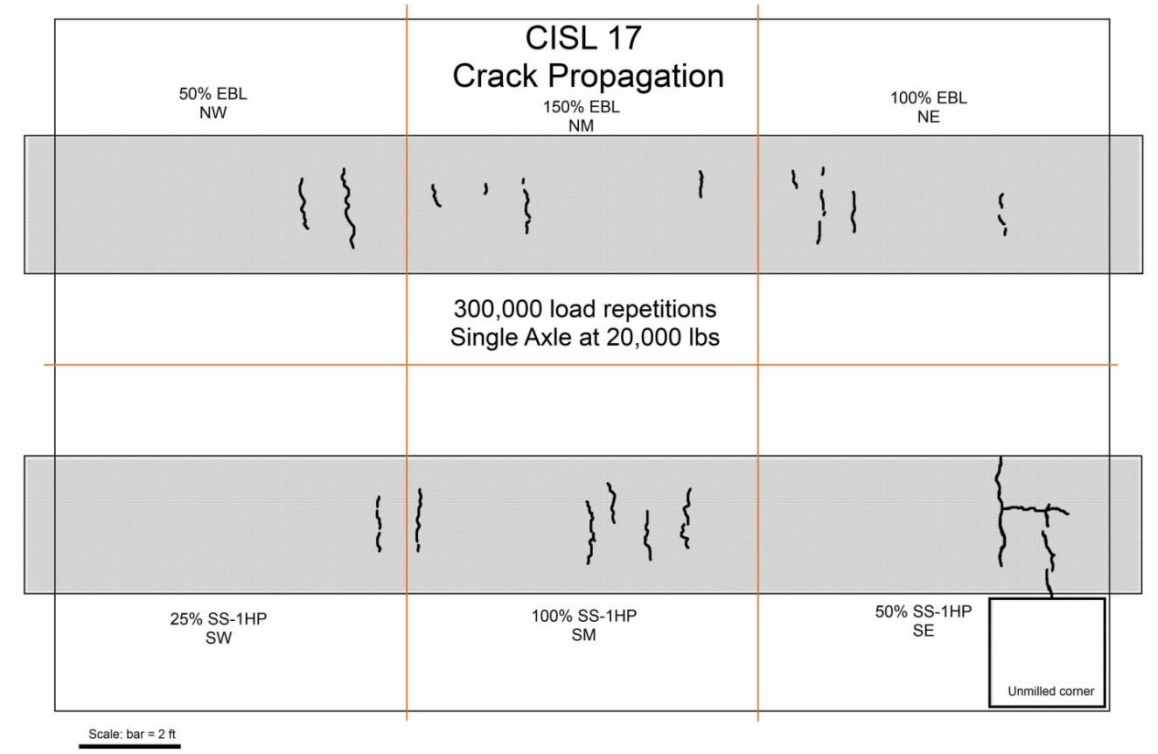

Figure 5.10 Cracks at 300,000 load repetitions

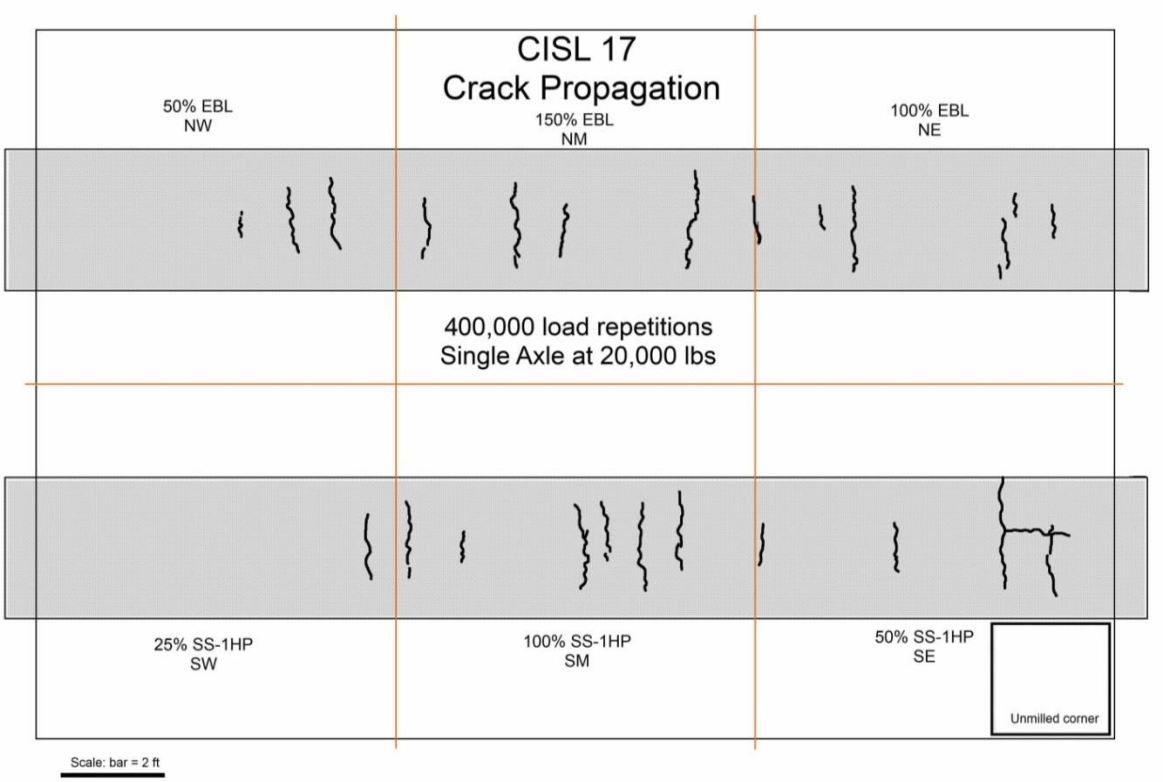

Figure 5.11 Cracks at 400,000 load repetitions

The results of these surveys indicate that the southwest and northwest sections each performed the best with respect to cracking in the wheelpath. Each of these sections had the least amount of tack coat applied in its lane. Northeast and Southeast sections measured the lowest longitudinal strain in their respective lanes. Based on the derivation of interface stiffness described in section 5.4, the northeast and southeast sections have the highest reaction modulus among test sections with the same tack coat material. These results indicate a relationship where high reaction modulus results in smaller longitudinal strains at the HMA layer interface, but could also result in greater surface cracking.

5.3 Sensitivity Analysis

Many input choices were made when creating the 3D-FEM that impacted predicted results, including material types and properties, geometry, boundary conditions, and loading. After the

working model was created, many of the factors were altered to determine their impact on predicted values and their correspondence to measured values from the CISL APT experiment. Sensitivity analyses were performed with regard to mesh size, global model size, and loading type. Loads were initially applied by step-wise rectangles, as described in Chapter 4, and again as one rectangle over the length of the wheel path for comparison.

Load application was also considered for sensitivity analysis. Every loading step added in the ABAQUS database increased computational time required for the solution. Therefore, equivalent loading was often used to simulate repeatedly applied loads. For this study, equivalent loads were applied by multiplying the time each pressure was applied over its respective area, and loading each area of the wheel path one time, thereby allowing each section of the wheel path to be loaded with a time equivalent to hundreds of thousands of load repetitions applied in the APT without coding hundreds of thousands of loading steps in the ABAQUS database. This type of loading should capture time-hardening creep modeled in HMA layers. The drawback to this type of simulation is that it negates potential impact of loading and unloading on each material's permanent deformation. To perform a sensitivity analysis on the impact of equivalent loading, a large loading step with one pass through the wheel path was compared to the equivalent time broken up over a few passes through the wheel path.

5.3.1 Mesh Size

Using a working model to simulate one of the six APT-tested pavement structures, sensitivity analysis was performed to observe the impact of mesh size parameters on key outputs. The key output for this study was longitudinal strain at the interface of the existing and overlaid HMA layers. These strains were measured in the APT experiment. Vertical deformation at the pavement surface was also considered because it was easily measured in the APT environment.

The model used in the sensitivity analysis represented the pavement section designated as MO-1. Layer material properties of this section are tabulated in Table 3.2. Cohesive stiffness of the tack coat interface was held at 740 lb/in^3, corresponding to the lower-bound of values found by Romanoschi and Metcalf (2001). Loads were applied step-wise for 5,000 sec. at 90-psi pressure load. Mesh sizes for the overlay, existing AC, granular base, and subgrade layers were initially 2, 4, 6, and 8 in., respectively. Vertical displacement was visualized with each mesh size iteration, and a path was created across overlay surface at its centerline of the section. This path was useful for creating data plots, as shown in Figure 5.12. Positive values in the z-direction relate to downward displacements. Key data from this path included maximum and minimum displacement values and rut depth, which is the difference of those values. Similarly, longitudinal strain at the top of the existing HMA layer, through its transverse centerline, is shown in Figure 5.13.

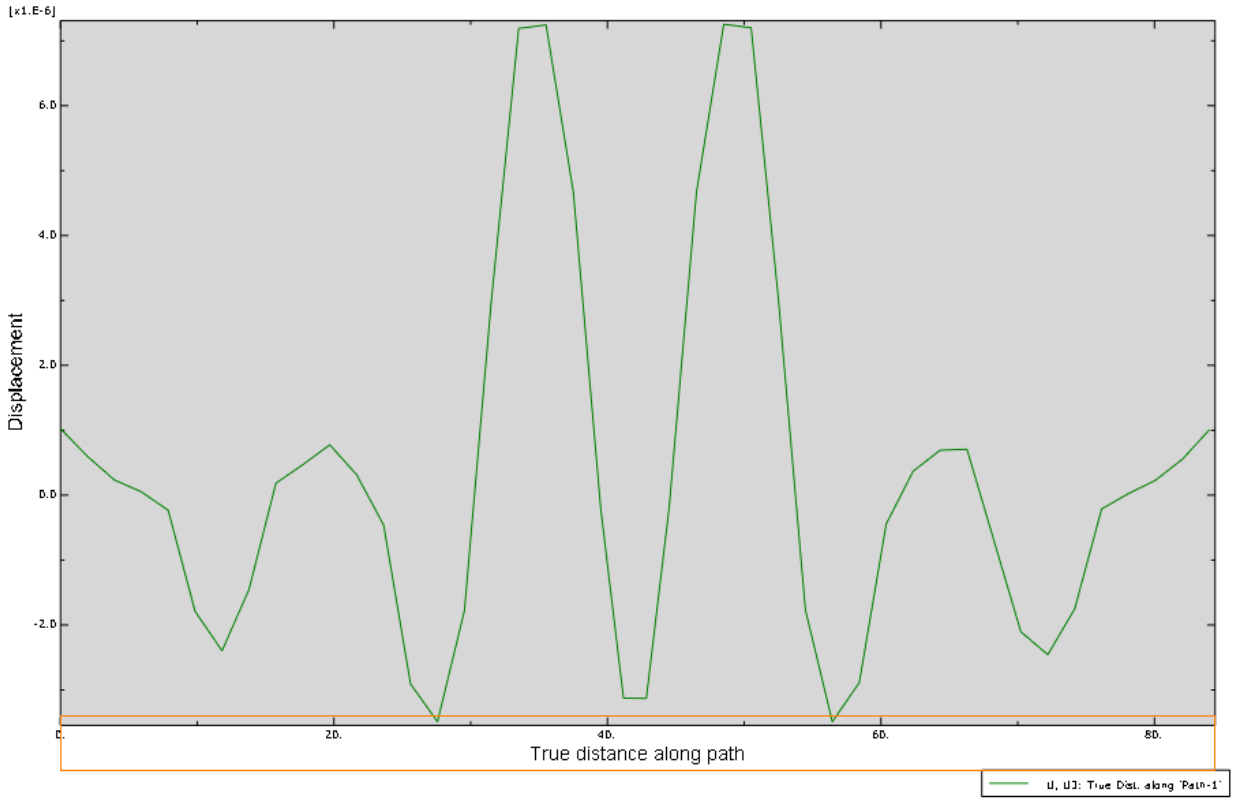

Figure 5.12 Vertical Displacement across Centerline Path

Strain along the transverse centerline of the existing HMA surface was significantly smaller than maximum and minimum longitudinal strains on the same surface. Therefore, sensitivity analyses were performed with respect to maximum and minimum longitudinal strains and centerline vertical deformations. The first analysis probed the influence of subgrade mesh size on vertical displacement and longitudinal strain outputs. These results are shown in Figures 5.14 and 5.15. Computational time increased significantly as the subgrade mesh size was reduced from 4 in. to 2 in. and smaller. When subgrade mesh size was set to 1 in., computational time was prohibitive.

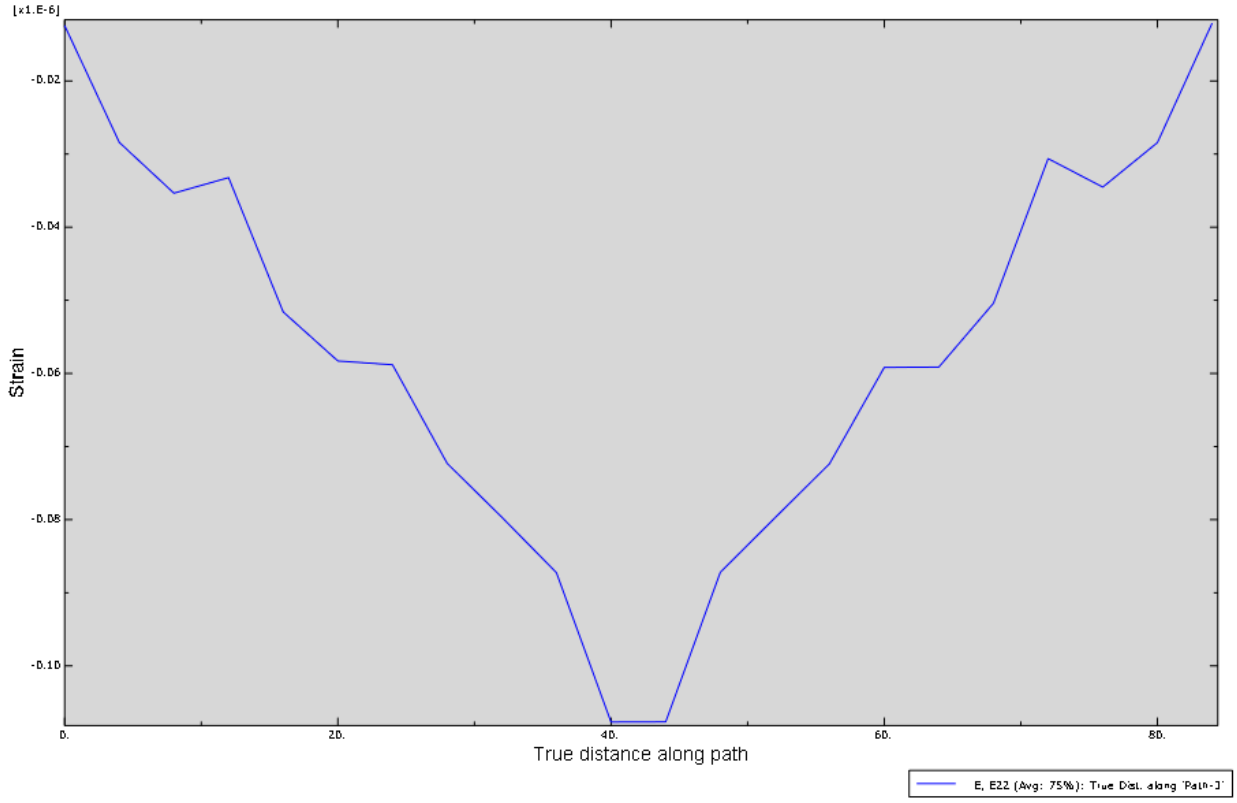

Figure 5.13 Longitudinal Strain on Top of Existing HMA layer along a Centerline Path

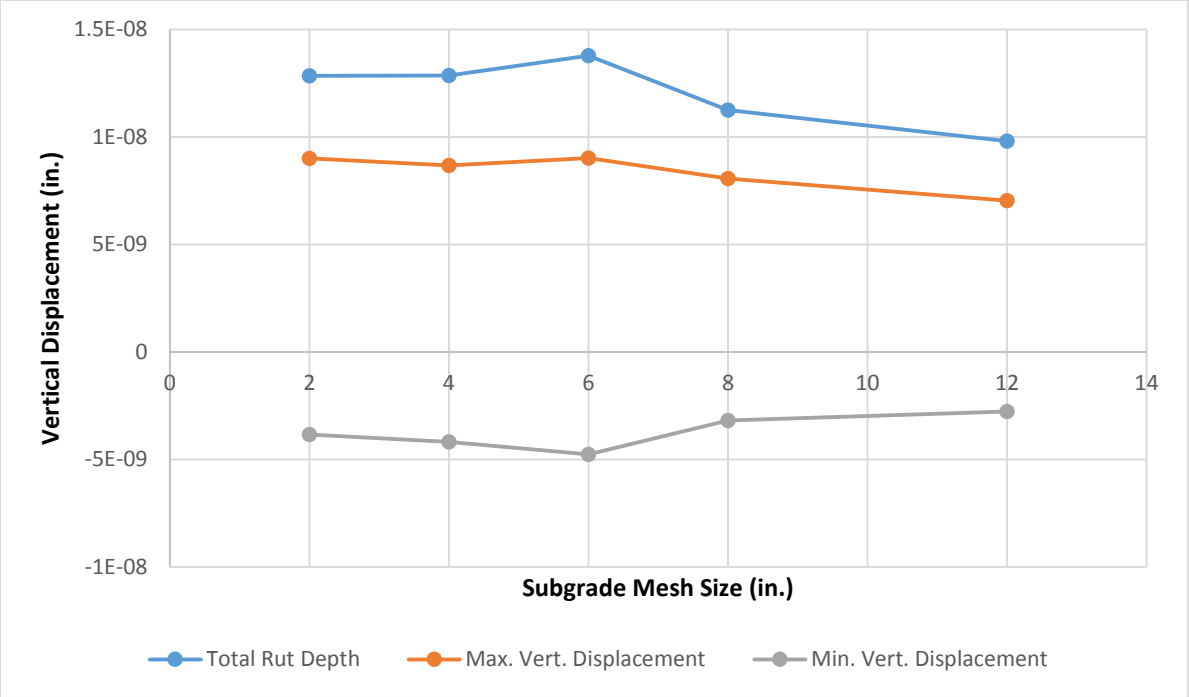

Figure 5.14 Vertical Displacement (in.) versus Subgrade Mesh Size (in.)

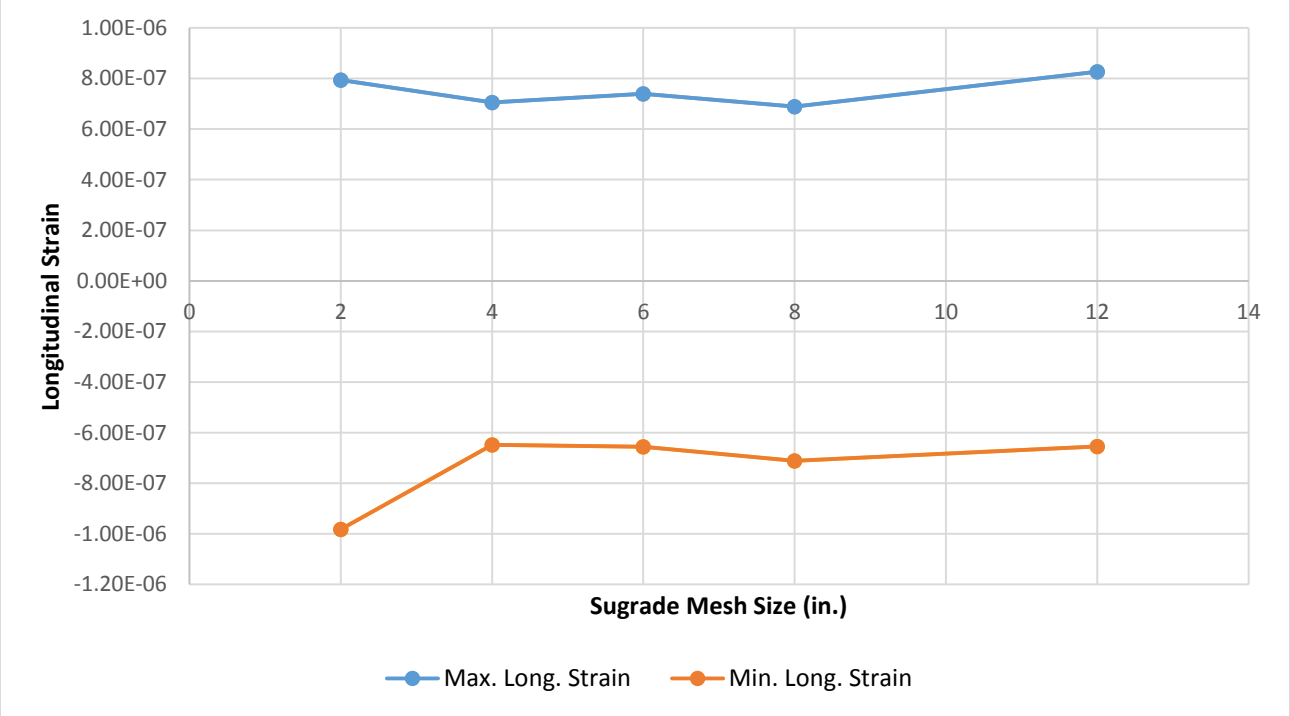

Figure 5.15 Maximum and Minimum Longitudinal Strain versus Subgrade Mesh Size (in.)

Similar analyses were completed to observe the influence of mesh size on the granular base layer with the same outputs. All other parameters were identical to the base mesh size analysis,

and mesh size for the subgrade was held at 4 inches. Figures 5.16 and 5.17 show results of that analysis.

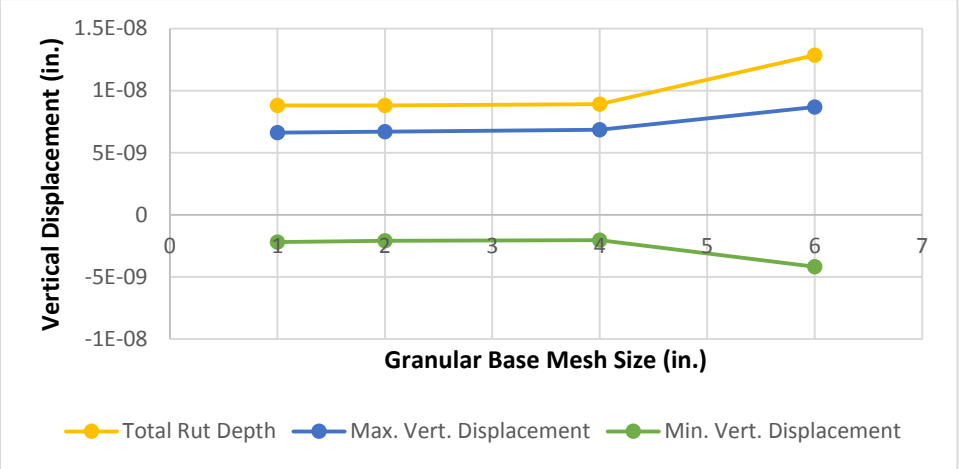

Figure 5.16 Vertical Displacement (in.) versus Granular Base Mesh Size (in.)

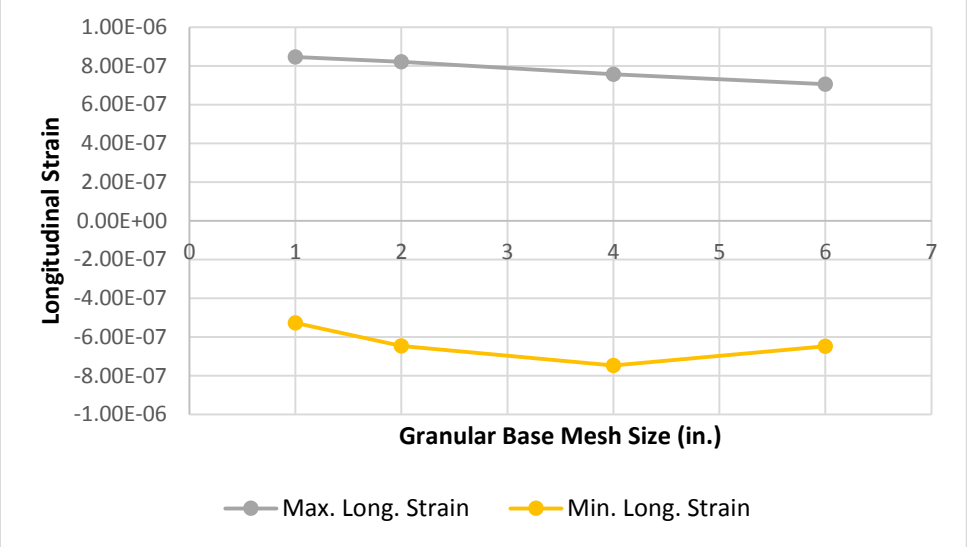

Figure 5.17 Maximum and Minimum Longitudinal Strain versus Granular Mesh Size (in.)

The same process was repeated for the existing AC layer. The model was identical to the model used in the granular base mesh size analysis; mesh size for the granular base layer was held to a constant 2 in**.** in this analysis. As the mesh size for the existing HMA layer became smaller than the mesh size of the overlay layer, results became discontinuous, with odd vertical spikes in the resulting deformed shape. Therefore, the overlay mesh size was decreased in tandem with the mesh size of the existing HMA layer. Figures 5.18 through 5.21 show results of mesh size

sensitivity analyses for both existing HMA and overlay layers. Based on these analyses, predictive models were built with mesh sizes of 1 in., 1 in., 2 in., and 4 in. for the overlay, existing HMA, granular base, and overlay layers, respectively.

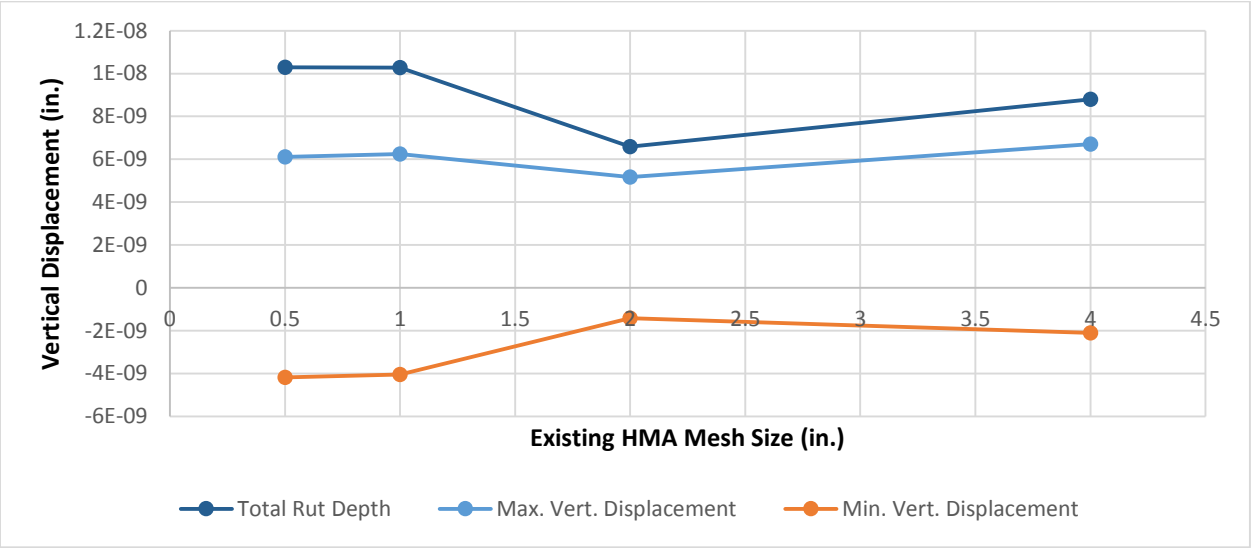

Figure 5.18 Vertical Displacement (in.) versus Existing HMA Mesh Size (in.)

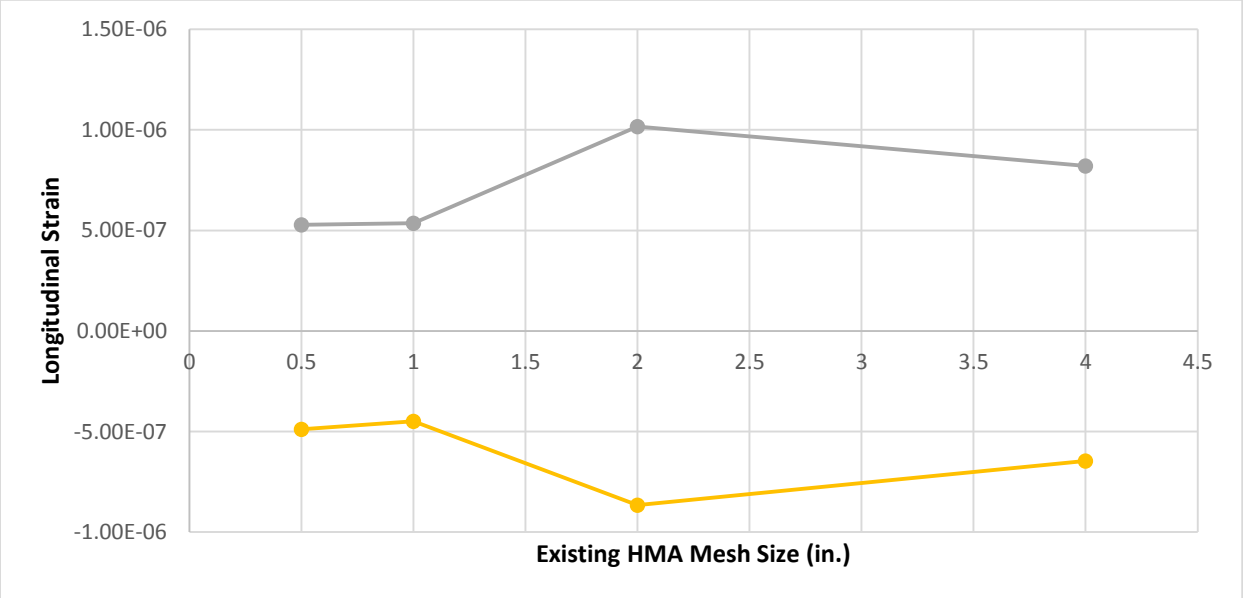

Figure 5.19 Maximum and Minimum Longitudinal Strain versus Existing HMA Mesh Size (in.)

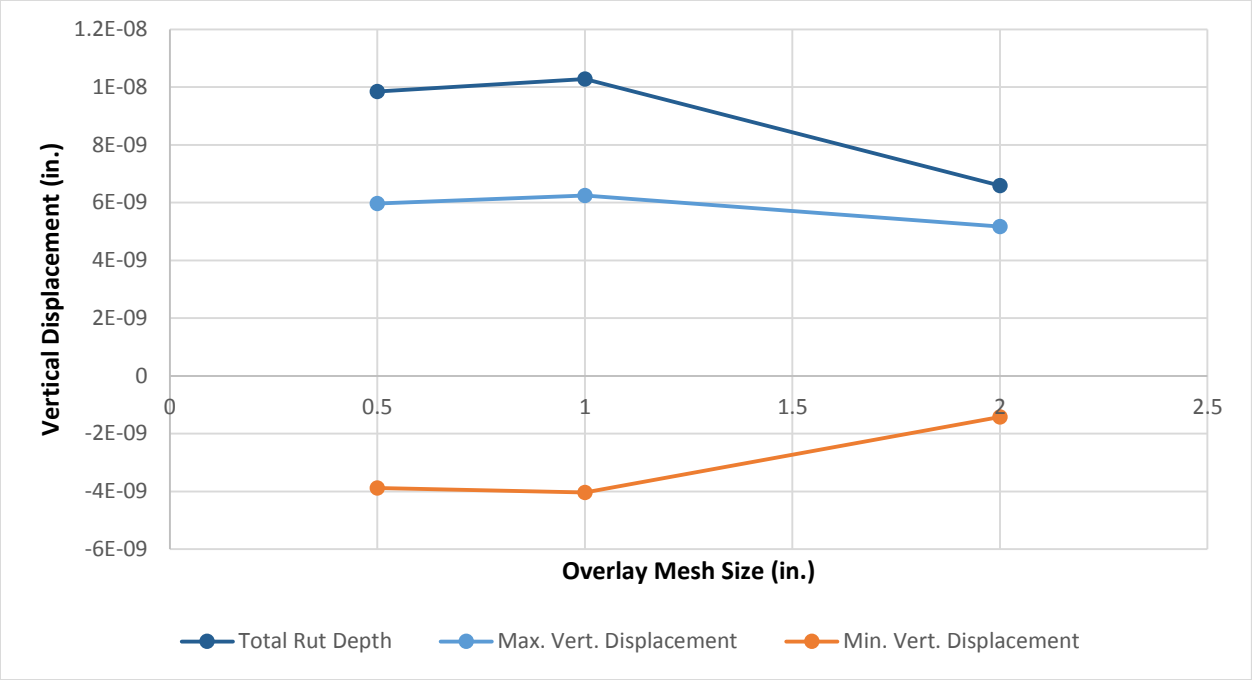

Figure 5.20 Vertical Displacement (in.) versus Overlay Mesh Size (in.)

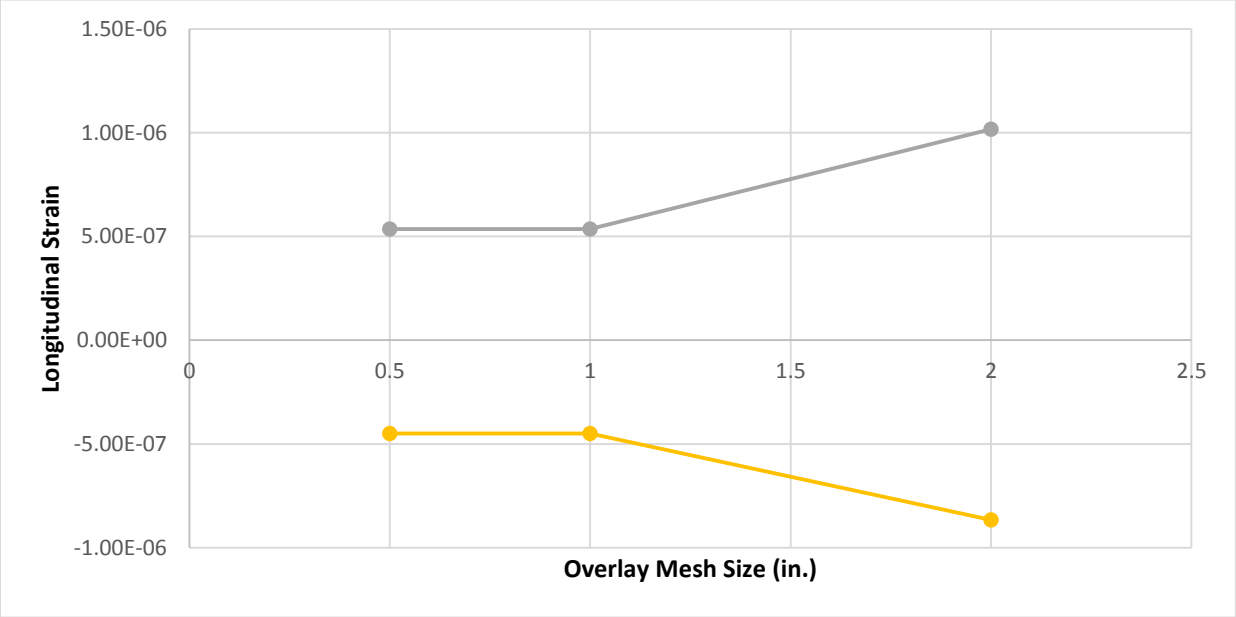

Figure 5.21 Maximum and Minimum Longitudinal Strain versus Overlay Mesh Size (in.)

5.3.2 Inclusion of Coefficient of Friction at Interface

Because this experiment occurred completely in the elastic region of the interface material, no observed failure was evident at the interface. Friction between the overlay and existing HMA layers never fully mobilized. The model confirmed this as the two models, identical in all ways

except the presence of frictional behavior at the interface, were run for vertical displacement and longitudinal strain. Both models behaved identically.

5.3.3 Load type

Differential permanent deformation was observed after the initial model was created. The dual tire assembly created rutted wheel paths as expected, and the magnitude of vertical displacements at the beginning of the wheel path was 20 times those observed at the end of the wheel path. These results are shown in Figure 5.22 when each wheel print was loaded for 5,000 sec., an equivalent of 100,000 wheel passes.

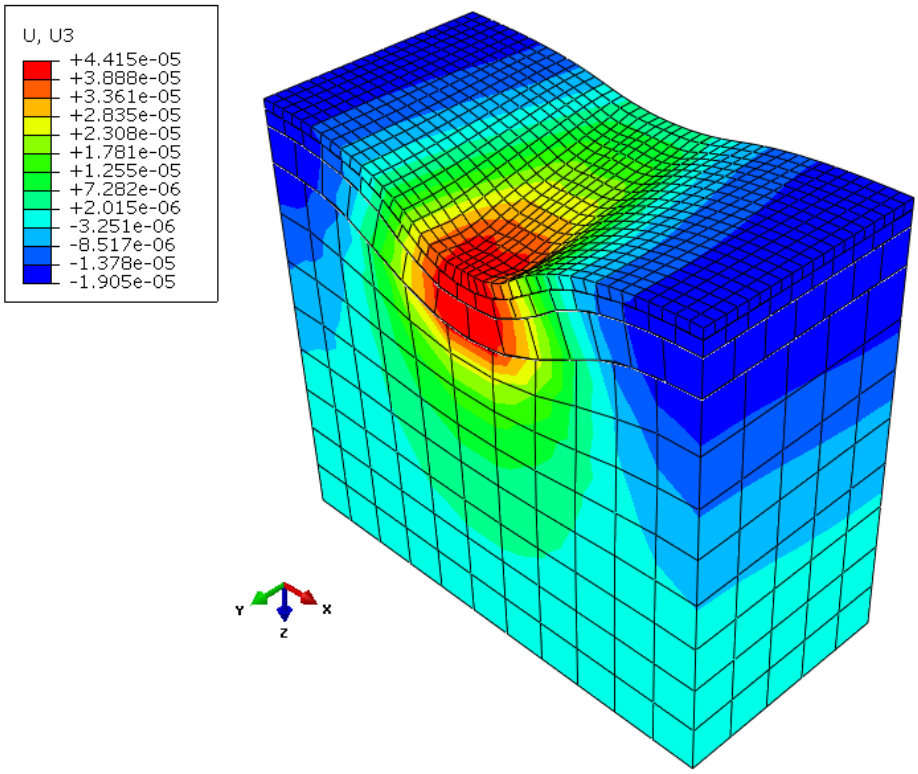

Figure 5.22 Predicted Differential Rutting

Onyango (2009) documented the same unexpected differential rutting, attributing it to "the load remaining constant at the magnitude associated with the end of the previous step," as described in the ABAQUS Users' Manual. An attempt was made to utilize trapezoidal load amplitudes to overcome this response, but results from the trapezoidal loading were unfavorable.

The next attempt was to load the entire wheel path at once. This approach seemed to stray further from actual loading of the APT experiment and in-service pavement, but it resulted in a uniformly deformed section in the longitudinal direction. These results proved to be satisfactory for rutting predictions. The entire wheel path was also loaded for 5,000 sec. and resulting deformation is shown in Figure 5.23. This approach yielded two distinct wheel paths, as was expected from an in-service or APT pavement.

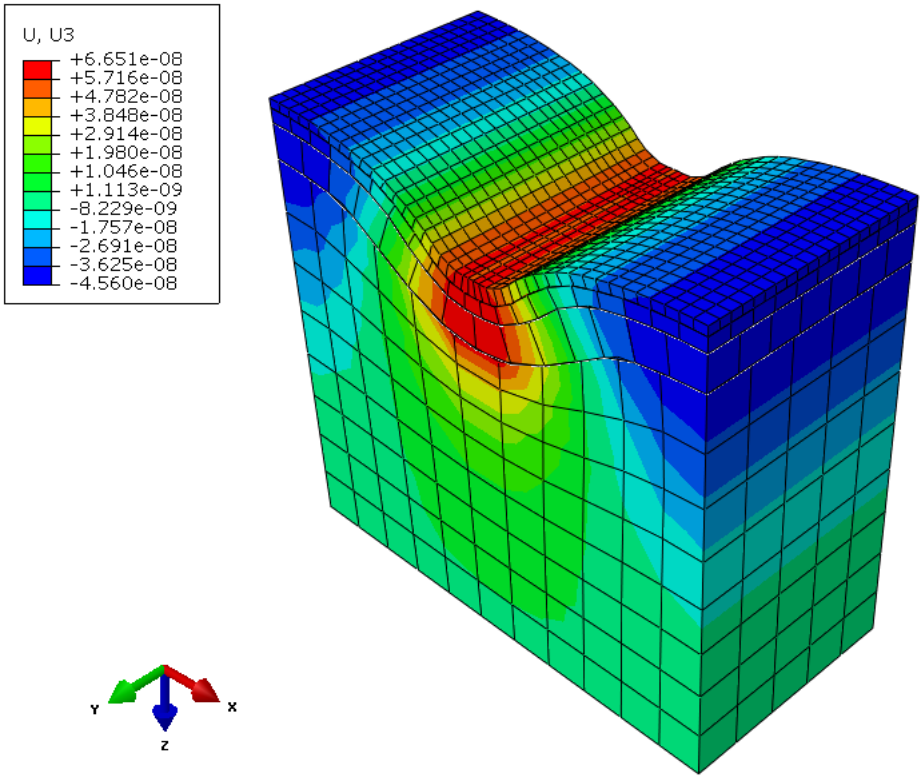

Figure 5.23 Predicted Uniform Rutting

Longitudinal strain calculated on the surface of the existing HMA layer by the FEM after full-path loading was many orders of magnitude smaller than those measured after step-wise loading. Therefore, full-path loading was not considered a useful approximation for this study. Table 5.4 demonstrates the stark contrast in predicted longitudinal strain and step-wise and full-path loading on two models.

Table 5.4 Maximum and Minimum Strain for Step-Wise and Full-Path Loading of Like Models

Model	Loading	Max. Strain (in.)	Min. Strain (in.)
1	Step-Wise	5.35E-07	-4.49E-07
1	Full-Path	3.07E-12	-3.45E-12
2	Step-Wise	5.28E-07	-4.90E-07
2	Full-Path	1.20E-11	-1.25E-11

Furthermore, maximum and minimum strain values for the full-path loaded Model 2 occurred as unusually concentrated strains at the model's boundary, as shown in Figure 5.24. Longitudinal strains on the existing HMA surface were very small, typically on the order of 10^{-13}in/in. In addition, small areas of concentrated strains could be seen at the boundaries, which were still several orders of magnitude smaller than those observed after step-wise loading. Although full-path loading was shown to be an adequate approximation for rutting measurements, it is not a viable option when analyzing interface strain.

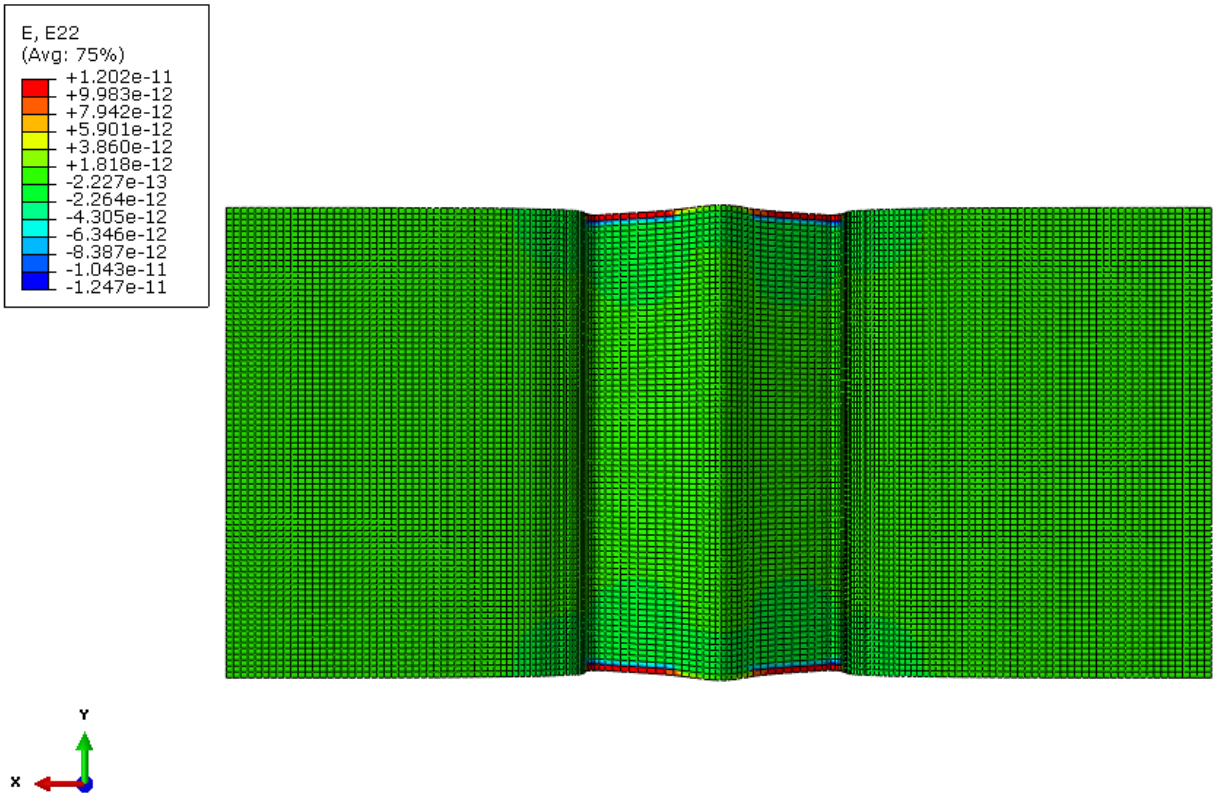

Figure 5.24 Longitudinal Strain on Existing HMA Surface

5.3.4 Model Size

All models were created using a y-direction symmetry boundary condition on the front and back of the model. Consequently, over a long enough section of pavement structure with uniform loading, displacements will be uniform in the longitudinal direction. Therefore, the longitudinal dimension of the model should become insignificant. The model may, therefore, be reduced in the longitudinal direction to a dimension equal to one wheel footprint. This reduction in model size increases the possibility for more accurate loading modeling. Specifically, more load cycles can be used without creating undue burden on computational resources.

Another model was created with identical material, boundary condition, meshing, and loading properties as the previous model. The longitudinal direction was set to 7 in., matching the longitudinal dimension of one loaded tire footprint. The single tire footprint was loaded for the

same length of time (5,000 sec.) as the previous model. The resulting deformation is shown in Figure 5.25.

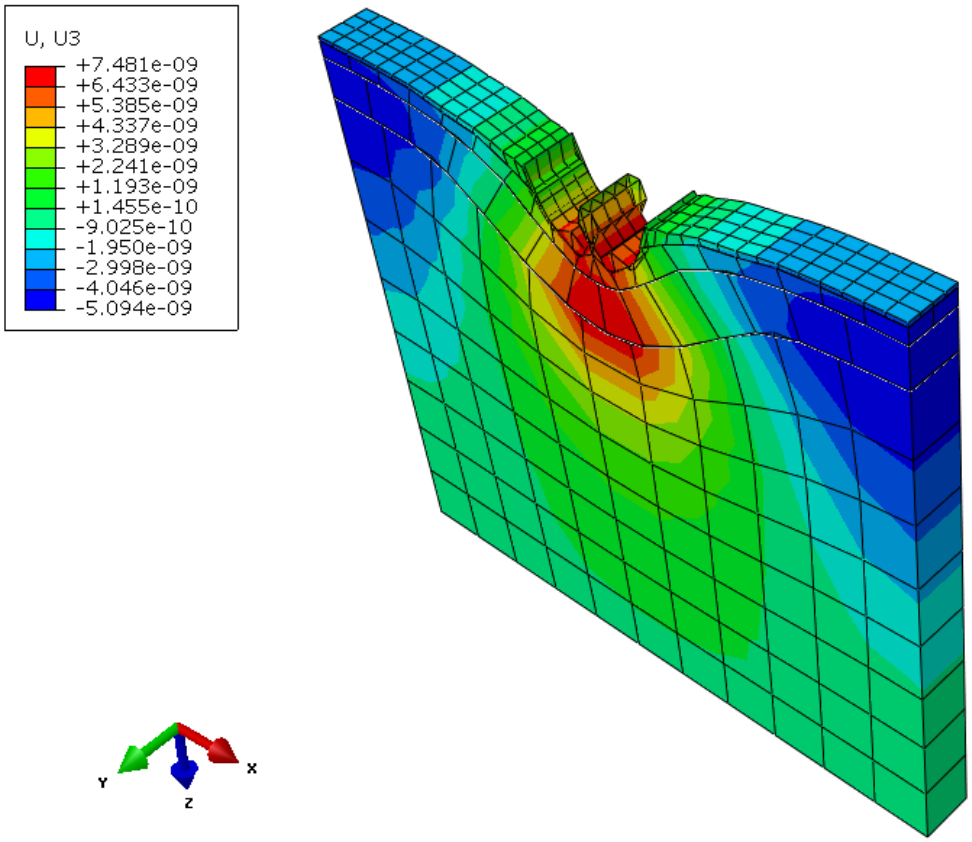

Figure 5.25 Deformation of 7-in. Model

The pattern shown in this deformation was similar to the larger model, but the magnitude of the vertical displacement was significantly different than the previous model. The 7-in. model was analyzed a second time with significantly smaller mesh sizes. As shown in Figure 5.26, the smaller mesh size results were very similar to the larger meshed model and did not improve the model toward the results of the larger model.

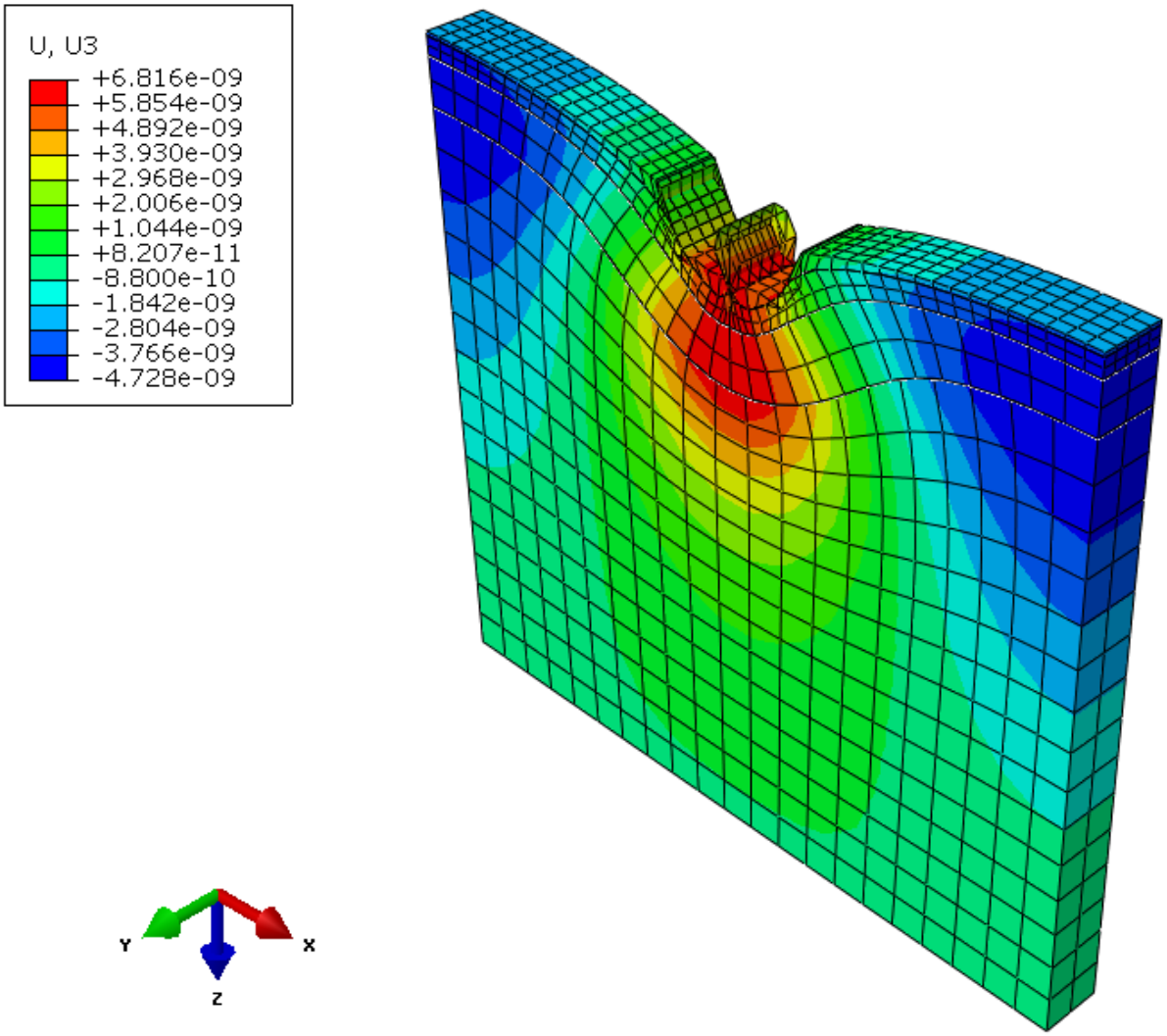

Figure 5.26 Deformation of 7-in. Model with Smaller Mesh Parameters

5.3.5 Loading Cycles

In-service and APT pavements are subjected to hundreds of thousands of repeated loads, a model environment must be created that captures that loading behavior as closely as possible. Constraints in computing resources and time, however, make modeling an equivalent number of time steps unfeasible. Model iterations in Figures 5.27 through 5.29 show vertical deformation when the total 5,000 seconds of loading was divided into greater numbers of equal-length time steps.

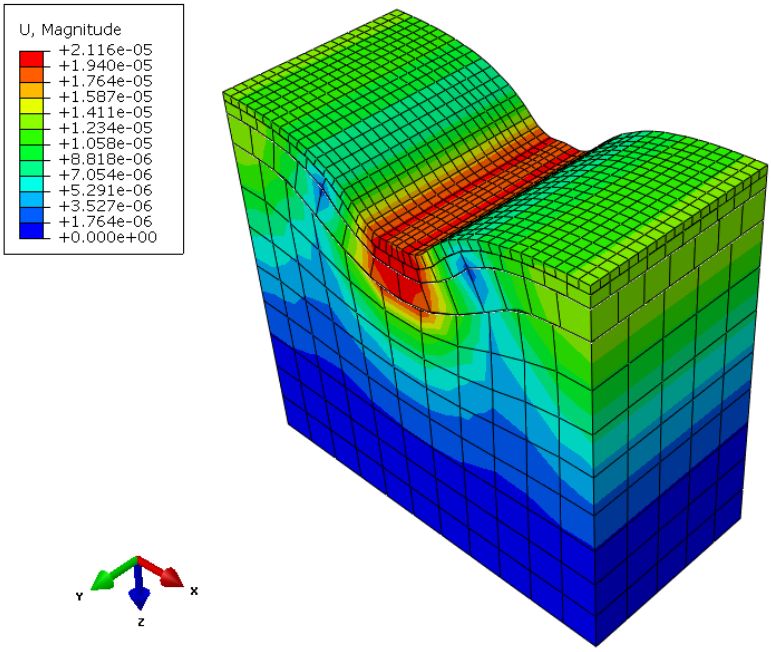

Figure 5.27 Vertical Deformation from Two 2500s Loading Steps

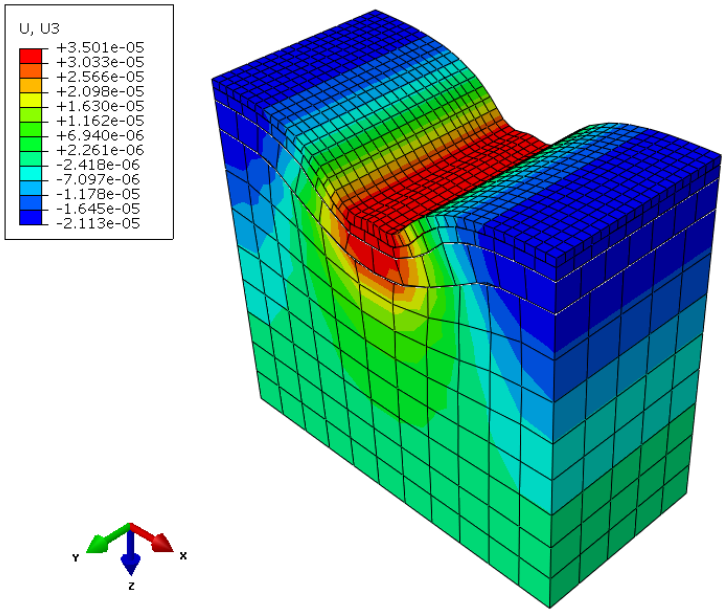

Figure 5.28 Vertical Deformation from Three 1666.67s Loading Steps

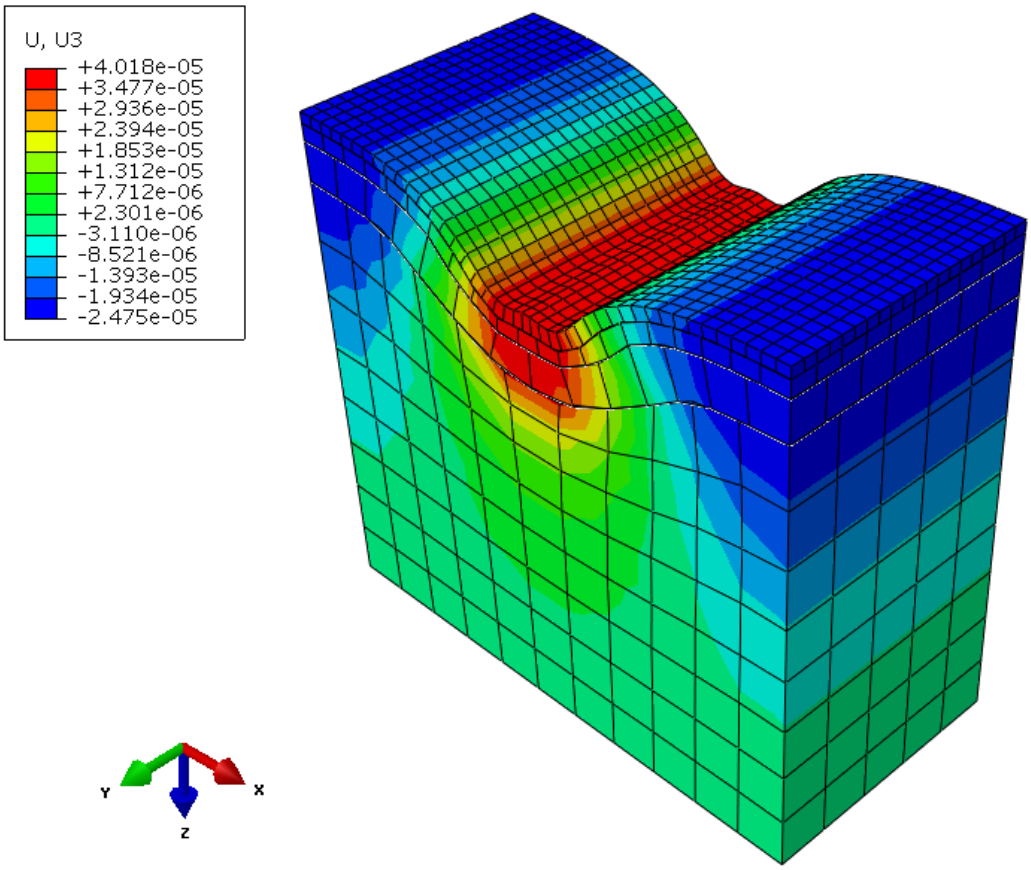

ll

Figure 5.29 Vertical Deformation from Four 1250s Loading Steps

In addition to comparing step-wise and full-path loading, careful consideration was given to potential variation from the single pass of a step-wise load to the hundreds of thousands of load repetitions that occur in APT experimentation and on in-service pavement structures. Permanent deformation and maximum and minimum strains were evaluated for load repetitions from 100,000 to 400,000. The applied pressure and total time that pressure was applied on each pavement segment were held constant at 90 psi and 5,000 sec., respectively. In order to consider multiple load passes, total loading time was divided by the number of passes to be considered. Applying five load passes, for example, involved creating five times the number of loading steps, with each step being given one-fifth the total load time. Model segments were loaded in the same sequence as before, with each load pass occurring in the same order. For example, when segments were

loaded from Segment 1 to Segment 7, Segment 1 was loaded immediately following the end of the step in which Segment 7 was loaded. Results showed that as the number of load repetitions increased, or loading time decreased, vertical displacements increased while strains decreased, as shown Figures 5.30 and 5.31.

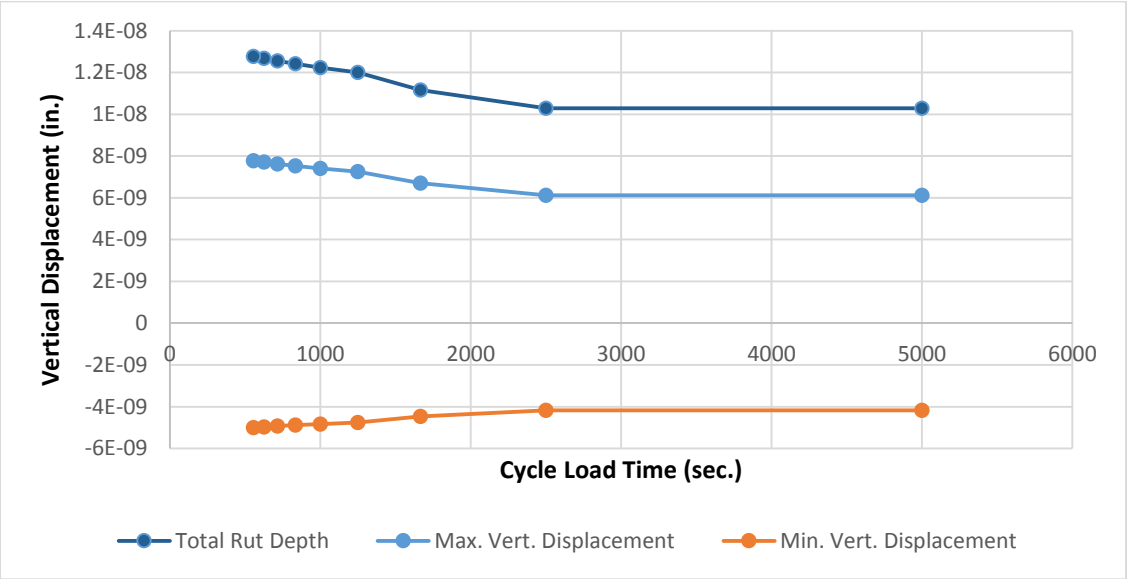

Figure 5.30 Vertical Displacement versus Cycle Load Time

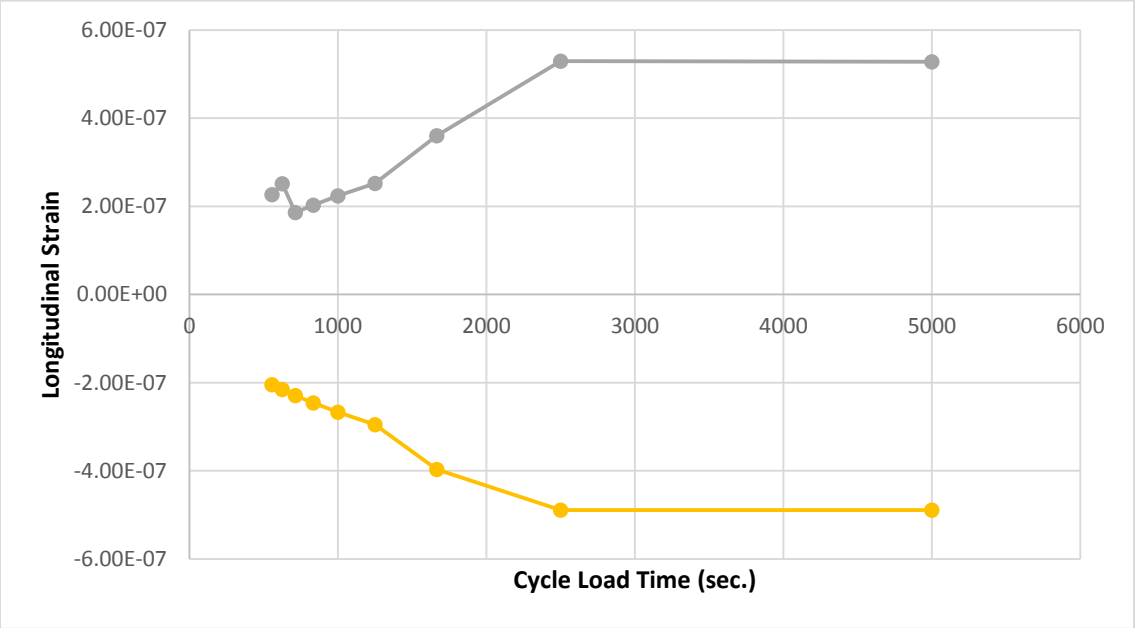

Figure 5.31 Maximum and Minimum Longitudinal Strain versus Cycle Load Time

Rut depths predicted in this portion of the study were significantly smaller than those measured in CISL 17. The high subgrade moduli input prevented the model from accurately predicting vertical permanent deformations. This unusually high subgrade modulus was obtained from a previously published study (Onyango 2009). A more accurate value has since been published (Romanoschi et al. 2014). The more accurate input was used in the final analysis of this study.

Detailed results from sensitivity analyses are tabulated in Appendix A.

5.4 Derivation of HMA Interface Stiffness

This study resulted in development of relationships between interface stiffness and longitudinal strain. These relationships are shown in Figures 5.1 and 5.2 for each of the six test sections of CISL 17. Because of failures in six of 12 placed H-bar strain gages, only four of the six test sections had recorded strain data. By comparing the early strain gage data to the FEM-developed strain versus interface stiffness relationships, each test section's interface stiffness could be evaluated. The results are shown in Table 5.5. Detailed results of longitudinal strain at the HMA layer interface are tabulated in Appendix B.

Table 5.5 HMA Interface Stiffness

Section	Material	APT Strain (microstrain)	Interface Stiffness (lb/in^3)
NE	EBL 100%	70	> 4400
NW	EBL 50%	80	> 4400
SE	SS-1HP 50%	125	> 4400
SM	SS-1HP 100%	140	4200

The strains predicted by the FEM tend to be higher than those measured in the APT. It is, therefore, necessary to extend the model analysis to higher reaction modulus values. Using the linear regression equations (6-9) discussed in Section 5.2.2., strains can be related to reaction

moduli that fall outside the normally modeled range. Table 5.6 shows the results of back-calculating interface stiffness (reaction modulus) values by using the linear regression equations.

Table 5.6 HMA Interface Stiffness (from linear regression equations)

Section	Material	APT Strain (microstrain)	Interface Stiffness (lb/in^3)
NE	EBL 100%	70	11,881
NW	EBL 50%	80	10,388
SE	SS-1HP 50%	125	8,545
SM	SS-1HP 100%	140	4,262

It appears that EBL at the recommended rate has the highest interface stiffness. Whereas SS-1HP at the currently specified rate has the lowest interface stiffness.

Chapter 6 – Conclusions and Recommendations

6.1 Summary

HMA pavements are an integral part of U.S. national and international infrastructure. Therefore, developments that produce longer-lasting and better-functioning roadways save public funds used to build and maintain those roadways and increase user productivity, thereby increasing commerce. Improved roadways also reduce the use of natural resources, promoting sustainability in transportation and engineering industries.

Proper bonding with tack coat remains an important step in designing and building better HMA pavements. Laboratory testing, in-situ testing, APT experiments, and FEM analysis are currently being used to increase the knowledge base regarding HMA layer bonding with tack coat. This study builds on previous developments by utilizing commercially available FEM software to characterize mechanistic responses of HMA pavement structures with various tack coat applications. Furthermore, the models developed in this study allowed for identification of a stiffness modulus or k-value based on pavement structure parameters and measured strain from the APT experiment.

6.2 Conclusions

The objective of this study was to develop a 3D-FEM that would accurately predict the mechanistic response of an HMA pavement structure relative to varying interface bonding conditions. Specifically, the goal of this study was to use FEM software and APT experimental data to appropriately characterize the reaction modulus for various types and application rates of tack coat material. That goal was accomplished, in part, because k-values were assigned to tack coat material and application rates used on most test sections of the CISL 17 APT experiment.

Additional conclusions can be drawn from this work with respect to modeling of repetitive loads on pavement structures. First, longitudinal strains measured directly under the applied load may be predicted by modeling independent of loading time. These strains were identically predicted regardless of the length of time over which the load was applied. This modeled strain was comprised almost entirely of elastic strain. Although plastic strains increased with loading time and were modeled through the material's creep parameters, they were many times smaller than induced elastic strains.

Although some studies, particularly studies focused on rutting, have used models that load the entire wheel path simultaneously, this study has shown that modeling to be inappropriate for measuring strain at the layer interface. Step-wise loading is preferred although it can be time-consuming and resource-draining to use dozens of loading steps. The output database for one job in this study, required 70 loading steps, was more than 1GB in size.

6.3 Future Work

Given the modeled k-values of Table 5.5, new phases of research can be identified. Although CISL 17 was limited to 400,000 load repetitions, the model may be used to analyze mechanistic responses in the pavement structure under extended loading. Similarly, the APT portion of the study could be extended to increase the number of load repetitions so that interface bonding fails. Beyond the point of failure, the interface should become completely dependent on friction between the layers. Modeling this behavior requires a user-defined interaction property similar to that used by Ozer et al. (2012).

The CISL 17 experiment used a direct tension test to evaluate bond strength of various tack coat applications. This method was chosen because it closely resembles the KT-78 test used by KDOT. Additional direct shear tests may be conducted. Direct shear tests as developed by

Romanoschi (1999) will allow a stiffness modulus to be determined in the laboratory and that k-value may be assigned in future FEM analysis related to future APT results.

CISL 17 test sections with EBL applied as the tack coat material showed very good performance, including very small interface strains. Further testing may be performed to validate this performance.

References

ABAQUS (2011). "ABAQUS 6.11 Analysis User's Manual". Dassault Systémes, Providence, RI.

Ali, B., Shahrour I., Dumont, A. G., and Perret, J. (2006). "Modeling of Rutting in Asphalt Flexible Pavement." *10th International Conference on Asphalt Pavements*, International Society for Asphalt Pavements, White Bear Lake, MN, 621-630.

ASTM D8-02, (2004) Standard Terminology Relating to Materials for Roads and Pavements, Annual Book of ASTM Standards, Vol. 04.03.

ASTM D4541-09e1, (2009) Standard Test Method for Pull-Off Strength of Coatings Using Portable Adhesion Testers, ASTM International, West Conshohocken, PA, www.astm.org.

Brown, E. R., Kandhal, P. S., Roberts, F. L., and Kim, Y. R. (2009). *Hot Mix Asphalt Materials, Mixture Design, and Construction*. NAPA Research and Education Foundation, Lanham, Maryland.

Canestrari, F., Ferrotti, G., Partl, M. N., and Santagata, E. (2005). "Advanced Testing and Characterization of Interlayer Shear Resistance." *Transportation Research Record: Journal of the Transportation Research Board, No. 1929*, Transportation Research Board, Washington, D.C., 2005, 69–78.

Clark, T.C., Todd, M. R., and Kevin, K. M. (2010). "Trackless Tack Coat Materials – A Laboratory Evaluation for Performance Acceptance." *TRB Preprint DVD Paper #10-0985, 89th Annual Meeting of the Transportation Research Board*, Transportation Research Board, Washington, D.C.

DeBondt, A. and Scarpas, A. (1994). "Theoretical analysis of shear interface setups," *Report 7-93-203-9, Road and Railway Research Laboratory*, Delft University of Technology, Delft, Netherlands.

Deysarkar, I. (2004). "Test Set-Up to Determine Quality of Tack Coat." Master's Thesis, Department of Civil Engineering, The University of Texas at El Paso, Dec.

Duncan, J. M., Monismith C. L., and Wilson, E. L. (1968). "Finite Element Analyses of Pavements." *Highway Research Board.* Transportation Research Board, Washington, D.C., 18-33.

Grove, J.D., Harris, G. K., and Skinner, B. J. (1993). "Bond Contribution to Whitetopping Performance on Low Volume Roads." *Construction Report, Iowa Highway Research Board Project No. HR-341*, Iowa Department of Transportation, January.

Hakimzadeh, S., Buttlar, W. G., and Santarromana, R. (2012). "Shear- and Tension-Type Tests to Evaluate Bonding of Hot-Mix Asphalt Layers with Different Tack Coat Application Rates." *Journal of the Transportation Research Board,* No. 2295, 54-62.

Hossain, M., Bortz, B. S., Melhem, H., Romanoschi, S. A., and Gisi, A. (2012). "Fourteen Years of Accelerated Pavement Testing at Kansas State University." *4th International Conference on Accelerated Pavement Testing,* CRC Press, Boca Raton, FL, 65-74.

Hu, X., and Walubita, L. F. (2011). "Effects of Layer Interfacial Bonding Conditions on the Mechanistic Responses in Asphalt Pavements." *Journal of Transportation Engineering*, Volume 137, No. 1, 2011, 28-36.

Hua, J. and White, T. (2002). "A study of nonlinear tire contact pressure effect on HMA rutting." *The International Journal of Geomechanics,* Volume 2, Number 3, 353–376.

Huang, B., Mohammad, L. N., and Rasoulian, M. (2001). "Three-Dimensional Numerical Simulation of Asphalt Pavement at Louisiana Accelerated Loading Facility." *Transportation Research Record*, No. 1764, 44-58.

Huang, Y. H. (2003). *Pavement Analysis and Design*. 2nd Edition, Pearson Education, Upper Saddle River, NJ.

Hugo, F. and ALE Martin (2004). "Significant Findings From Full-Scale Accelerated Pavement Testing." *NCHRP Synthesis of Highway Practice.* Issue 325, p. 211. Transportation Research Board, Washington, D.C.

KDOT (2007). Kansas Department of Transportation Special Provisions to the Standard Specifications, Edition 2007.

Khweir, K., and Fordyce, D. (2003). "Influence of Layer Bonding on the Prediction of Pavement Life." *Proceedings of the Institution of Civil Engineering – Transport,* Transport Research Library, Workingham, Berkshire, United Kingdom, Vol. 156, 73-83.

King, G, and May, R. (2003). "New Approaches to Tack Application." *Presentation made to the 83rd Annual Meeting of the Transportation Research Board,* Transportation Research Board, Washington, D.C.

Leng, Z., Ozar, H., Al-Qadi, I.L., and Carpenter, S.H. (2008). "Interface Bonding between Hot-Mix Asphalt and Various Portland Cement Concrete Surfaces: Laboratory Assessment, Transportation Research Record." *Journal of the Transportation Research Board*, No. 2057, 2008, pp. 46-53.

Lewis, P. (2008). "Lessons Learned From the Operations Management of an Accelerated Pavement Testing Facility." *Proceedings of the 3rd Intl. Confc. On Accelerated Pavement Testing,* Madrid, Spain.

Liu, L., and Hao, P. (2012). "Effect of Bonding Condition between Asphalt Layers on Behavior of Pavement." *Twelfth COTA International Conference of Transportation Professionals*. American Society of Civil Engineers, Reston, VA, 2955-2964.

Maina, J.W. and Matsui, K. (2004). "Developing Software for Elastic Analysis of Pavement Structure Responses to Vertical and Horizontal Surface Loading." *Transportation Research Record: Journal of the Transportation Research Board*, No. 1896, 2004, 107-118.

Mealiff, D. (2015). "Evaluation of Interface Bond of Hot-Mix Asphalt Overlays." Master's Thesis. Department of Civil Engineering, Kansas State University, Manhattan, KS.

Metcalf, J.B. (1996). "NCHRP Synthesis of Highway Practice 235: Application of Full-Scale Accelerated Pavement Testing." Transportation Research Board, National Research Council, Washington, D.C.

Mohammad, L., Elseifi, M., Bae, A., Patel, N., Button, J., and Scherocman, J. (2012). "Optimization of Tack Coat for HMA Placement." *NCHRP Project 09-40*. p. 146. Transportation Research Board, Washington, D.C.

Onyango, M. (2009). "Verification of Mechanistic Prediction Models for Permanent Deformation in Asphalt Mixes Using Accelerated Pavement Testing." Doctoral Dissertation. Department of Civil Engineering, Kansas State University, Manhattan, KS.

Ozer, H., Al-Qadi, I. L., and Leng, Z. (2008). "Fracture-Based Friction Model for Pavement Interface Characterization." *Transportation Research Record,* Volume 2057, No. 2057, 54-63.

Ozer, H., Al-Qadi, I. L., Wang, H., and Leng, Z. (2012). "Characterisation of interface bonding between hot-mix asphalt overlay and concrete pavements: modelling and in-situ response to accelerated loading." *International Journal of Pavement Engineering*. Volume 13, No. 2, 181-196.

Paul, H. R., and Scherocman, J. A. (1998). "Friction Testing of Tack Coat Surfaces." *Transportation Research Record: Journal of the Transportation Research Board,* Volume 1616, 6-12.

Roffe J.C., and Chaignon, F. (2002). "Chatacterisation Tests on Bond Coats: Worldwide Study, Impact, Tests, and Recommendations." *3rd International Conference Bituminous Mixtures and Pavements*, Thessaloniki, Greece.

Ritter, J., Rabe, R. and Andreas, A. (2012). "Analysis of the Long-Term Structural Performance of Flexible Pavements Using Full-Scale Accelerated Pavement Tests." *Procedia – Social and Behavioral Sciences.* Volume 48. 1244-1253. ISSN: 1877-0428.

Romanoschi, S.A. (1999). "Characterization of Pavement Layer Interfaces." Ph.D. Dissertation, Louisiana State University, Baton Rouge.

Romanoschi, S. A., and Metcalf, J.B. (2001). "Characterization of Asphalt Concrete Layer Interfaces." *Journal of the Transportation Research Board,* Volume 1778, 132-139.

Romanoschi, S.A., Lewis, P., Gedafa, D. and Hossain, M. (2014) "Verification of Mechanistic-Emperical Design Models for Flexible Pavements through Accelerated Pavement Testing." *Final Report No. FHWA-KS-14-02,* Kansas Department of Transportation, Topeka, KS

Saevarsdottir T. and Erlingsson S. (2014). "Modelling of responses and rutting profile of a flexible pavement structure in a heavy vehicle simulator test." *Road Materials and Pavement Design*, DOI: 10. 1080/14680629.2014.939698

Salinas, A., Al-Qadi, I. L., Hasiba, K. I., Ozer, H., Leng, Z., and Parish, D. C. (2013). "Interface Layer Tack Coat Optimization." *Transportation Research Record: Journal of the Transportation Research Board*, No. 2372, 53-60.

Webster, S. L. (1992). "Geogrid reinforced base courses for flexible pavements for light aircraft: literature review and test section design." *Miscellaneous Paper GL-92-6.* U.S. Army Corps of Engineers Waterways Experiment Station, Vicksburg, MS.

West, R. C., Zhang, J., and Moore, J. (2005). "Evaluation of Bond Strength Between Pavement Layers." *NCAT Report 05-08. National Center for Asphalt Technology,* Auburn University, Auburn, AL.

Willis, J. and Timm, D. (2007). "Forensic Investigation of Debonding in Rich-bottom Pavement." *Transportation Research Record: Journal of the Transportation Research Board*, No. 2040, 2007, 107-114.

Woods, M. E. (2004) "Laboratory Evaluation of Tensile and Shear Strength of Asphalt Tack Coats." M.S Thesis, Department of Civil Engineering, Mississippi State University, Mississippi, December.

Wu, Z. (2001). "Finite Element Simulation of Rutting on Superpave Pavements." PhD Dissertation, Kansas State University, Manhattan, KS.

Yan-qing, Z., Chang-hong, Z., and Yi-qiu, T. (2009). "Effects of Layer Interface Conditions on Fatigue Behavior of Asphalt Pavements with Semi-rigid Bases." *ICCTP 2009: Critical Issues in Transportation Systems Planning, Development, and Management*, ASCE, Reston, VA, 2426-2435.

Yoo, P. J., and Al-Qadi, I. L. (2008). "The Truth and Myth of Fatigue Cracking Potential in Hot-Mix Asphalt: Numerical Analysis and Validation." *Journal of the Association of Asphalt Paving Technologists*, 549-590.

Zou, X., Gong, H., Tang, B., Xiao, D., and Zhao, D. (2012). "Effects of Shear Stress on Pavement Cracking and Interface Debonding: Case Study in Arkansas." DVD-ROM Preprint of the *Transportation Research Board 92nd Annual Meeting*, Transportation Research Board, Washington, D. C., p 17.

Appendix A - Sensitivity Analyses

A.1 Mesh Size and Global Geometry Size Sensitivity

Table A.1.1 Sensitivity to Subgrade Mesh Size

				Centerline	Surface	
Subgrade Mesh (in)	Max z-displacement	Min z-displacement	Rut Total	Min Strain (E22)	Max Strain	Min Strain
12	7.04E-06	-2.77E-06	9.8105E-06	-2.38E-07	8.27E-07	-6.54E-07
8	8.06E-06	-3.18E-06	1.1241E-05	-1.08E-07	6.89E-07	-7.11E-07
6	9.01E-06	-4.76E-06	1.3773E-05	-7.45E-08	7.40E-07	-6.55E-07
4	8.67E-06	-4.18E-06	1.2856E-05	-5.78E-08	7.05E-07	-6.48E-07
2	9.00E-06	-3.84E-06	1.284E-05	-2.27E-08	7.94E-07	-9.82E-07

Table A.1.2 Sensitivity to Granular Base Mesh Size

Granular Base Mesh (in)	Max z-displacement	Min z-displacement	Rut Total	Min Strain (E22)	Max Strain	Min Strain
4	6.86E-06	-2.04E-06	8.9043E-06	-6.34E-08	7.56E-07	-7.46E-07
2	6.70E-06	-2.10E-06	8.8007E-06	-3.76E-08	8.21E-07	-6.47E-07
1	6.63E-06	-2.18E-06	8.8092E-06	-2.18E-08	8.45E-07	-5.28E-07
0.5	6.63E-06	NA	NA	NA	NA	NA

Table A.1.3 Sensitivity to Existing AC Mesh Size

Existing AC mesh (in)	Max z-displacement	Min z-displacement	Rut Total	Min Strain (E22)	Max Strain	Min Strain
2	5.17E-06	-1.42E-06	6.5886E-06	-5.72E-08	1.02E-06	-8.66E-07
1	5.27E-05	-9.13E-06	6.1809E-05	-1.44E-07	NA	NA
0.5	NA	NA	NA	NA	NA	NA

Table A.1.4 Sensitivity to Overlay Mesh Size

Overlay mesh (in)	Existing AC mesh (in)	Max z-displacement	Min z-displacement	Rut Total	Min Strain (E22)	Max Strain	Min Strain
1	1	6.24E-06	-4.04E-06	1.0283E-05	-9.95E-08	5.35E-07	-4.49E-07
0.5	1	5.97E-06	-3.88E-06	9.8485E-06	-7.46E-09	5.35E-07	-4.49E-07
0.5	0.5	6.12E-06	-4.17E-06	1.0288E-05	NA	5.28E-07	-4.90E-07

Table A.1.5 Sensitivity to Global Model Size

Model Size (in.)	Max z-displacement	Min z-displacement	Rut Total	Max Strain	Min Strain
14	7.62E-06	-3.73E-06	1.14E-05	4.04E-07	-4.92E-07
21	8.97E-06	-3.76E-06	1.27E-05	3.13E-07	-3.31E-07
40	6.12E-06	-4.17E-06	1.03E-05	5.28E-07	-4.90E-07
56	5.13E-06	-4.00E-06	9.14E-06	5.51E-07	-6.81E-07
80	4.94E-06	-3.87E-06	8.80E-06	2.25E-07	-4.78E-07

A.2 Loading Sensitivity

Table A.2.1 Sensitivity to Full-Path and Step-Wise Loading

Loading	Overlay mesh (in)	Existing AC mesh (in)	Max z-displacement	Min z-displacement	Rut Total	Max Strain	Min Strain
Step-wise	1	1	6.24E-06	-4.04E-06	1.0283E-05	5.35E-07	-4.49E-07
Full Path	1	1	2.50E-08	-9.07E-09	3.4027E-08	3.07E-12	-3.45E-12
Step-wise	0.5	0.5	6.12E-06	-4.17E-06	1.0288E-05	5.28E-07	-4.90E-07
Full Path	0.5	0.5	2.33E-08	-1.67E-08	3.9927E-08	1.20E-11	-1.25E-11

Table A.2.2 Sensitivity to Step-Wise Loading Cycles

Load Cycles	Max z-displacement	Min z-displacement	Rut Total	Max Strain	Min Strain
1	6.12E-06	-4.17E-06	1.0288E-05	5.28E-07	-4.90E-07
2	6.12E-06	-4.17E-06	1.0288E-05	5.30E-07	-4.90E-07
3	6.70E-06	-4.47E-06	1.1165E-05	3.60E-07	-3.97E-07
4	7.25E-06	-4.75E-06	1.2004E-05	2.52E-07	-2.95E-07
5	7.41E-06	-4.83E-06	1.2237E-05	2.24E-07	-2.67E-07
6	7.53E-06	-4.89E-06	1.2414E-05	2.03E-07	-2.46E-07
7	7.63E-06	-4.93E-06	1.2557E-05	1.86E-07	-2.29E-07
8	7.71E-06	-4.97E-06	1.2674E-05	2.51E-07	-2.16E-07
9	7.77E-06	-5.00E-06	1.2775E-05	2.27E-07	-2.05E-07
10	7.83E-06	-5.03E-06	1.2861E-05	1.83E-07	-1.95E-07

Appendix B - Interface Strain Results

B.1 Strain Results for Varying Stiffness Moduli

Table B.1.1 Strain Results for 5000s Loading (Section NM, 1-in. mesh)

Time	K-Value	Microstrain
5000	740	1.208E+02
5000	1000	1.185E+02
5000	1800	1.120E+02
5000	2600	1.056E+02
5000	3400	1.006E+02
5000	4200	9.578E+01
5000	4400	9.461E+01

Table B.1.2 Strain Results for 10,000s Loading (Section NM, 1-in. mesh)

Time	K-Value	Microstrain
10000	740	1.210E+02
10000	1000	1.187E+02
10000	1800	1.122E+02
10000	2600	1.062E+02
10000	3400	1.009E+02
10000	4200	9.600E+01
10000	4400	9.485E+01

Table B.1.3 Strain Results for 15,000s Loading (Section NM, 1-in. mesh)

Time	K-Value	Microstrain
15000	740	1.212E+02
15000	1000	1.189E+02
15000	1800	1.123E+02
15000	2600	1.063E+02
15000	3400	1.010E+02
15000	4200	9.614E+01
15000	4400	9.500E+01

Table B.1.4 Strain Results for 20,000s Loading (Section NM, 1-in. mesh)

Time	K-Value	Microstrain
20000	740	1.213E+02
20000	1000	1.191E+02
20000	1800	1.124E+02
20000	2600	1.065E+02
20000	3400	1.011E+02
20000	4200	9.600E+01
20000	4400	9.512E+01

Table B.1.5 Strain Results for 5000s Loading (Section NM, 0.5-in. mesh)

Time	K-Value	MicroStrain
5000	740	1.470E+02
5000	1000	1.446E+02
5000	1800	1.374E+02
5000	2600	1.310E+02
5000	3400	1.252E+02
5000	4200	1.198E+02
5000	4400	1.186E+02

Table B.1.6 Strain Results for 10,000s Loading (Section NM, 0.5-in. mesh)

Time	K-Value	MicroStrain
10000	740	1.473E+02
10000	1000	1.448E+02
10000	1800	1.376E+02
10000	2600	1.312E+02
10000	3400	1.254E+02
10000	4200	1.201E+02
10000	4400	1.188E+02

Table B.1.7 Strain Results for 15,000s Loading (Section NM, 0.5-in. mesh)

Time	K-Value	MicroStrain
15000	740	1.474E+02
15000	1000	1.449E+02
15000	1800	1.378E+02
15000	2600	1.313E+02
15000	3400	1.255E+02
15000	4200	1.202E+02
15000	4400	1.190E+02

Table B.1.8 Strain Results for 20,000s Loading (Section NM, 0.5-in. mesh)

Time	K-Value	MicroStrain
20000	740	1.476E+02
20000	1000	1.451E+02
20000	1800	1.379E+02
20000	2600	1.315E+02
20000	3400	1.257E+02
20000	4200	1.201E+02
20000	4400	1.191E+02

B.2 Strain Results by Section and Stiffness Modulus

Table B.2.1 Strain Results for NM Section

Section	K	Microstrain
NM	740	1.470E+02
NM	1000	1.446E+02
NM	1800	1.374E+02
NM	2600	1.310E+02
NM	3400	1.252E+02
NM	4200	1.198E+02
NM	4400	1.186E+02

Table B.2.2 Strain Results for NE Section

Section	K	Microstrain
NE	740	1.369E+02
NE	1000	1.347E+02
NE	1800	1.287E+02
NE	2600	1.232E+02
NE	3400	1.183E+02
NE	4200	1.138E+02
NE	4400	1.128E+02
NE	5000	1.097E+02
NE	5800	1.059E+02
NE	6600	1.024E+02
NE	7400	9.913E+02

Table B.2.3 Strain Results for NW Section

Section	K	Microstrain
NM	740	1.470E+02
NM	1000	1.446E+02
NM	1800	1.374E+02
NM	2600	1.310E+02
NM	3400	1.252E+02
NM	4200	1.198E+02
NM	4400	1.186E+02

Table B.2.4 Strain Results for SM Section

Section	K	Microstrain
SM	740	2.259E+02
SM	1000	2.097E+02
SM	1800	1.672E+02
SM	2600	1.326E+02
SM	3400	1.111E+02
SM	4200	1.099E+02
SM	4400	1.097E+02

Table B.2.5 Strain Results for SE Section

Section	K	Microstrain
SE	740	2.489E+02
SE	1000	2.327E+02
SE	1800	1.897E+02
SE	2600	1.547E+02
SE	3400	1.253E+02
SE	4200	1.099E+02
SE	4400	1.097E+02

Table B.2.6 Strain Results for SW Section

Section	K	Microstrain
SW	740	2.300E+02
SW	1000	2.139E+02
SW	1800	1.713E+02
SW	2600	1.366E+02
SW	3400	1.098E+02
SW	4200	1.089E+02
SW	4400	1.088E+02